Stress Characterization in Thick Walled Cylinders with Elliptical Cross-Bores

Christiaan Adika Adenya

A thesis submitted in partial fulfillment for the Degree of Master of Science in Mechanical Engineering in the Jomo Kenyatta University of Agriculture and Technology

2009

DECLARATION

This thesis is my original work and has not been presented for a degree in any other University.

Signature:…… Date:……..…….....…….

Christiaan Adika Adenya

This thesis has been submitted for examination with my approval as University Supervisor.

Signature:…… Date:……..…….....…….

Eng. Prof. John M. Kihiu

JKUAT, Kenya.

DEDICATION

This work is dedicated to the memory of my late parents, Doricah Musabi and Hudson Adenya. As my very first two teachers you inculcated in me the valuable principles of love of work and academic excellence. Your confidence in me motivated me towards the same. You believed and invested dearly in me. Thank you.

ACKNOWLEDGEMENTS

Special thanks to my lecturer and project supervisor Eng. Prof. J. M. Kihiu for introducing me to the field of Finite Element Method. Your guidance, insights and support in the course of this research work has been invaluable. You have been patient enough to impart in me the principles of the Finite Element Method.

I am grateful to the Management and Administration of Jomo Kenyatta University of Agriculture and Technology for granting me study leave and sponsorship to carry out this research work. Special thanks to the Chairman of the Department of Mechanical Engineering, Dr. Eng. P. K. Kibicho for ensuring that the facilities needed for this research were made available. Thanks to the Chief Technician of the Department of Mechanical Engineering, Mr. E. Kibiro for ensuring that essential softwares and other office supplies were made available for this research.

Appreciation to my colleagues Mr. M. Njuguna, Mr. P. Kamau, Mr. D. Ondoro, Mr. J. Kimotho, Mr. O. Muvengei, Mr. A. Gitahi, Mr. H. Ndiritu, Ir. A. Muchiri and Mr. B. Kariuki for their ever present moral support. I am also thankful to the entire staff members of the Department of Mechanical Engineering for their direct and indirect support.

Special thanks to my grandma Zipporah Kambiha who is always keen to know my progress. To my siblings, Solomon, Lewis, Edwin, Rodgers and the late Joan, you

have been a great source of motivation. I appreciate your concern, encouragement and moral support. My appreciation to the Tunjes for their ever present support and love.

To my dear wife Dorcas Supa and our daughter Abigail Amanda, your support, understanding and patience during my deep involvement in this research is appreciated. You are a great inspiration in my life.

All the Glory and Honour be to the Almighty and Faithful God for enabling me to complete this work.

TABLE OF CONTENTS

LIST OF TABLES

LIST OF FIGURES

LIST OF APPENDICES

LIST OF ABBREVIATIONS

AOR	The angle of rotation of the elliptical cross-bore major axis with respect to the cylinder axis. The major axis of the elliptical cross-bore is initially parallel to the cylinder axis.
FEM	Finite element method.
SCF	Stress concentration factor.

LIST OF SYMBOLS

a	Ellipse semi-major axis (m)
A	Constant in the Lame's Equations (N/m^2)
b	Ellipse semi-minor axis (m)
B	Constant in the Lame's Equations (N)
d	Cross-bore to cylinder bore radius ratio
E	Young's modulus (N/m^2)
k	Thickness ratio
K_t	Hoop stress concentration factor
r	Radial distance from the cylinder axis (m)
r_i	Inner radius of the cylinder (m)
r_o	Outer radius of the cylinder (m)
p	Internal pressure (N/m^2)
σ_a	Axial stress (N/m^2)
σ_c	Hoop stress (N/m^2)
σ_{eff}	Effective stress (N/m^2)
σ_r	Radial stress (N/m^2)
σ_y	Uniaxial yield stress (N/m^2)
σ_{xx}	Stress in the x – direction (N/m^2)
σ_{yy}	Stress in the y – direction (N/m^2)
σ_{zz}	Stress in the z – direction (N/m^2)

$\sigma_1, \sigma_2, \sigma_3$	Principal normal stresses (N/m^2)
ν	Poisson's ratio
τ_{xy}	Shear stress in the x – direction on planes y = constant (N/m^2)
τ_{yz}	Shear stress in the y – direction on planes z = constant (N/m^2)
τ_{zx}	Shear stress in the z – direction on planes x = constant (N/m^2)
τ_{max}	Maximum shear stress (N/m^2)
τ_{oct}	Octahedral shear stress (N/m^2)
τ_y	Yield stress in shear (N/m^2)
ξ, η, ρ	Natural co-ordinates

ABSTRACT

An investigation was conducted to determine the elastic stress profiles in a thick walled closed ended cylinder with a radial elliptical cross-bore. The orientation of the elliptical cross-bore with respect to the cylinder axis was varied. Various cross-bore to cylinder bore radius ratios were investigated. Investigations were also done for various geometries of the elliptical cross-bore.

The aim of this research was to determine the stress profiles and stress concentration factors in the vicinity of an elliptical cross-bore with regard to changing orientation of the cross-bore. The research was also aimed at determining stress trends when the cross-bore geometry was changed.

Investigations were done by computer simulation. An elastic three-dimensional finite element method computer programme in FORTRAN code was developed. The displacement formulation was used. Cylinder geometries of thickness ratios $k=2.0$, $k=2.25$ and $k=2.5$ were considered. Cylinder length was taken to be 9 times the wall thickness. The cross-bore was positioned at the centre of the cylinder to avoid any end effects. The Bauschinger effect was ignored.

The results obtained showed that the maximum stress concentration factor was experienced when the major axis of the elliptical cross-bore lay in the meridional

plane, whereas, the minimum stress concentration factor was experienced when the major axis of the elliptical cross-bore lay in the transverse plane.

For an elliptical cross-bore of cross-sectional area equivalent to that of a circular cross-bore of cross-bore to cylinder bore radius ratio of 0.15, the stress concentration factor (SCF) was a constant at 2.1 for angle of rotation (AOR) of 74.5° for semi-minor axis to semi-major axis ratio (*b/a*) between 0.3 and 0.7. For an elliptical cross-bore of cross-sectional area equivalent to that of a circular cross-bore of cross-bore to cylinder bore radius ratio of 0.20, the SCF was a constant at 2.1 for AOR = 73° for *b/a* between 0.3 and 0.7. For an elliptical cross-bore of cross-sectional area equivalent to that of a circular cross-bore of cross-bore to cylinder bore radius ratio of 0.25, the SCF is a constant at 2.1 for AOR = 72.5° for *b/a* between 0.3 and 0.7.

The results obtained from this research give details on the stress profiles and SCF that arise for a radial elliptical cross-bore at any orientation with respect to the cylinder axis. These results form a good basis for re-evaluating existing data for design of cylinders with elliptical cross-bores. The program developed can be commercialized and used to collect further data for design.

CHAPTER 1

INTRODUCTION

1.1. OVERVIEW

Pressure vessels are leak-proof containers. High pressures, extremes of temperatures and severity of functional performance requirements pose exacting design problems. These have necessitated the study of modes of failure, study of methods of stress analysis in pressure vessels, study of selection of material type and its environmental behaviour. Knowledge of material behaviour is required not only to avoid failures, but also to permit maximum economy of material used [1].

The development of high pressure technology was driven by three primary applications: gun barrel development, the polyethylene process and isostatic pressing [2]. Early attempts to improve gun barrel design concentrated on increasing strength of the barrel materials and better projectile loading methods. Polyethylene industry contributed to the understanding of the fatigue and fracture of pressurized cylinders, and the design of pressure seals and high pressure compressors. The process of compacting powders at high pressure and high temperature (hot isostatic pressing), led to the development of a wide variety of hot isostatic pressing vessels operating at pressures up to 345 MPa and temperatures up to 1650 °C.

Developments of space exploration, nuclear and chemical industries have placed new demands on materials suitable for extremes of temperature, impact and fatigue [1]. Sometimes these applications also require consideration of other environmental effects such as corrosion, neutron bombardment and hydrogen embrittlement. The chemical industry has greatly increased the importance of correct design for pressure containers [3]. The combined effects of corrosion, high temperatures, and fluctuating loads have raised the demands beyond those which can be met by straight forward interpretation of ordinary theoretical methods.

Thick pressure vessels are now widely used in nuclear power plants for steam and power generation [4]. Other pressure vessel applications might involve as high as 1380 MPa and temperatures of up to 300 °C resulting in the pressure vessel material holding immense potential energy exerted by the working fluid [4]. Such high pressure vessels require proper understanding of the stress concentration levels and distributions for fail-safe design. With pressure vessels holding high potential energy exerted by working fluid, it is important to minimize or even eliminate accidental losses due to poor designs that may result from inadequate understanding of the stresses [5].

Past pressure vessel catastrophic failures arising from the lack of understanding of the stress levels, material properties and fluid/structure environmental interactions, particularly in the past century, were very expensive in terms of losses in materials and human life [4]. These failures were the main impetus for early studies in

cylinders of various materials. Later on, the stress distribution in critical sections and metallurgical failure aspects were given more emphasis.

High pressure vessels are now of great importance in many industries and their economic use of material often depends upon the occurrence of small, controlled permanent deformations [4]. Autofrettage is the process by which beneficial residual stresses are introduced into a thick walled pressure vessel by initially subjecting the vessel to a high internal pressure that causes plastic deformation. As a result, the load carrying capacity of the thick walled pressure vessel is increased due to the presence of residual stresses [1].

It is frequently required to provide a pressure tapping into a thick walled pressure vessel. Situations arise when it becomes necessary to provide these openings in the pressure vessel wall for a flow circuit, temperature measurement, internal pressure measurement, fluid inlets or outlets, safety valves, and bursting disc [6]. These openings constitute a major source of weakness. The cross-bores once introduced create regions of high stress concentrations. The severity of the stress concentrations depend on the geometrical configuration of the cross-bore at the junction of the main bore. These stress concentrations not only reduce the pressure carrying capacity of the vessel but also reduce the fatigue life of the vessel [6].

Proper understanding of the stress profile in the cylinder and around the cross-bore is essential in estimating the maximum permissible operating pressure. This problem

can be overcome by forming a radius, chamfer or counter-bore at the intersection of the main cylinder bore and the cross-bore. However, even then, a clear understanding of the stress profile would help in better design [7]. For high pressure applications, a clear understanding of the state of stress in a vessel with side bores is needed because fatigue life is very critical and limitations of strength and ductility in commercial pressure vessel materials prevent high factors of safety [8].

1.2. STATEMENT OF THE PROBLEM

Situations arise where a cross-bore is required in the wall of a thick walled cylinder. A cross-bore introduces a point of discontinuity in the cylinder wall. This results in a point of high stress concentrations and consequently the weak point in the cylinder. Failure is likely to occur at this point.

To avoid the enormous losses of property and human life that may occur due to a high pressure vessel failure, it is imperative to know the stress concentration factors and the stress profiles that arise in the vicinity of the elliptical cross-bore when the cylinder is loaded with an internal pressure while in service.

There is a continuous search for designs that would give the least SCF while at the same time remaining functional and economical. This information will aid in the design considerations and also guide on the operational limits of a pressure vessel.

Moreover, existing finite element method (FEM) commercial softwares are very expensive and inaccessible. This therefore necessitates the development of a FEM computer program.

1.3. OBJECTIVES

The objectives of this research work were:

1. To determine the elastic stress profiles and the stress concentration factors in the vicinity of a radial elliptical cross-bore.
2. To determine the effect of the orientation of an elliptical cross-bore on the stress profile and the stress concentration factors.
3. To determine the elliptical cross-bore geometry and orientation that gives the minimum stress concentration factor.

1.4. JUSTIFICATION

This research work will provide more insight into the stress profiles and the stress concentration factors that exist in the vicinity of a radial elliptical cross-bore. It will also give the much needed data on the geometry and orientation of the elliptical cross-bore that gives the minimum stress concentration factor. This information and data will guide the design of pressure vessels and consequently help minimize the losses that may occur due to failure of a high pressure vessel while in service.

1.5. OUTLINE OF WORK DONE

The first part of the study involved the development a finite element method (FEM) computer program to analyze elastic stresses in a plain thick walled cylinder. The program developed used the frontal solution method in solving the linear equations resulting from the finite element method formulation. This was to overcome the computer memory limitation that occurs with the Gaussian elimination when dealing with a large number of elements.

The second part of the study involved further development of the FEM computer program to include an elliptical cross-bore. This program was used to carry out investigations for various cross-bore geometries and for various cross-bore orientations with respect to the cylinder axis. Elliptical cross-bores of area equivalent to a given circular cross-bore were studied.

CHAPTER 2

LITERATURE REVIEW

An approximate analytical solution was derived for the stresses in the main pipe near the branch holes [9]. This was based on the theoretical solution for a hole in an infinite plate under uniform tension. Research was done using a frozen stress photo-elastic technique. The peak values of stresses predicted by the theory were too large. Theoretical value of SCF was 32 % greater than the measured value of 2.80.

A theoretical and experimental study has been done on stress concentration induced in a cylinder under internal pressure by the presence of circular side holes and elliptical side holes with major axis of the ellipse perpendicular to the meridional axis of the cylinder [8]. The theoretical study was based on analyses for holes in infinite elastic plates subjected to axial or biaxial stresses. The experimental analysis was done using both strain gauges and photo-elasticity method. Hoop stress concentration factor for closed-ended cylinder with a small circular cross-bore was found to be 2.5.

Research has been done on fatigue strength of cylinders with cross-bore [10]. The existence of a cross-bore was found to reduce by a factor greater than 2 the repeated pressure which a tube can withstand. For 2.5 % nickel chromium-molybdenum steel, hardened and tempered to an ultimate strength of 773 MPa, thickness ratio 2.25, bore

diameter 0.0254 m, cross-bore diameter 0.0032 m and 0.0048 m, theoretical analysis gave stress concentration factor of 2.9 and experimental analysis gave stress concentration factor of 2.1.

A theoretical analysis has been done to determine stress concentrations in thick walled cylinders which have side holes of size near that of the cylinder bore [11]. Approximate analyses were conducted on cylinders under internal pressure and also for cylinders under external shrink-fit pressure. For a cylinder with cross-bore subjected to internal pressure the stress concentration factor increased with decreasing cross-bore diameter, for a fixed bore diameter and approaches asymptotic values. For internal shrink-fit pressure, the stress concentration factor decreases with increasing thickness ratio. It also decreases with decreasing side hole diameter. For external shrink-fit pressure, the stress concentration factor approaches 3 for small cross-bore. For case of cross-bore diameter greater than cylinder bore, lowest concentration factor experienced when intersecting diameters have the same diameter.

Experiments have been done to assess the strength of a cylinder containing a cross-bore of circular cross section [12]. Static burst tests and fatigue tests were carried out on cylinders with cross-bores in various off set positions. Brittle material, grey cast iron was chosen to ensure no plastic flow of material around the cross-bore. Maximum normal stress criterion was used. Tests showed that the fatigue life of a cylinder containing a small cross-bore can be greatly improved if the cross-bore is

offset. The fatigue life for a cylinder having an optimally positioned cross-bore was found to be greater than one having a radial cross-bore by approximately 100 % for k = 1.8 and by approximately 170 % for k = 1.4.

Research has been done using a combination of analytical formulae and the numerical boundary integral equation (BIE) method for cylinders with thickness ratios 2.0 and 2.25 and for cross-bore to main bore radius ratio of 0.25 [13]. Analytical formulae were used to determine residual stresses in an autofrettaged cylinder while BIE was used to determine resultant stresses on introduction of a cross-bore. The superposition principle was used to combine the two to determine stress redistribution in partially autofrettaged tubes when a cross-bore is introduced after autofrettage. Overstrain was determined as 35 % and 27.5 % for the radius ratios of 2.0 and 2.25 respectively. The variations of resultant residual stresses across the cylinder wall near the cross-bore and in radial plane containing its axis were found to be bi-linear. Results showed no advantage in introducing a radial cross-bore after cylinder has been autofrettaged.

Finite element method has been used to study the stress distribution and fatigue behaviour of a thick walled closed ended pressure vessel containing cross-bore with various blending geometries at the intersection with the main cylinder bore [6, 14]. A curved beam model specimen was adopted and the PAFEC 75 package used. 20 nodded brick isoparametric elements were used. Thickness ratios of 2, 1.8, and 1.4 were considered. Plain cross-bores were surprisingly shown to have superior fatigue

behaviour, when compared to radiused and chamfered cross-bores, for a thickness ratio of 2 and 1.4. The effect of chamfer angle on stress distribution was found to be insignificant for 1.42 mm chamfer length that was investigated. For thickness ratio of 2.0, the SCF for the plain, radiused and chamfered cross-bores were 3.03, 1.48, and 1.86 respectively. For thickness ratio of 1.8, the SCF for the plain, radiused and chamfered cross-bores were 2.97, 1.45, and 1.95 respectively. For thickness ratio of 1.4, the SCF for the plain, radiused and chamfered cross-bores were 2.84, 1.43, and 2.11 respectively.

A 3-dimensional finite element approach was used to perform plastic analysis for cylinders with thickness ratios of 2 and 1.4 [15]. Experiments were done on cylinders of 826M40 steel with 25 mm inside diameter. 20 nodded brick type isoparametric elements were used. The effect of cross-bore diameter on the hoop stress at the intersection of cross-bore and main cylinder bore was found to result in the lowest peak stress for cross-bore of 4mm diameter. The size of a cross-bore and its surface roughness significantly affected the fatigue behaviour. A power form relation was found to exist between fatigue life and the applied maximum internal pressure.

3-dimensional finite element analyses were done for closed ended thick-walled cylinders under internal pressure with: circular cross-bore at radial position, or circular cross-bore at offset positions from the radial line, or elliptical radial cross-bores, using the LUSAS finite element package [16, 17]. Effects of cross-bore

diameter on the principal stress distribution and the SCF along the plain cross-bores were investigated for cylinders of 25 mm internal diameter and thickness ratio of 2.0. The results showed that hoop stress distributions, maximum hoop stress and SCF depended on the cross-bore diameter size. The SCF at the bore for of the circular radial hole, optimally shaped radial elliptical hole and an optimally offset circular cross bore were 2.30, 1.53 and 1.33 respectively.

Research has been done using the hoop stress to pressure ratio along with a simple notch strain estimation procedure based on kinematic hardening rule for quick residual stress estimation at a critical plane of a block containing cross-bores [18]. Neuber's rule was used as a notch strain estimation procedure. Neuber's rule slightly underestimated the residual stresses relative to FEM results. Finite element models of blocks containing cross-bores were used. Three cross-bore block configurations were examined. First, all sides were equal. Second, all sides to bore ratios were equal. Third, bore ratios were equal and hoop stress to pressure ratios was found for different sides to bore ratios. Hoop stress to pressure ratios were used in Neuber's rule to pre-select an appropriate autofrettage pressure and to estimate residual stresses at the critical plane, i.e., the plane containing both bore center lines.

Research has been done to establish and quantify the influence of cross-bore entry geometry on the elastic and elastic-plastic stresses and their distribution in thick walled cylinders under internal pressure [19]. The analysis was done by computer simulation using 3-dimensional FEM procedures. Pressure vessel material was high

strength SA-372 steel. Model cylinders had varying thickness ratio, varying cross-bore diameters, and cross-bores with varying cross-bore to main bore entry geometry. Plain cross-bores, radiused cross-bores and chamfered cross-bores were considered. For plain cross-bored cylinders, for thickness ratio between 1.75 and 3, the stress concentration factor was determined as a constant value of 2.753 for cross-bore to main bore radius ratio of 0.2. When the cross-bore to main bore radius ratio is less than 0.2, the stress concentration factor increases with increasing thickness ratio, whereas, when the cross-bore to main bore radius ratio is more than 0.2, the stress concentration factor increases with decreasing thickness ratio. For radiused entry cross-bored cylinder the stress concentration factors and stress gradients were lower than those of an equivalent plain cross-bored cylinder. Maximum hoop stress was located near the upper end of the entry radius in the meridional plane. Stress concentration factor reduces with increase in cross-bore entry radius. For chamfered entry cross-bore, varying the chamfer angles may result in minimum stress concentration factor lower than those in an equivalent plain cross-bored cylinder, but higher than those in an equivalent radiused entry cross-bored cylinder.

A technique for elastic-plastic analysis of a thick-walled cylinder under internal pressure was developed involving two parametric functions and piecewise linearization of the stress strain curve [20]. A deformation type of relationship is combined with Hooke's law in such a way that stress-strain law has the same form in all linear segments. The technique involves the use of deformed geometry to satisfy the boundary conditions. The proposed method provides a general elastic-plastic

solution to thick wall cylinders, which accounts for the effect of deformed geometry due to high internal pressure.

A 3-dimensional FEM computer program in FORTRAN code was developed to determine the optimum overstrain for autofrettage in a thick walled plain cylinder [4]. Using the program, the elastic, elastic-plastic residual and service stresses and displacements in a closed ended thick walled cylinder under internal pressure were established. The benefits of autofrettage were demonstrated and the optimum overstrain of 16 % established for a cylinder with thickness ratio of 2.

A 3-dimensional FEM computer program was developed to establish the stress distribution and stress concentration factors in thick walled cylinders with plain cross-bores under internal pressure [21]. The displacement formulation and eight nodded brick isoparametric elements were used. The frontal solution technique was used. For a thickness ratio of less than 1.75, cross-bore to main bore radius ratio was a found to be a geometric constant equal to 0.11 where the stress concentration factor is 2.67. For a thickness ratio of more than 1.75, cross-bore to main bore radius ratio was found to be a geometric constant equal to 0.2 where the stress concentration factor is 2.734.

A 3-dimensional finite element method computer program was developed to establish the elastic-plastic, residual and service stress distributions in a thick walled cylinder with flush and non-protruding plain cross-bores under internal pressure [5].

For a cylinder of thickness ratio of 2.25 and a cross-bore to main bore radius of .01, an optimum overstrain ratio of 37 % was established.

Research has been done to evaluate the effect of introducing a radial cross-bore in an autofrettaged thick-walled cylinder using the ANSYS 3-dimensional SOLIDS 95, 20 nodded finite element [7]. A radial cross-bore was introduced by element killing, (i.e. stiffness of selected elements is reduced to a very small value, thereby representing a material removal/machining effect), after the cylinder was autofrettaged and residual stress distribution were evaluated in the thick walled cylinder and around the vicinity of the cross-bore. A cylinder of 105 mm inside diameter, 220 mm outside diameter and 800 MPa autofrettage pressure was considered using von Mises yield criterion. Analysis was done for cross-bore diameters of 10 mm, 15 mm and 20 mm. It was observed that there is severe localized change in the residual stress profile in the vicinity of the cross-bore. The residual hoop stress increases in compression at the bore and increases in tension at the outside diameter. It was also observed that increasing the radial hole diameter reduces the residual hoop stress at the bore whereas it increases the residual hoop stress at the outer diameter of the main cylinder.

Research has been done to establish the stress distributions and stress concentration factors in chamfered cross-bore cylinders under internal pressure [22]. Each combination of thickness ratio and cross-bore to main bore radius ratio resulted in a unique universal SCF value at certain chamfer angles for all chamfer length ratio. In

optimal chamfered cylinders with thickness ratio between 2.25 and 3, the SCF increases with decrease in thickness ratio. For thickness ratio between 1.25 and 2, a cross-bore to main bore radius ratio of 0.075 was found to be a geometric constant with SCF of 2.65.

The stress concentration can be reduced by making the cross-bore either elliptical in section with its axis coincident with a radial centre-line or by using a round-section cross-bore which has its axis offset from the radial centre-line [23]. To minimize stress concentration, the dimensions of the outlet ellipse, formed where the cross-bore breaks into the main bore, should be such that the maximum stress at the ends of the major and minor axes are equal. To fulfill this requirement, the major axis of the outlet ellipse should be approximately twice that of the minor axis.

From this literature review, limited study has been done on elliptical cross-bores. Where an elliptical cross-bore is required in a thick walled cylinder, there is need to understand its effect on the stress profiles in the cylinder wall. Furthermore, the study of the elastic stress profiles and the SCF in a thick walled cylinder with a radial elliptical cross-bore whose orientation with respect to the cylinder axis is varying has not been done. This research will aim to get this data and also highlight details on the stresses in the vicinity of the elliptical cross-bore. Various cylinder geometries and elliptical cross-bore geometries will be analyzed and the results presented and discussed in graphical and tabular formats.

The finite element method will be used for the analysis since the information on its implementation procedures is readily available. Based on the finite element method, a computer algorithm will be developed using the FORTRAN programming code which is accessible to the researcher. FORTRAN is simple and is the most widely used language for technical and scientific computations. FORTRAN is good at numerical analysis which is being done in this research work.

CHAPTER 3

THEORETICAL BACKGROUND

3.1. THE ELLIPSE

An ellipse is the locus of a point the sum of whose distances from two foci are equal. The shape of an ellipse is indicated in Figure 3-1, where *a* is the semi-major axis and *b* is the semi-minor axis.

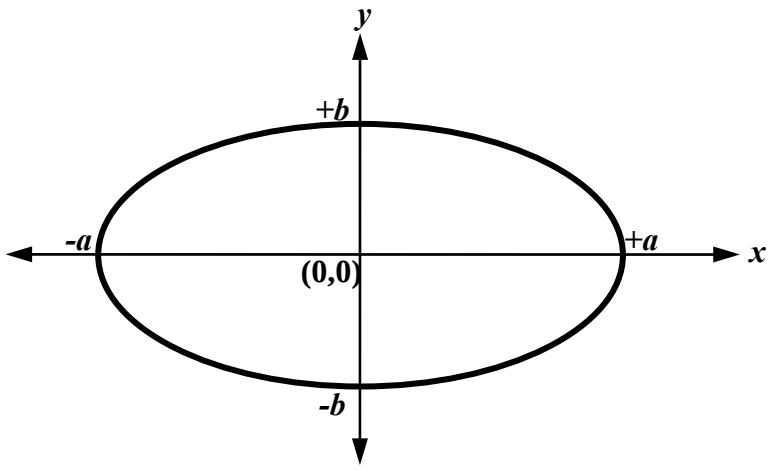

Figure 3-1 The Ellipse

The equation for an ellipse whose centre is located at (0,0) is given by:

$$\left(\frac{x}{a}\right)^2 + \left(\frac{y}{b}\right)^2 = 1 \qquad (3.1)$$

The area of an ellipse is given by:

$$A_{ellipse} = \pi ab \tag{3.2}$$

The eccentricity e of an ellipse is given by:

$$e = \sqrt{1 - \left(\frac{b}{a}\right)^2} \tag{3.3}$$

3.2. VON MISES EFFECTIVE STRESS

According to von Mises yield criterion, yielding occurs when the shear stress on the octahedral planes, τ_{oct}, reaches a critical value, i.e. $\tau_{oct} = \tau_y$ (at yielding).

$$\tau_y = \frac{1}{3}\sqrt{(\sigma_1 - \sigma_2)^2 + (\sigma_2 - \sigma_3)^2 + (\sigma_3 - \sigma_1)^2} \tag{3.4}$$

The plane on which the uniaxial stress acts is related to the octahedral plane by a rotation through an angle $\cos^{-1}(1/\sqrt{3})$, which is equal to 54.7° [24].

For principal stresses, the effective stress is given by the following equation [24]:

$$\sigma_{eff} = \sqrt{\frac{(\sigma_1 - \sigma_2)^2 + (\sigma_2 - \sigma_3)^2 + (\sigma_3 - \sigma_1)^2}{2}} \tag{3.5}$$

For any state of stress, the effective stress given by [24].

$$\sigma_{eff} = \sqrt{\frac{(\sigma_{xx} - \sigma_{yy})^2 + (\sigma_{yy} - \sigma_{zz})^2 + (\sigma_{zz} - \sigma_{xx})^2 + 6(\tau_{xy}^2 + \tau_{yz}^2 + \tau_{zx}^2)}{2}} \tag{3.6}$$

3.3. STRESS-STRAIN RELATION

For three-dimensional case, the elastic stress-strain matrix for isotropic material is given by [25]:

$$C = \frac{E(1-v)}{(1+v)(1-2v)} \begin{bmatrix} 1 & \frac{v}{1-v} & \frac{v}{1-v} & 0 & 0 & 0 \\ \frac{v}{1-v} & 1 & \frac{v}{1-v} & 0 & 0 & 0 \\ \frac{v}{1-v} & \frac{v}{1-v} & 1 & 0 & 0 & 0 \\ 0 & 0 & 0 & \frac{1-2v}{2(1-v)} & 0 & 0 \\ 0 & 0 & 0 & 0 & \frac{1-2v}{2(1-v)} & 0 \\ 0 & 0 & 0 & 0 & 0 & \frac{1-2v}{2(1-v)} \end{bmatrix} \tag{3.7}$$

3.4. STRESS CONCENTRATION FACTOR

The elementary stress formulas used in the design of structural members are based on the members having a constant section or a section with gradual change of contour. The presence of shoulders, grooves, holes, keyways, threads, and so on results in modifications of the simple stress distributions so that localized high stresses occur. This localization of high stress is known as stress concentration, measured by the stress concentration factor (SCF) [26]. The SCF can be defined as the ratio of the peak stress in the body (or stress in the perturbed region) to some other stress (or stress-like quantity) taken as a reference, given by:

$$K_t = \frac{\sigma_{\max}}{\sigma_{nom}} \tag{3.8}$$

Where σ_{max} is the maximum stress and σ_{nom} is the reference stress.

Abrupt changes in cross-section give rise to great irregularities in stress distribution [27]. The irregularities are of particular importance in design of machine parts subjected to variable external forces and to reversal of stresses. Irregularity of stresses at such places means that at certain points the stress is far above the average value, and under the action of reversal of stresses, progressive cracks are likely to start [27]. Therefore, a cross-bore gives rise to a region of high stress concentrations in the pressure vessel wall. The stress concentration factor is the most important parameter in the pressure vessel analysis studies and is the one used for design purposes [19].

If a circular hole is made in a plate subjected to uniform tensile stress, the theoretical stress concentration factor is 3. If an elliptical hole is made in a plate with its major axis perpendicular to the direction of the uniform tensile stress as shown in Figure 3-2, the maximum stress will be at the end of the major axis. The theoretical stress concentration factor is given by [27].

$$K_t = \left(1 + 2\frac{a}{b}\right) \tag{3.9}$$

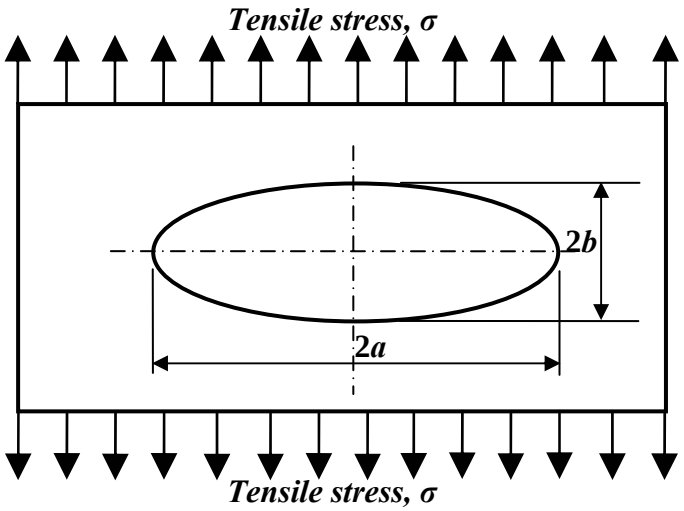

Figure 3-2 An elliptical hole in a flat plate under tension

By using the classical solution to the problem of a circular hole in an infinite plate subjected to uniform tension, the elastic stresses surrounding a small circular cross-bore drilled radially through the wall of a cylinder can be approximated. The hoop stress concentration factor can be shown to be given by the following equation [12]:

$$K_t = \left(\frac{4k^2 + 1}{k^2 + 1} \right) \tag{3.10}$$

where k is the cylinder thickness ratio, while the maximum shear stress concentration factor is equal to a constant value of 2.5 [12]. The strength of a pressure vessel will, in many situations, be dependent on the magnitude of the stress concentration factor. A reduction of the stress concentration factor should increase the load carrying capacity of the pressure vessel.

The hoop stress concentration factor is the ratio of the maximum principal stress at the intersection of the cross-bore and the cylinder bore to the Lame's hoop stress at the bore of a vessel without a cross-bore, and is given by the following equation [28].

$$K_t = \frac{\sigma_{\max - principal}}{\sigma_{Lame' - hoop}} \tag{3.11}$$

3.5. THE FINITE ELEMENT METHOD

3.5.1. Introduction

The Engineer's task is a quantitative analysis and synthesis of physical objects. Experiments on physical models or prototypes became imperative and were frequently the only tools available during the first half of the 20th century. With the invention of the digital computer, with its remarkable arithmetic capabilities, the attitude of Engineers has changed. By using approximate numerical processes, the 'experiment' can be cast in digital form and rapidly analyzed by the computer at no great cost. Optimization by experiment was both expensive and hazardous. The computer is now established as an essential part of life in a wide range of engineering activities, such as aerospace and electronics, and indeed the work of many Mechanical and Civil Engineers is already unthinkable without its use [29]. Nuclear explosions can also be simulated on computer.

Once a part or product has been designed, it must be tested to ensure it will perform according to specifications in the real world. Rather than go through the expensive and time-consuming process of building prototypes and subjecting them to destructive testing, the standard practice has been to test a model of the part or product on the computer using finite element analysis. The objective of finite element analysis of real world models is to simulate destructive testing using a minimum amount of computer memory, computation time and modeling time [30].

Recent advances in numerical techniques such as the finite element method have ensured that solutions can readily be obtained for three-dimensional solid structures [31]. With emphasis gradually shifting to ultimate load analysis for efficient design, the inclusion of non-linear behaviors is desirable. This is particularly so in technologically advanced fields such as reactor vessel design where non-linear effects are of paramount importance in assessing the performance of the structure.

Derivation of governing equations for most problems is not unduly difficult, but their solution by exact methods of analysis is a formidable task. Approximate methods of analysis provide alternative means to finding solutions [32]. More recently, the method of finite elements has been found to be a powerful approach to stress analysis problems. Part of its advantage stems from the ability to handle irregular shapes of boundaries and mixed boundary conditions [33].

The finite element method overcomes the disadvantages of traditional variational methods, like Rayleigh-Ritz and Galerkin, by providing a systematic procedure for the derivation of the approximation functions over sub-regions of the domain [32]. The finite element method is endowed with three basic features that make it superior over other competing methods (e.g., finite difference method, and the variational methods) [32]:

1. A geometrically complex domain of the problem is represented as a collection of geometrically simple domains, called finite elements.
2. Over each finite element, the approximation functions are derived using the basic idea that any continuous function can be represented by a linear combination of algebraic polynomials.
3. Algebraic relations among the undetermined coefficients (i.e., nodal values) are obtained by satisfying the governing equations, often in a weighted integral sense, over each element.

3.5.2. The Finite Element Method Displacement Formulation

The procedure for the finite element displacement formulation includes the following [32, 34-37]:

1. Discretization of the structure into elements. This involves locating the nodes, numbering and specifying their coordinate values.
2. Determination of element properties from material and loading data. This involves specifying the approximation equation for force-displacement

relationships. Equations are written in terms of the unknown nodal displacements.

3. Determination of the stiffness matrix and the corresponding nodal loads for each element.
4. Assembly of the element stiffness matrices and load vectors to generate the global stiffness matrix and the global load vector respectively.
5. Application of boundary conditions on the assembled global stiffness matrix and global load vector.
6. Solving the resulting system of equations to determine the nodal displacements.
7. Evaluation of strains and stresses for each element using the nodal displacements and the element properties.

3.5.3. Isoparametric Elements

The concept of Isoparametric elements is based on the transformation of the parent element in local or natural coordinate system to an arbitrary shape on the Cartesian coordinate system [36]. Isoparametric elements have the geometry and displacements of the element described in terms of the same parameters and are of the same order [38]. The shape functions defining geometry and displacement functions are the same [37]. The same points define the geometry and the finite element analysis points.

3.5.4. Eight Noded Brick (Hexahedral) Element

For linear three-dimensional analysis the superiority of general shaped hexahedral elements over simple tetrahedral is now generally accepted [39]. See Figure 3-3.

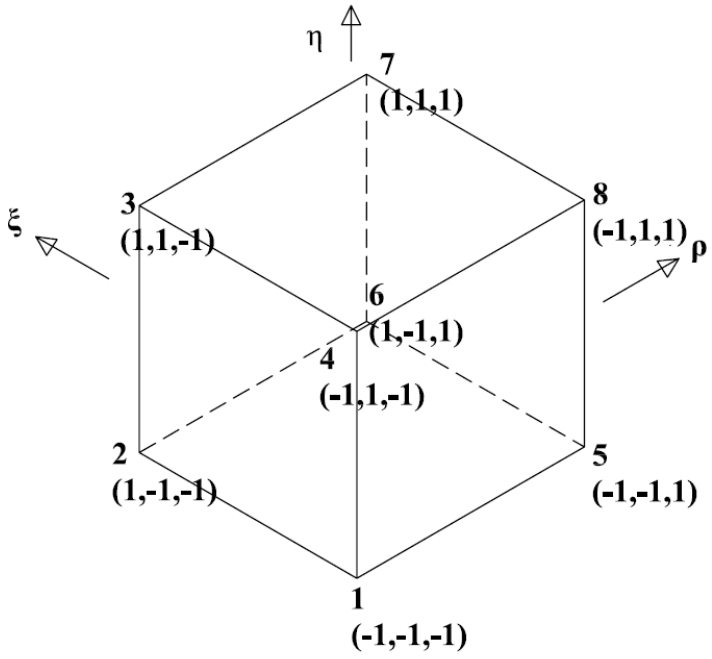

Figure 3-3 Eight Noded Brick Element

The shape function defining the geometry and variation of displacement for the eight-noded (brick) isoparametric element is given by the following equation [36]:

$$N_i = \frac{1}{8}(1+\xi\xi_i)(1+\eta\eta_i)(1+\rho\rho_i) \quad i = 1, 2, \ldots, 8 \tag{3.12}$$

Where ξ, η, ρ are natural coordinates of the Gaussian sampling points and ξ_i, η_i, ρ_i are the values of natural coordinates for node *i*.

The natural coordinate of the Gaussian sampling points for the eight noded element are given in the Table A-1 in the appendix. The weighting factor for each Gauss point is unity. Stresses are determined at the sampling points and then extrapolated to the nodes.

CHAPTER 4

METHODOLOGY

4.1. INTRODUCTION

This work involved the study of the stress profiles and the stress concentration factors in a thick-walled cylinder with a radial elliptical cross-bore. Due to symmetry, the thick walled cylinder was represented by a quarter of the structure [19] for the plain cylinder. Half of the structure was used to represent the cylinder with an elliptical cross-bore, due to the special shape of the ellipse and the need to rotate the cross-bore. Using portions of the cylinder instead of the whole cylinder greatly reduced the computer storage requirements and computer run time.

For comparison purposes, elliptical cross-bores of cross-sectional area equivalent to that of a given circular cross-bore were studied. This was to ensure equal material weight removal.

In this research work:

1. An eight noded brick isoparametric element, shown in Figure 3-3, was used.
2. Serendipity family element shape functions were used for their simplicity. These are given by equation (3.12).

3. Displacement formulation was used. The displacements of nodal points are the basic unknown parameters of the problem [37].
4. Numerical integration procedure was used for evaluating the stiffness matrix using Gauss quadrature. The 2x2x2 scheme was adequate for 8-noded linear element [36].
5. The pressure vessel material was a high strength SA 372 steel of yield stress 450 MPa, Young's modulus of 209 GPa and Poisson's ratio of 0.29 [40].
6. A FORTRAN computer program was developed for the analysis.
7. The simulation results were presented in form of graphs.

4.2. DISCRETIZATION DETAILS

Discretization was done to obtain the nodal numbers and nodal coordinates, element numbers and identify the nodes for each element. The eight noded brick element was entirely used for this analysis.

4.2.1. Plain Thick Walled Cylinder

A plain cylinder, that is, a cylinder without a cross-bore, was studied to give data that would be used to test the validity, accuracy and therefore reliability of the elastic finite element method analysis used for this research. The stress profiles were easily compared to the analytical profiles generated by the Lame's equations. See equations (A.6) and (A.7) in the appendix.

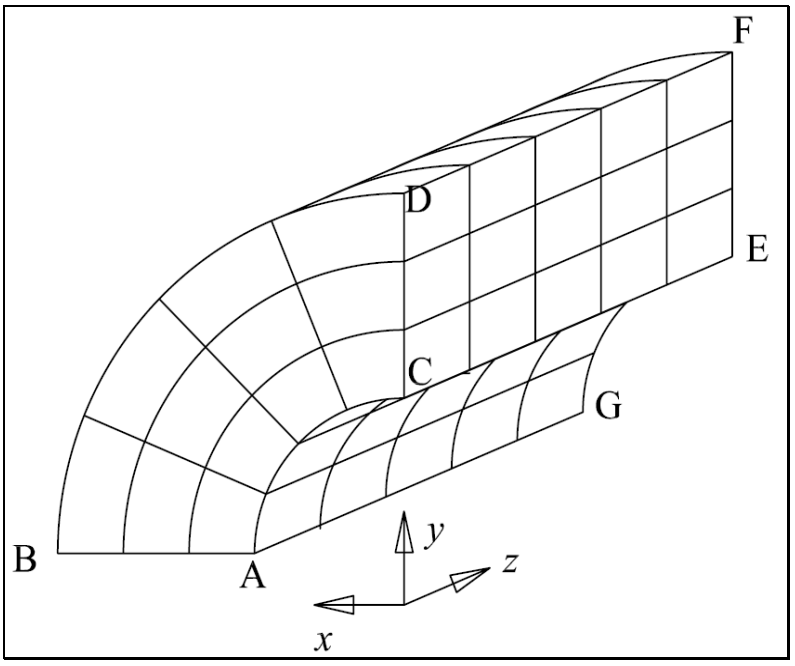

Figure 4-1 Discretization of a plain cylinder

For a cylinder without a cross-bore, quarter of the cylinder was considered as shown in Figure 4-1. The geometric inputs were the inside radius, the cylinder thickness ratio, the material's Young's modulus, the Poisson's ratio, the internal load pressure, number of elements in the radial direction (along AB), number of elements along in the circumferential direction (along AC), number of elements in the axial direction (along CE) and the geometric ratio of elements in the radial direction. The inside radius was 12.5 mm, thickness ratio was 2, Young's modulus was 209 GPa, Poisson's ratio was 0.29, internal pressure was 50 MPa, 14 elements in the radial direction, 8 elements in the circumferential direction, 8 elements in the axial direction.

This resulted in a structure with 1,215 nodes, 896 elements, 3,645 degrees of freedom and a frontal width of 438. The global stiffness matrix coefficients were reduced by 98.6 %, thus only 1.4 % of the potential memory requirement was needed. The results obtained for the plain cylinder were very accurate when compared with the analytical results. Therefore the discretization was sufficient.

4.2.2. Cross-Bored Thick Walled Cylinder

For a cylinder with an elliptic cross-bore, half of the cylinder was considered as shown in Figure 4-2. The meridional cross-sectional view of the cylinder with a cross-bore is shown in Figure 4-3 whereas the transverse cross-sectional view is shown in Figure 4-4.

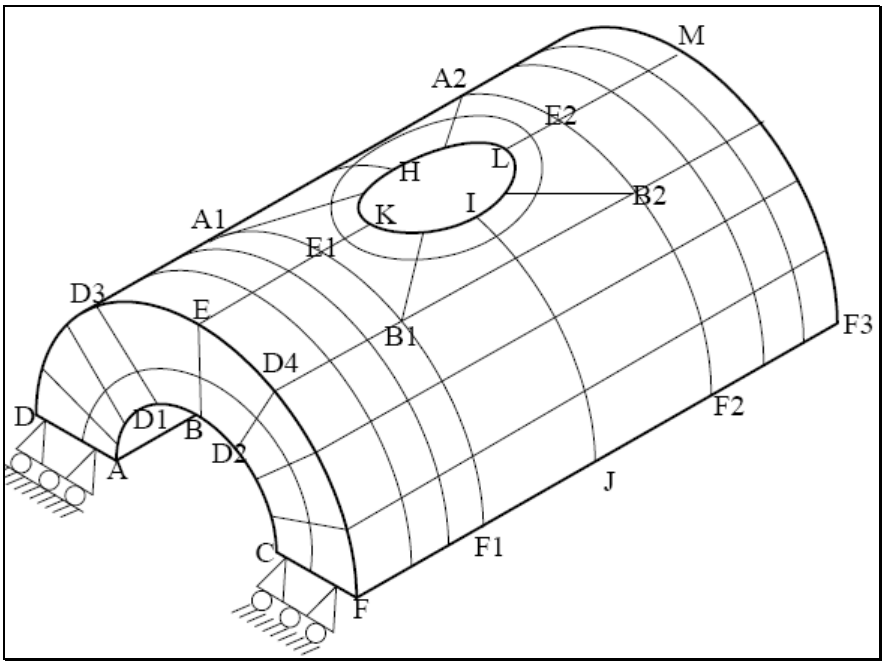

Figure 4-2 Discretization of a cylinder with an elliptical cross-bore

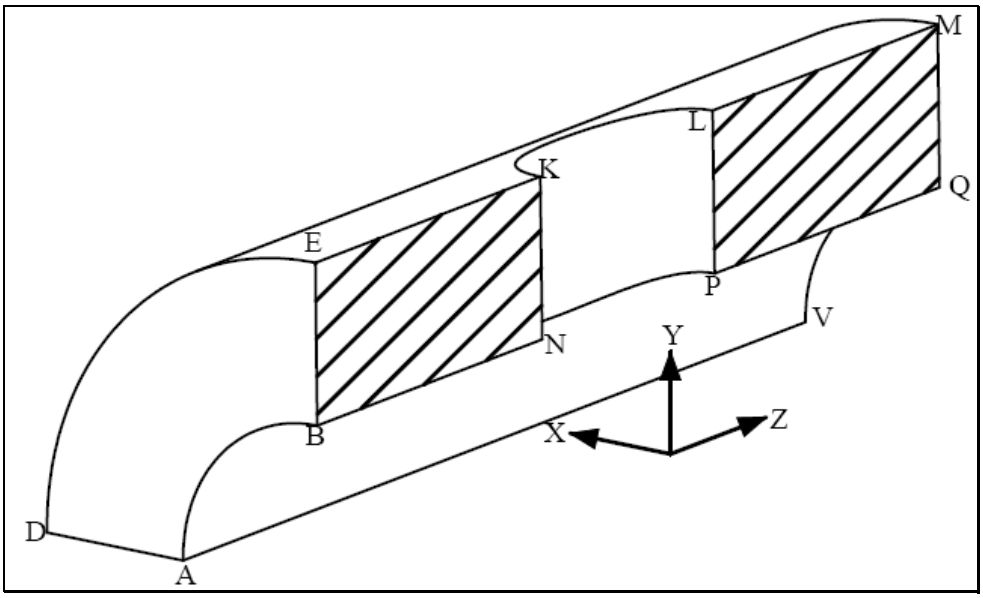

Figure 4-3 Meridional cross-sectional view of cylinder with cross-bore

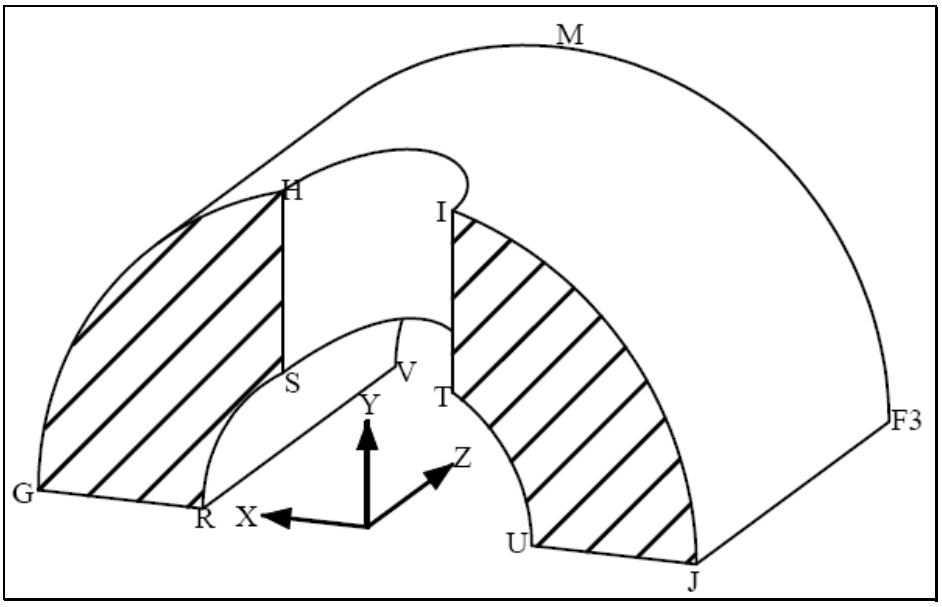

Figure 4-4 Transverse cross-sectional view of cylinder with cross-bore

The half cylinder was divided into five parts. Part I included elements bound by the transverse planes passing through points D-D3-E-D4-F and points A1-E1-B1-F1.

Part II included elements between the transverse plane with points A1-E1-B1-F1 and the transverse plane with point A2-E2-B2-F2 and also between the horizontal plane with points A-D-V and the vertical plane passing through points A1-A2. Part III included elements around the cross-bore, that is, between the vertical plane passing through points A1-A2 and the vertical plane through points B1-B2. Distance E1-K was 10 % of the cylinder inside radius. This was made small to ensure that the high stress profiles expected in this section around the cross-bore are noted. This section near the cross-bore was finely meshed compared to the other parts. Part IV included elements between transverse plane with points A1-E1-B1-F1 and the transverse plane with points A2-E2-B2-F2 and also between the horizontal plane with points C-F-F3 and the vertical plane with points B1-B2. Part V included elements between the transverse plane with points A2-E2-B2-F2 and the transverse plane with points M-F3-V.

The geometric inputs were the inside radius, the cylinder thickness ratio, ratio of cross-bore radius to main bore radius, ratio of the semi-minor axis to the semi-major axis of the elliptical cross-bore, angle of rotation of the elliptical cross-bore. The direction of rotation of the elliptical cross-bore was anticlockwise. The angle of rotation was varied in the anticlockwise direction from the cylinder axis. This angle was varied from 0° to 90°.

The inside radius for this case was 12.5 mm, thickness ratio was varied, Young's modulus was 209 GPa, Poisson's ratio was 0.29, and internal pressure was 50 MPa.

The number of elements in the radial direction were 14, number of elements along curve HL were 6, number of elements along E1-K were 5, number of elements along E-E1 were 5, the number of elements along curve A-D1 were 5. This resulted in a structure with 5,760 nodes, 4,760 elements, 17,280 degrees of freedom and a frontal width of 2,196. The global stiffness matrix coefficients were reduced by 98.4 %. Thus only 1.6 % of the potential memory requirement was needed. The cylinder radial geometric ratio was 1.2, geometric ratio along E1-K was 1.35, geometric ratio along curve H-L was 1.1, geometric ratio along E-E1 was 2.0, and geometric ratio along curve A-D1 was 1.5.

The high geometric ratios were chosen where high stress gradients were anticipated and to ensure that on moving from one part to the other, the element edges have about the same size [19]. The geometric ratios were also used in controlling the element aspect ratios and volume ratios. Choice of number of elements and geometric ratios in each division or line edges was based on the following [19]:

i. To ensure that the far field stresses are close to the exact solution of a plain cylinder, that is for points away from the cross-bore.
ii. To ensure that stress concentration factor reasonably converges while minimizing the frontal width and processing time, that is, for points in the cross-bore area.

4.2.3. Boundary Conditions

Referring to Figure 4-1, the boundary conditions for a plain cylinder were:

i. Nodes in the *y*-*z* plane have no displacement in the *x*-direction.

ii. Nodes in the *x*-*z* plane have no displacement in the *y*-direction.

iii. Nodes in the *x*-*y* plane have no displacement in the *z*-direction.

Referring to Figure 4-2, Figure 4-3, and Figure 4-4, the boundary conditions for a cross-bored cylinder were:

i. Nodes in the *x*-*z* plane have no displacement in the *y*-direction.

ii. Nodes in the *x*-*y* plane have no displacement in the *z*-direction.

4.3. PROGRAM FLOW CHART

Below is the flow chart for the FEM analysis program. The main program module is shown in the appendix.

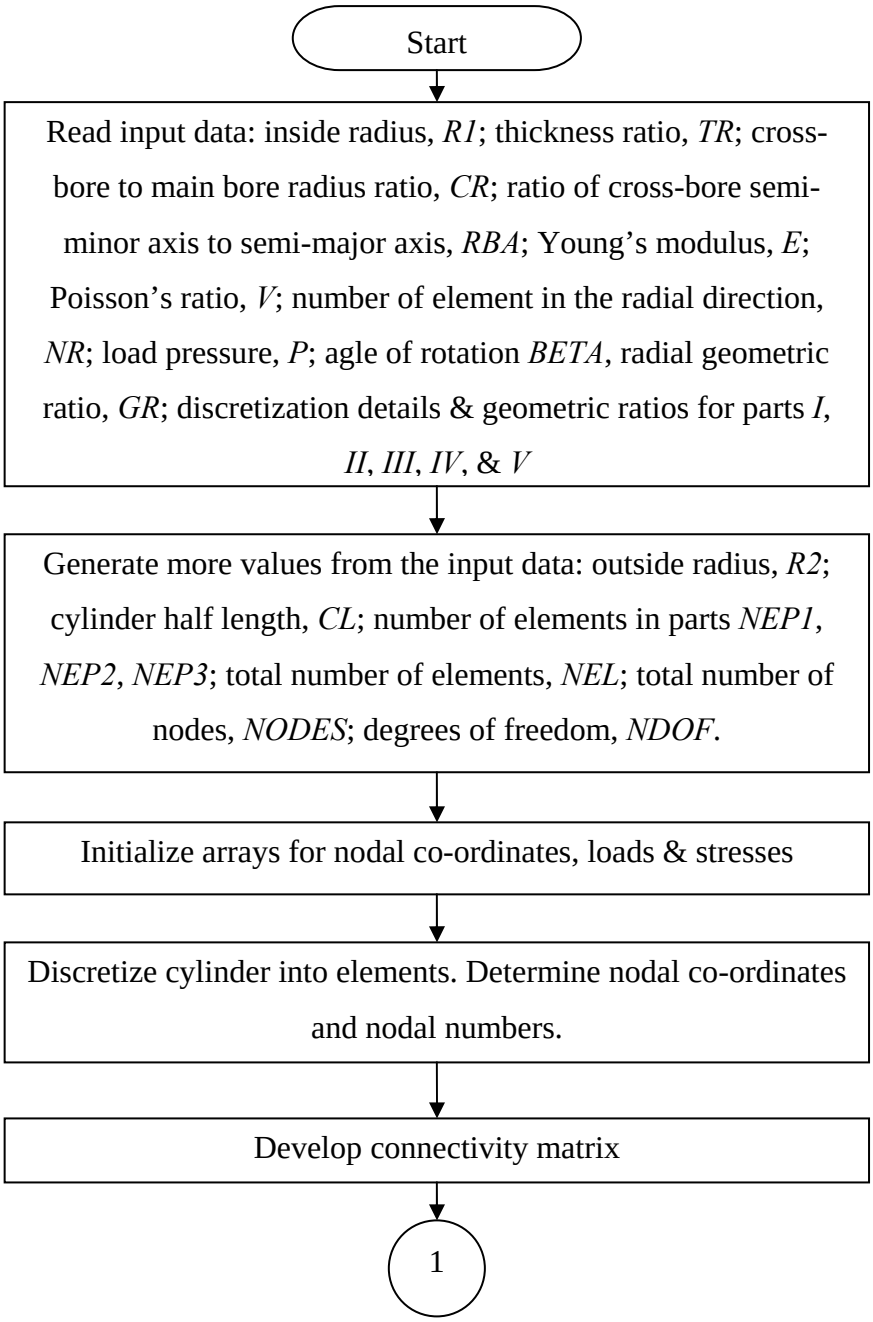

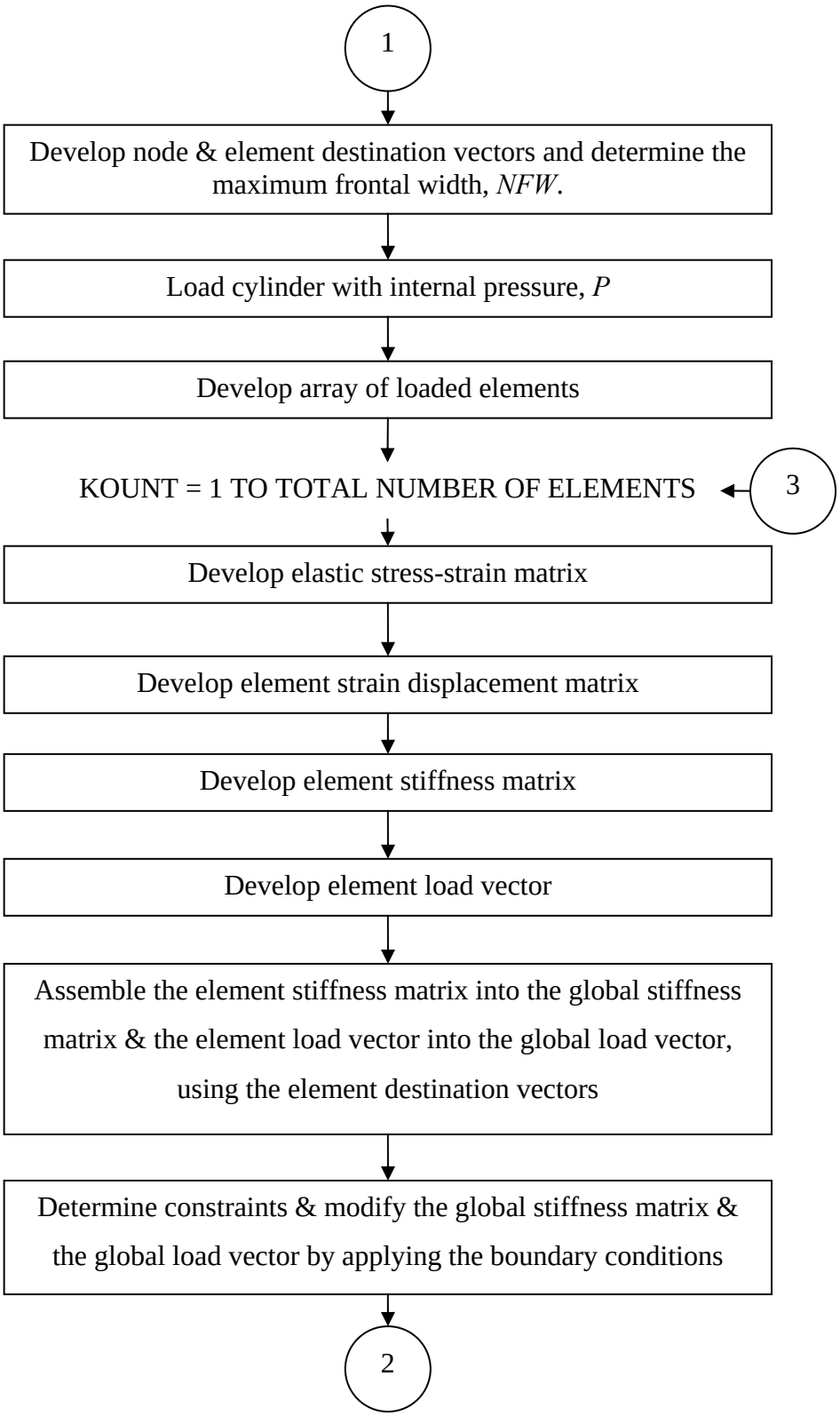
1
Develop node & element destination vectors and determine the maximum frontal width, NFW.
Load cylinder with internal pressure, P
Develop array of loaded elements
KOUNT = 1 TO TOTAL NUMBER OF ELEMENTS
3
Develop elastic stress-strain matrix
Develop element strain displacement matrix
Develop element stiffness matrix
Develop element load vector
Assemble the element stiffness matrix into the global stiffness matrix & the element load vector into the global load vector, using the element destination vectors
Determine constraints & modify the global stiffness matrix & the global load vector by applying the boundary conditions
2

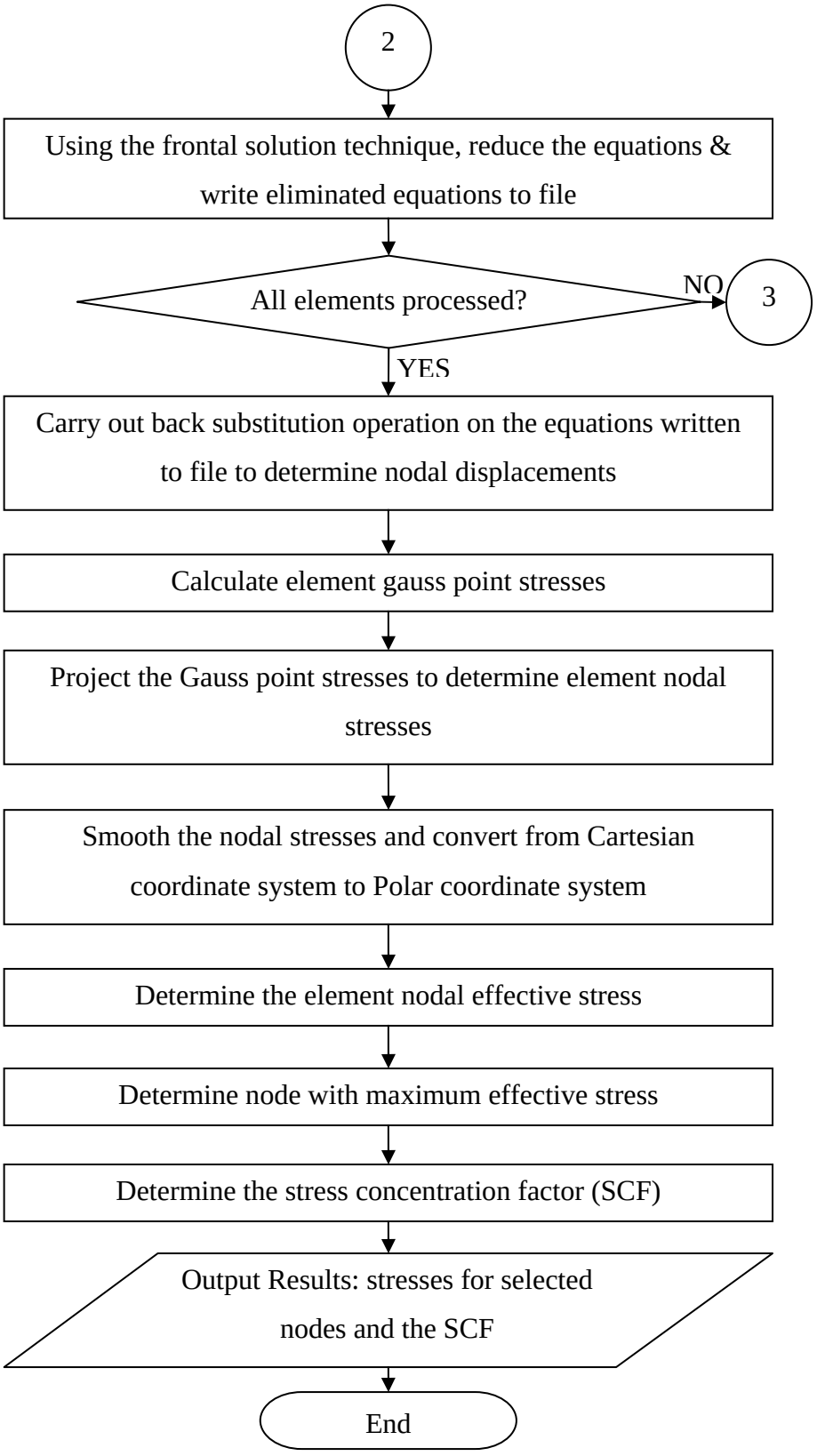
2
Using the frontal solution technique, reduce the equations & write eliminated equations to file
All elements processed?
NO
3
YES
Carry out back substitution operation on the equations written to file to determine nodal displacements
Calculate element gauss point stresses
Project the Gauss point stresses to determine element nodal stresses
Smooth the nodal stresses and convert from Cartesian coordinate system to Polar coordinate system
Determine the element nodal effective stress
Determine node with maximum effective stress
Determine the stress concentration factor (SCF)
Output Results: stresses for selected nodes and the SCF
End

4.4. STEPS OF THE FINITE ELEMENT PROGRAM

The finite element program developed for this research has the following steps.

1. Execute the finite element method computer program. Implemented by PROGRAM MAIN that calls the subroutines.
2. Read the cylinder and cross-bore geometry details, orientation of the elliptical cross-bore, pressure (load), discretization details, and material properties from the stored data.
3. Discretize the cylinder into elements.
4. Develop the global connectivity matrix.
5. Develop the nodal and element destination vectors by processing and modifying the global connectivity matrix. Determine the element in which each node appears last and set the last appearance of the node in the connectivity matrix to a negative number [41]. Determine the maximum frontal width.
6. Use the shape functions to obtain the strain-displacement matrices and the Jacobian of the transformation.
7. Develop the elastic stress-strain matrix for each element.
8. With reference to the Gauss points, generate the elastic stiffness matrix of each element in turn.
9. Using an elastic load, generate the element nodal loads.
10. Using the element and nodal destination vectors assemble the element stiffness matrix and the element load vector on the active global stiffness matrix and active global load vector respectively.

11. Using the modified connectivity matrix, determine when a node ceases to be active. Determine nodes with known displacements e.g. the fixed nodes for which displacement is zero. Apply the boundary conditions on the active global stiffness matrix and active global load vector. Carry out a Gaussian elimination. Store the stiffness matrix and load coefficients associated with the condensed node in a data file.
12. Continue assembly and elimination till the last element.
13. Do Gaussian back substitution using the stored stiffness matrix and load coefficients to get displacements at the nodes.
14. Calculate the Gauss point stresses, then calculate and store the effective stress for each element.
15. Transform the stresses from Cartesian coordinate system to Cylindrical coordinate system using the laws of stress transformation [42] to get hoop, radial and axial stresses.
16. Carry out smoothing and projection to obtain global nodal stresses.
17. Determine the maximum effective stress and calculate the stress concentration factor with respect to far field stresses in the cylinder.

4.5. ORDER OF NUMERICAL INTEGRATION

Having selected a numerical integration scheme, the order of numerical integration to be used in the evaluation of various finite element integrals needs to be determined. The choice of the order of numerical integration is important in practice because,

first, the cost of analysis increases when a higher order integration is employed, and second, using a different integration order, the results can be affected by a very large amount [25].

In general, the appropriate integration order depends on the matrix that is evaluated and the specific finite element being considered. If a high enough order is used, all matrices will be evaluated accurately. Using too low an order of integration, will lead to inaccurate evaluation of the matrices, and the problem solution may not be possible. For the eight noded elements, displacements vary linearly in the ξ, η, and ρ directions. Hence two point integration is sufficient in each direction. Thus 2 x 2 x 2 Gauss integration is required to evaluate the exact stiffness matrix for the eight noded element [25].

4.6. FRONTAL SOLUTION METHOD

Instead of assembling the complete structure stiffness matrix, the equations are assembled and reduced at the same time [25]. Only those equations that are actually required for the elimination of a specific degree of freedom are assembled, the degree of freedom considered is statically condensed out. The complete procedure consists of statically condensing out one degree of freedom after the other and always assembling only those element stiffness matrices that are actually required during the specific condensation to be performed. The finite elements that must be considered for the static condensation of the equations corresponding to one specific node define

the wave front at that time. Since the equations are assembled in the order of the elements, the length of the wave front and therefore the half-bandwidth dealt with are determined by element numbering.

Frontal solution for finite elements is far more efficient than a band solution, and also more convenient to use than a band solver. It is evolved from a full Gaussian reduction, with the whole triangle of structural stiffness in the solution area. It operates only on those columns containing non-zero coefficients. The reducing equation written to file store decreases from an equation of a length equal to the maximum front width, to a variable equation containing only those coefficients between the first and last non-zero coefficients [43].

The frontal technique uses less storage and arithmetic than the best Gaussian band algorithm. Nevertheless, the band algorithm can be simpler and more straightforward. The frontal technique discards the active variables in an order different from that which it picks them up. Elements are presented in a certain order, which is critical – just as node numbering is critical in a band algorithm – although the best order is not always unique[44].

The operations of a front solver can be split into three logical parts [41]:

i. Prefront;
ii. Reduction and pre-constraints;
iii. Back-substitution and post-constraints.

The pre-constraints and post-constraints impose specified displacements on the nodal variable. Prefront determines the nodal destination vector and the maximum front width. The nodal destination vector contains the locations allocated to each node. It is from this vector that the element destination vectors are determined [41].

4.7. NODAL STRESS EXTRAPOLATION AND SMOOTHING

In a number of programs the stresses are determined at the nodes, since the nodal positions are readily located and it is convenient to output the displacements and stresses at the same points. A better alternative is to calculate the stresses at Gauss points, in which it will be found that because of superior accuracy no averaging is necessary. A least square smoothing technique is used to yield surface function from which accurate nodal stresses are obtained [41].

In finite element analysis involving numerically integrated elements, integration points are known to be the best sampling points. However, in problems involving determination or estimation of stresses and high stress gradients at the boundary or a bi-material interface of a structure, nodes are the most useful output locations for stresses. Since nodes happen to be the worst sampling points, the analyst often goes with the value at the closest Gaussian integration point [45].

Discrete stress data obtained from finite element Gauss points can be smoothed and extrapolated to the boundaries of the domain using conventional least-square

smoothing. In this conventional procedure, a smooth polynomial surface is derived from the discrete data distribution. In a problem with stress concentration evaluation using Moir'e fringe analysis, Hinton and Irons indicated that such polynomials tend to behave erratically near the boundaries of the region and thus pose a special disadvantage since poor results were obtained at the boundaries where they were often needed [45].

Alternatively in finite element solutions, stress in individual element can be obtained at the Gauss points and then extrapolated to the element periphery, that is, at the nodes according to the shape function of the element. Such an extrapolation technique in least-square local smoothing of discrete Gauss point stress was introduced by Hinton and Campell. The nodal stresses obtained by linear least-square extrapolation were then averaged to obtain local smoothing of the stress distribution [45]. By using the least squares fit, the following expression has been obtained to get smoothed nodal stresses [39]:

$$\begin{Bmatrix} \tilde{\sigma}_1 \\ \tilde{\sigma}_2 \\ \tilde{\sigma}_3 \\ \tilde{\sigma}_4 \\ \tilde{\sigma}_5 \\ \tilde{\sigma}_6 \\ \tilde{\sigma}_7 \\ \tilde{\sigma}_8 \end{Bmatrix} = \begin{bmatrix} e & f & g & f & f & g & h & g \\ f & e & f & g & g & f & g & h \\ g & f & e & f & h & g & f & g \\ f & g & f & e & g & h & g & f \\ f & g & h & g & e & f & g & f \\ g & f & g & h & f & e & f & g \\ h & g & f & g & g & f & e & f \\ g & h & g & f & f & g & f & e \end{bmatrix} \begin{Bmatrix} \sigma_I \\ \sigma_{II} \\ \sigma_{III} \\ \sigma_{IV} \\ \sigma_V \\ \sigma_{VI} \\ \sigma_{VII} \\ \sigma_{VIII} \end{Bmatrix} \tag{4.1}$$

where $\tilde{\sigma}_1$ - $\tilde{\sigma}_8$ are the smoothed nodal values, σ_I - σ_{VIII} are the Gauss points stresses, and the coefficients *e, f, g* and *h* are given by the following equations:

$$e = \frac{5+3\sqrt{3}}{4}, \qquad f = -\frac{\left(\sqrt{3}+1\right)}{4}, \qquad g = \frac{\sqrt{3}-1}{4} \quad \text{and} \quad h = \frac{5-3\sqrt{3}}{4} \tag{4.2}$$

The smoothed stress resultants are then modified by finding the average of the nodal stress resultant of all elements meeting at a common node [36].

CHAPTER 5

RESULTS AND DISCUSSION

5.1. INTRODUCTION

The numerical and analytical results for displacement and stresses are presented and discussed in this chapter. The stress concentration factors are also presented. An arbitrary load pressure of 50 MPa was used in all cases. This was to ensure elastic loading only. The stress profiles are presented in an easy read non-dimensional form of $\frac{\sigma}{\sigma_y}$, where σ is the stress and σ_y is the material yield stress.

The results of a plain cylinder, that is, a cylinder without a cross-bore, are presented as proof of the validity, accuracy and, therefore, reliability of the elastic finite element method analysis used for this research.

Cylinders of thickness ratios 2.0, 2.25 and 2.5 were considered. A radial plain elliptical cross-bore was considered. The cross-bore was initially circular. Its dimensions were then varied to form an elliptical cross-bore of the same cross-sectional area. In this work, the cross-bore to cylinder bore radius ratio refers to that of the circular cross-bore. The circular cross-bore to cylinder bore radius ratios 0.15, 0.20, and 0.25 were considered. For stress profiles presented in this chapter, a

cylinder of thickness ratio of 2.0 and a cross-bore to cylinder bore radius ratio of 0.15 were considered. The other thickness ratios and cross-bore to cylinder bore radius ratios were considered for stress concentration factors. The stress profiles obtained for cross-bores with a cross-bore to cylinder bore radius ratio of 0.20 and 0.25 were very similar to those discussed for a cross-bore to cylinder bore radius ratio of 0.15. The stress profiles were very similar with very small variations.

Initially, the elliptical cross-bore major axis was parallel to the cylinder axis, that is, it lied in the meridional cross-section shown in Figure 4-3, whereas the cross-bore minor axis was in the transverse cross-section shown in Figure 4-4. The direction of rotation of the elliptical cross-bore was anticlockwise. The angle of rotation was measured anticlockwise from the cylinder axis. Stress profiles can be generated for any angle of rotation between 0° to 90°.

In the course of this research, several challenges we encountered. The main one was discretization for a cylinder with an elliptical cross-bore whose orientation was variable. Initially quarter of a cylinder was used but the variable orientation of the cross-bore could not be attained as new nodal points needed to be introduced with every new position of the cross-bore. This was overcome by use of half of the cylinder. Consequently, this resulted in very many nodes (and elements) and hence wider frontal width which required more computer memory space to run. Using the frontal solution technique reduced the memory requirements greatly. Due to the

relatively long run times and the need to study several cases, the program was run on several computers to save on time.

5.2. PLAIN CYLINDER

The results obtained for a plain cylinder with a thickness ratio of k = 2.0 are discussed in this section. A quarter of the cylinder as shown in Figure 4-1 was used for this analysis.

5.2.1. Displacements

Figure 5-1 and Figure 5-2 compare the radial displacements obtained by the finite element method to those obtained analytically along edges AB and CD respectively, for the plain cylinder shown in Figure 4-1.

It can be seen that the numerical displacements obtained by the finite element method are very close to the analytical values. The maximum error in determining the displacements was -0.40 %. The average error for all the points studied across the cylinder wall was -0.39 %. This therefore shows the reliability of the FEM program developed.

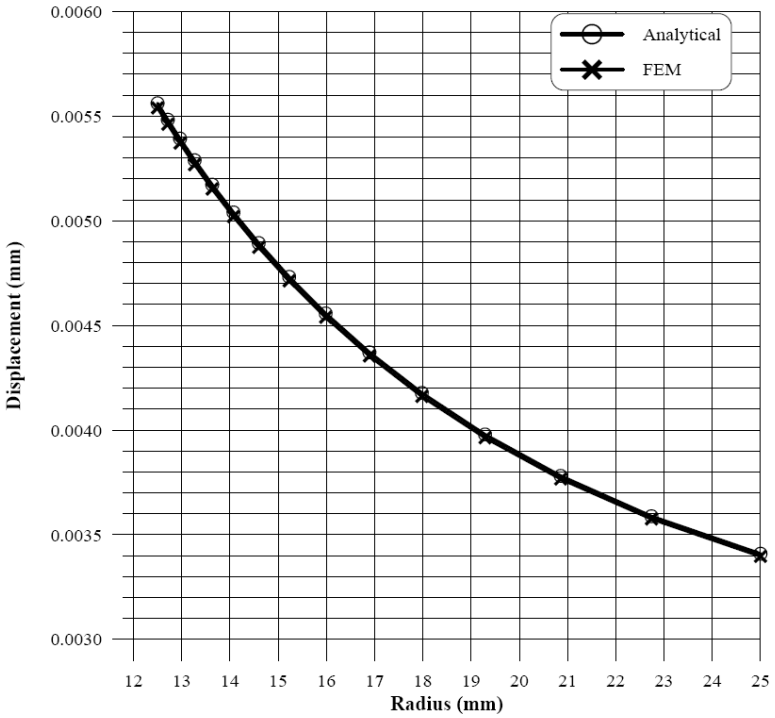

Figure 5-1 Radial displacement along edge AB

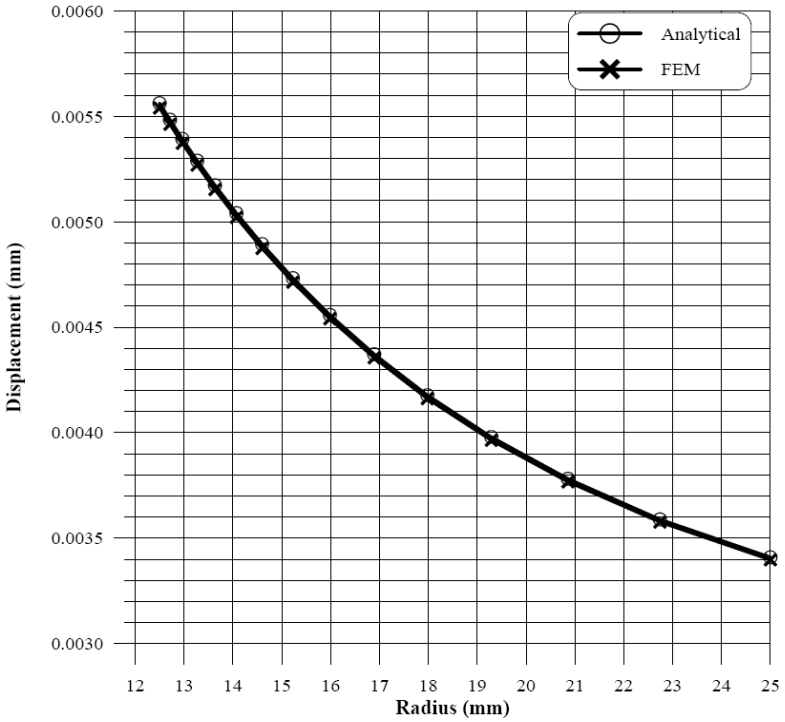

Figure 5-2 Radial displacement along edge CD

5.2.2. Stresses

Figure 5-3 shows the non-dimensional elastic stress distribution across a plain cylinder wall. It compares the elastic stresses obtained by both the analytical and the finite element method for hoop stress, radial stress and axial stress. The stress profiles obtained from the finite element program agreed very well with the analytical stress profiles.

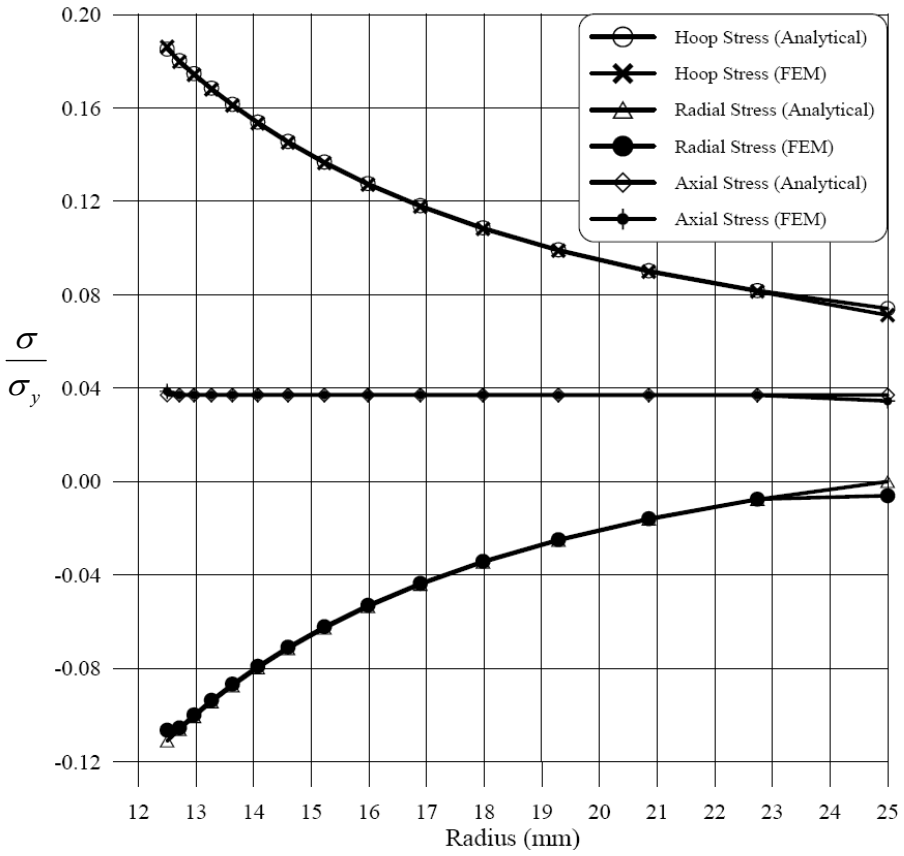

Figure 5-3 Stress distribution through a plain cylinder wall

Nodes inside the material gave very accurate stress values. They were very close to the analytical values. Maximum stress errors were experienced at the cylinder's outside surfaces. These can be accommodated as the critical points are at the cylinder bore. Hoop stress error at the inside surface was 0.53 %. Hoop stress error at the outside surface was 3.87 %. For nodes inside the material, the hoop stress errors varied between 0.31 % and 0.48 %. Radial stress error at the inside surface was 4.17 %. At the outside surface the radial stress varied slightly from the theoretical zero value. For nodes inside the material, the radial stress errors varied from 0.74 % to 2.02 %. Axial stress error at the inside surface was 4.32 %. Axial stress error at the outside surface was 6.96 %. For nodes inside the material, the axial stress errors varied from 0.03 % to 0.18 %. The finite element method showed very high accuracy for nodes inside the material. Therefore, the results of the FEM are admissible.

The discrepancy between the finite element results and the analytical values of stress at the outside and inside surfaces of the cylinder can be attributed to the system of stress projection and averaging [19]. The average stresses of the inner and outer elements are not averaged since they have neighbours in only one direction.

From these results obtained for displacements and stresses, it can be concluded that the finite element method program can be depended upon for accurate results. It can also be projected that if the finite element program is further developed and modified

to include a radial circular and elliptical cross bore, the results that are obtained are reliable and acceptable.

5.3. FAR FIELD STRESSES FOR CYLINDER WITH CROSS BORE

For a cylinder with a cross-bore, a half cylinder as shown in Figure 4-2 was considered. Half cylinder was chosen so as to cater for the rotation of the elliptical cross-bore. A thick walled cylinder with a thickness ratio of k = 2.0 and a circular cross-bore of cross-bore to cylinder bore ratio of d = 0.15 was considered.

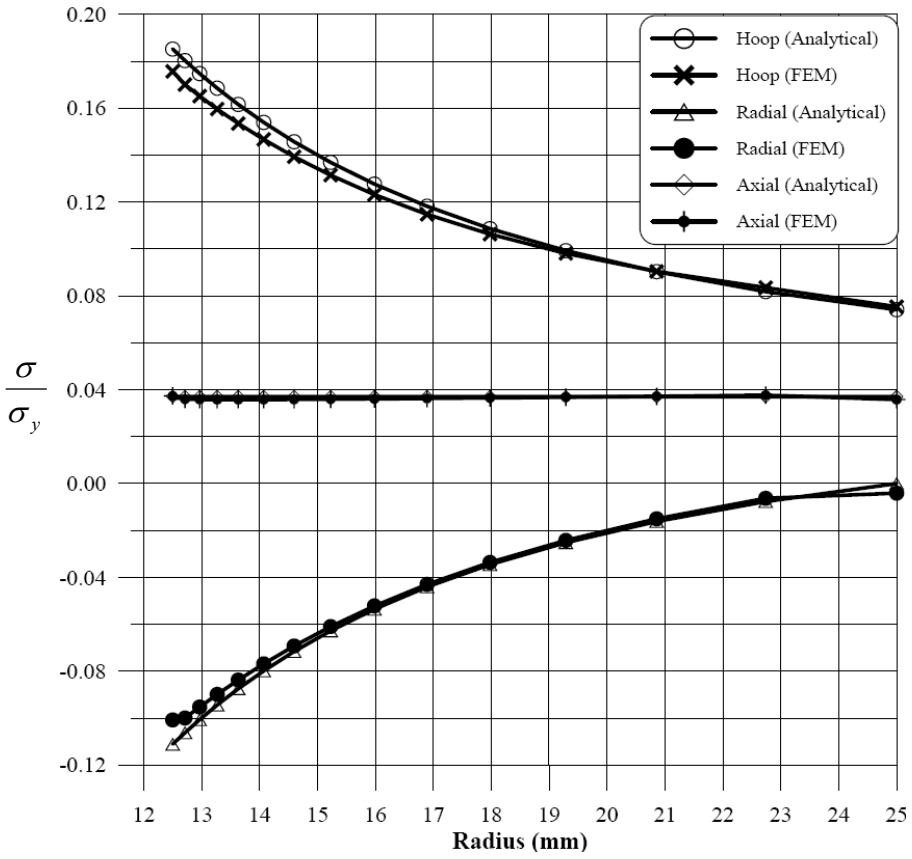

Figure 5-4 Far field stresses along edge AD or CF

The far field non-dimensional elastic stresses along edges AD or CF are shown in Figure 5-4. The non-dimensional elastic stresses along BE are shown in Figure 5-5.

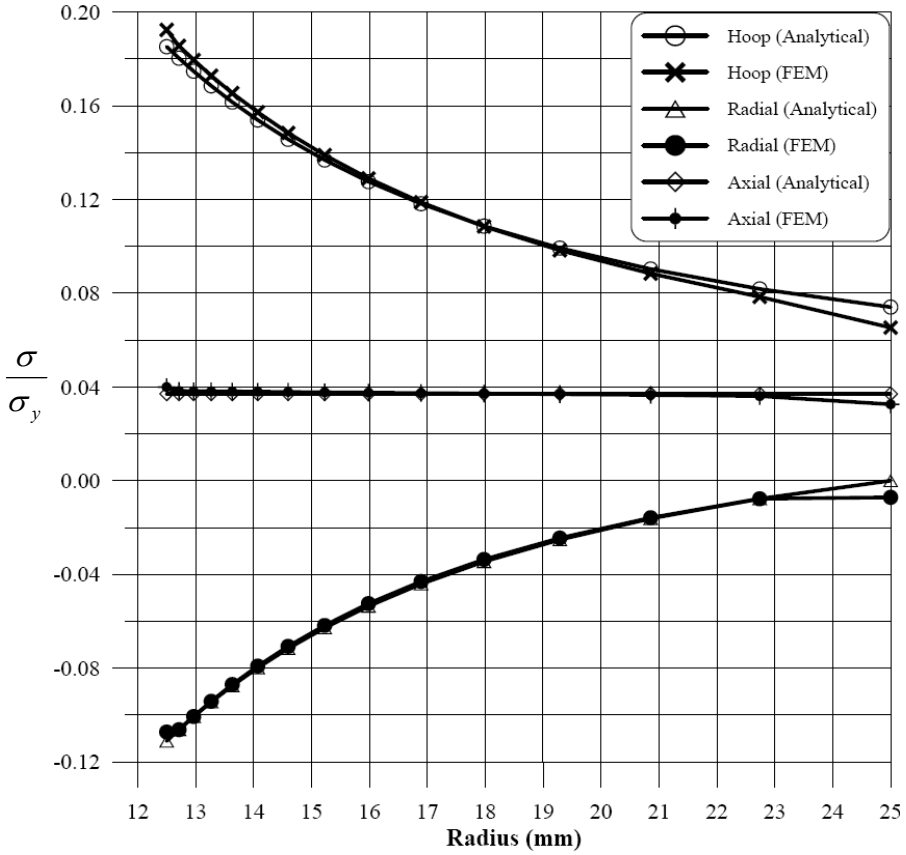

Figure 5-5 Far field stresses along edge BE

The stresses are compared to the analytical stresses. At the cylinder bore hoop stress error varied between 3.22 % and 4.58 %, radial stress error varied between 3.63 % and 9.22 % and axial stress error varied between 0.93 % and 8.24 %. For nodes inside the material, the hoop, radial and axial stresses were much closer to the analytical values. The stress profiles along BE were more accurate than those obtained along edges AD and CF. This was because the stresses along AD and CF

were affected by the boundary edge effects. The stress profiles obtained were admissible.

Following the discussion above, it can be seen that, using half a cylinder and further dividing the cylinder into five parts made the finite element method for this case more complex than that of a plain cylinder. This case therefore resulted in more memory requirements than the plain cylinder case. Comparing with the case of a plain cylinder, where quarter cylinder was used, the half cylinder also resulted in larger but acceptable errors as discussed above.

5.4. CIRCULAR CROSS-BORE

In this section, the elastic stresses arising due to the presence of a radial circular cross-bore are considered. A half cylinder was considered as shown in. Figure 4-2. A cylinder with thickness ratio k = 2.0 and a circular cross-bore of cross-bore to cylinder bore ratio of d = 0.15 was considered.

5.4.1. Meridional Stresses

The stresses discussed here are the elastic stresses along the meridional section shown in Figure 4-3 along the surface BNK or QPL. Figure 5-6 shows the non dimensional elastic meridional stresses for a cylinder with a circular cross-bore.

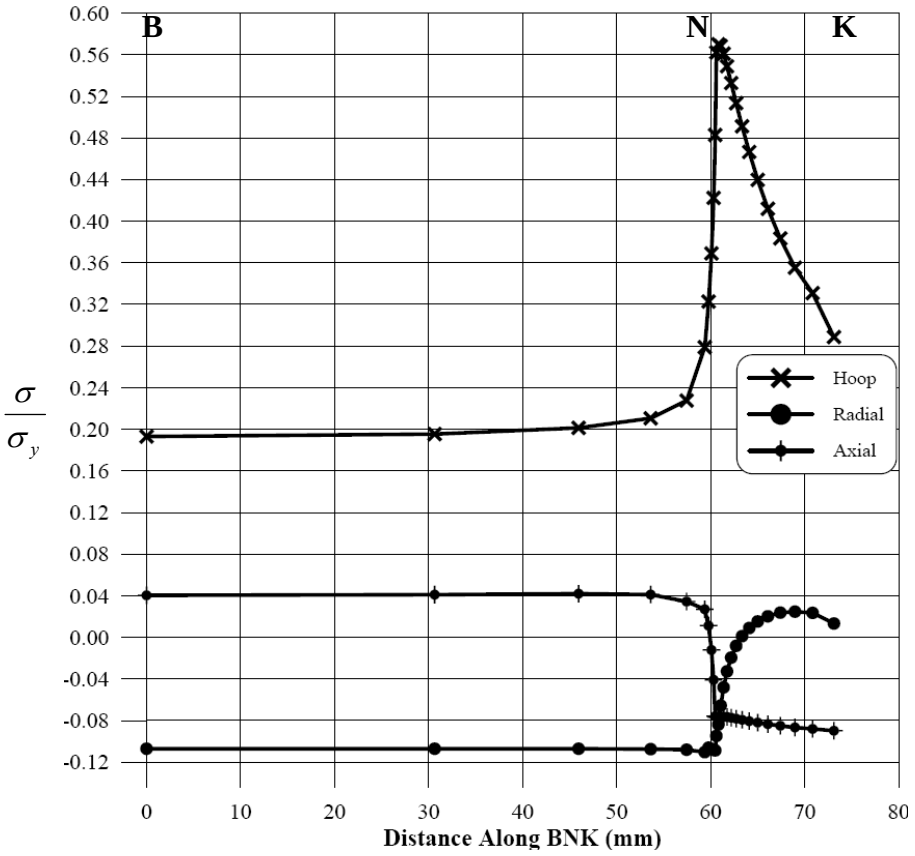

Figure 5-6 Meridional stresses – circular cross-bore

Hoop stress was about 87 MPa at point B and was constant along the cylinder bore. In the vicinity of the cross-bore, the hoop stress increased sharply to about 253 MPa at point N. Along the vertical line NK it immediately increased to about 257 MPa. The maximum hoop stress does not occur at the crotch corner. The hoop stress then drop to about 130 MPa at point K on the cylinder surface.

Axial stress was about 18 MPa at point B and remained constant along the cylinder bore. In the vicinity of the cross-bore the axial stress suddenly dropped to about -35 MPa at point N. Along the vertical line NK it then dropped to -40 MPa at point K.

Radial stress was about -48 MPa at point B. It remained constant along the cylinder bore. Along the vertical line NK it increased sharply and then quickly leveled off to a value of 10 MPa and then dropped slightly to 6 MPa.

These profiles were expected. They can be explained by considering the cross-bore and the cylinder bore as two interacting cylinders, each with its coordinate system and loaded by the same internal pressure. Take the cross-bore as a hole in an irregular block.

Approaching the cross-bore, the hoop stress increased tremendously. This occurred because in the meridional plane, the hoop stresses due to the two cylinders superimpose positively. They add up. From N to K the magnitude of the hoop stress reduces since the hoop stress due to the cylinder bore loading reduces.

Approaching the cross-bore the radial stress reduces sharply and then reduces very slowly. The interaction of the cylinder axial stress and the cross-bore radial stress in the meridional plane is negative. The magnitude of the tensile axial stress is reduced by the compressive radial stress arising due to the loading of the cross-bore.

Along NK the radial stresses due to the loading of the cylinder bore are experienced. There is no interaction with any other stresses arising from the loading of the cross-bore. Therefore the profile obtained is that for radial stress in an internally loaded cylinder.

5.4.2. Transverse Stresses

The stresses discussed here are the elastic stresses along the transverse section shown in Figure 4-4 along the surface RSH or UTI. Figure 5-7 shows the non-dimensional elastic transverse stresses for circular cross-bore with a cross-bore to cylinder bore radius ratio of 0.15.

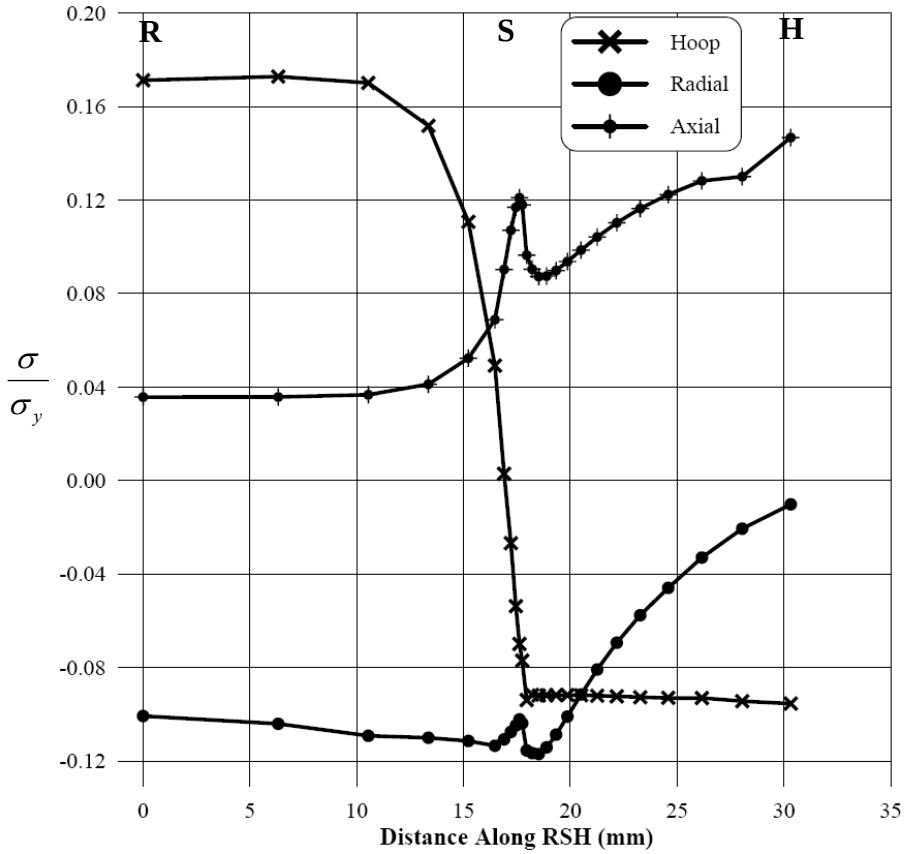

Figure 5-7 Transverse stresses – circular cross-bore

Hoop stress was about 77 MPa at point R. Approaching the cross-bore it dropped quickly to a value of about -34 MPa at point S. Along the vertical line SH it dropped

further to about -41 MPa, remained constant for several points and then dropped very slightly to about -43 MPa at point H.

Axial stress was about 16 MPa at point R. It remained constant along cylinder bore. In the vicinity of the cross bore it increased to about 54 MPa at point S. Along vertical line SH it dropped slightly to 39 MPa and then increased gradually to 66 MPa at point H.

Radial stress was about -45 MPa at point *R*. It dropped slightly to -50 MPa in the vicinity of the cross-bore. At point *S* it increased to about -46 MPa. Up the cross-bore it immediately dropped further to about -52 MPa before starting to rise gradually up to about -5 MPa at the cross-bore cylinder outside surface intersection.

These stress profiles are explained by considering the cross-bore and the cylinder bore as two interacting cylinders, each with its coordinate system and loaded by the same internal pressure. Take the cross-bore as a hole in an irregular block.

Approaching the cross-bore the hoop stress dropped sharply from tensile to compressive. This is due to its interaction with the compressive radial stresses arising from the loading of the cross-bore. The compressive radial stresses counter the tensile hoop stresses arising from the cylinder bore loading.

Axial stress increased when approaching the cross-bore. At the cross-bore these stresses interact with the hoop stresses arising from the cross-bore loading. Since both stresses are tensile, they positively add up.

Radial stress does not interact directly with the other stresses arising due to the cross-bore loading. Therefore it takes the same profile of the radial stresses in an internally loaded cylinder.

5.4.3. Cross-Bore-Main Bore Intersection Stresses

The stresses discussed here are the stresses at the intersection of the circular cross-bore and the cylinder bore. Figure 5-8 shows the non-dimensional elastic stress profiles for a cross-bore to cylinder bore radius ratio of 0.15.

The cross-bore had tensile hoop stress of about 253 MPa at points *N* and *P*. Points *S* and *T* had a compressive hoop stress of about -35 MPa. Moving from *N* to *S* or *P* to *T*, the hoop stress dropped quickly from 253 MPa to -35 MPa. Moving from *S* to *P* or *T* to *N*, the hoop stress increased quickly from -35 MPa to 253 MPa.

Points *N* and *P* had a compressive axial stress of a value of about -35 MPa. Points *S* and *T* had a tensile axial stress of about 53 MPa. Moving from *N* to *S* or *P* to *T*, the axial stress increased from -35 MPa to 55 MPa and then dropped to 53 MPa. Moving

from *S* to *P* or *T* to *N*, the axial stress increased from 53 MPa to 55 MPa and then fell to -35 MPa.

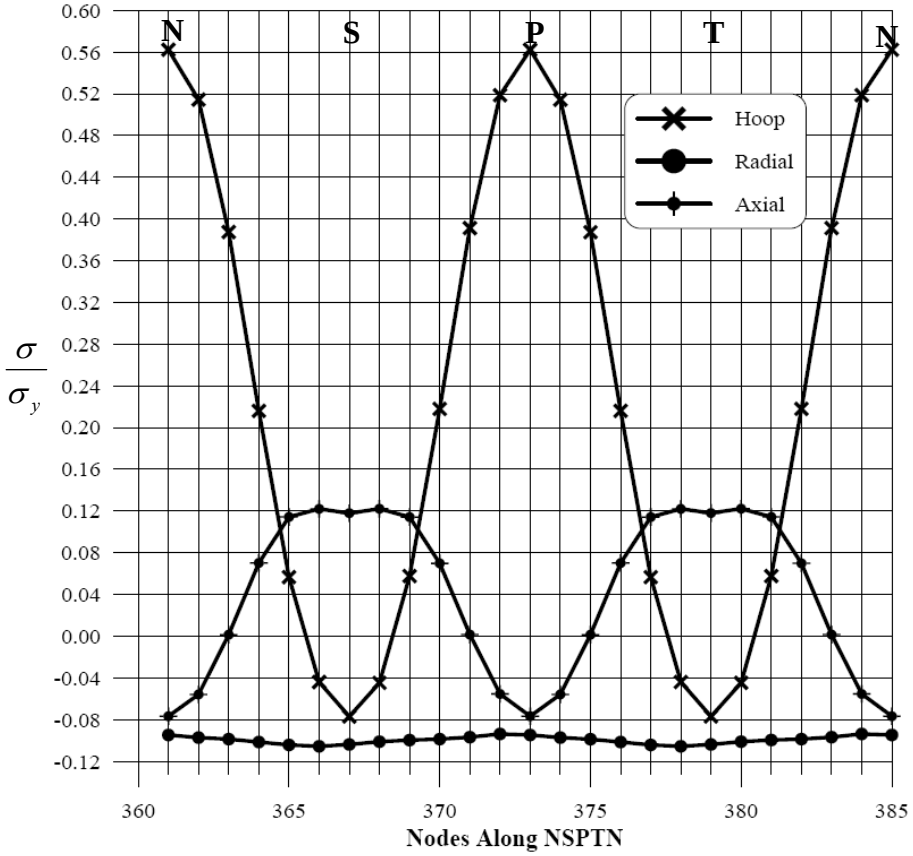

Figure 5-8 Cross-bore-main bore intersection stresses – circular cross-bore

Radial stress varied marginally. Moving from *N* to *S* to *P* and back to *N* it formed a smooth curve with very small deflections. At points *N* and *P* the radial stress was -42 MPa. At points *S* and *T*, the radial stress was -47 MPa.

The hoop stress was highest at the crotch corner, points *N* and *P* and lowest at points *S* and *T*. At points *N* and *P* the tensile hoop stresses due to cylinder loading and

cross-bore loading add up. At points *S* and *T* the tensile hoop stress is countered by the compressive radial stresses arising from cross-bore loading. Therefore the hoop stress reduces from a maximum to a minimum.

Axial stress was highest near points *S* and *T* and lowest at points *N* and *P*. At points *N* and *P* the tensile axial stress is countered by the compressive radial stress arising from the cross-bore loading. At points *S* and *T* the cylinder axial stress add up with hoop stress arising from the cross-bore loading.

Radial stresses had very little interactions with the stresses arising from the cross-bore loading. It therefore had very little variations.

5.4.4. Cross-Bore Mid-Way Stresses

The stresses discussed here are the stresses midway along a circular cross-bore. Figure 5-9 shows the non-dimensional elastic stress midway along the cross-bore for a cross-bore to cylinder bore radius ratio of $d = 0.15$.

Points N and P had tensile hoop stress of about 221 MPa. Points S and T had a compressive hoop stress of about -41 MPa. Moving from N to S or P to T, the hoop stress dropped quickly from 221 MPa to -41 MPa. Moving from S to P or T to N, the hoop stress increased quickly from -41 MPa to 221 MPa.

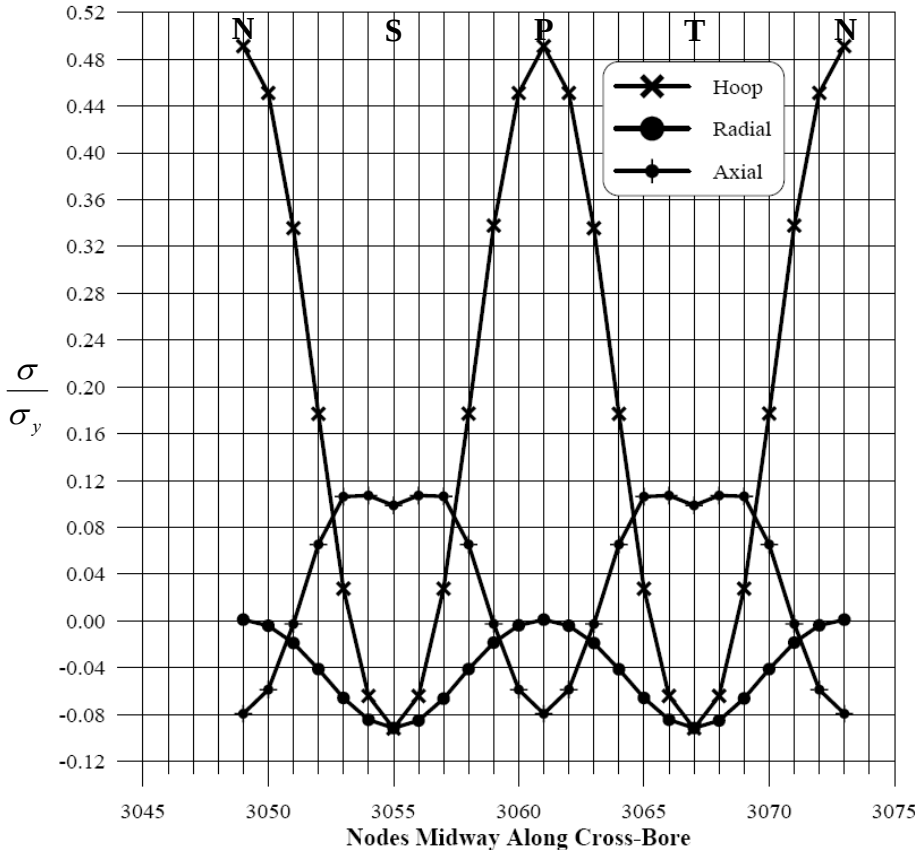

Figure 5-9 Cross-bore midway stresses – circular cross-bore

Points N and P had a compressive axial stress of a value of about -36 MPa. Points S and T had a tensile axial stress of about 44 MPa. Moving from N to S or P to T, the axial stress increased from -36 MPa and leveled off to 48 MPa. At points S and T, it dropped slightly to about 44 MPa. Moving from S to P or T to N, the axial stress increased slightly to 48 MPa and then falls to -36 MPa.

Points N and P had almost no radial stress. Points S and T had a compressive radial stress of about -41 MPa. Moving from N to S or P to T, the radial stress varied

smoothly from 0 MPa to -41 MPa. Moving from S to P or T to N, the radial stress increased smoothly from -41 MPa to 0 MPa. It forms a smooth curve.

Comparing these stresses with those at the cross-bore cylinder bore intersection in section 5.4.3, it is seen that the hoop stress has reduced. Moving up the cross-bore the hoop stress reduced as discussed in sections 5.4.1 and 5.4.2. The maximum axial stress reduced slightly. The maximum axial stress occurred at points S and T in the transverse section. From section 5.4.2 it can be seen that moving up the cross-bore, the radial stress reduced for several points before it started increasing again. The magnitude of the radial stresses at points N and P in the meridional plane reduced from their compressive values to zero. Algebraically it increased from the negative values to zero as discussed in section 5.4.1.

5.4.5. Cross-Bore Cylinder-Outside Surface Intersection Stresses

The stresses discussed here are the stresses at the intersection of the circular cross-bore and the cylinder outside surface. Figure 5-10 shows the non-dimensional elastic stresses at the intersection of the cross-bore and the cylinder outside surface for a cross-bore to cylinder bore radius ratio of $d = 0.15$.

Points K and L had tensile hoop stress of about 130 MPa. Points H and I had a compressive hoop stress of about -43 MPa. Moving from K to H or L to I, the hoop

stress dropped quickly from 130 MPa to -43 MPa. Moving from H to L or I to K, the hoop stress increased quickly from -43 MPa to 130 MPa.

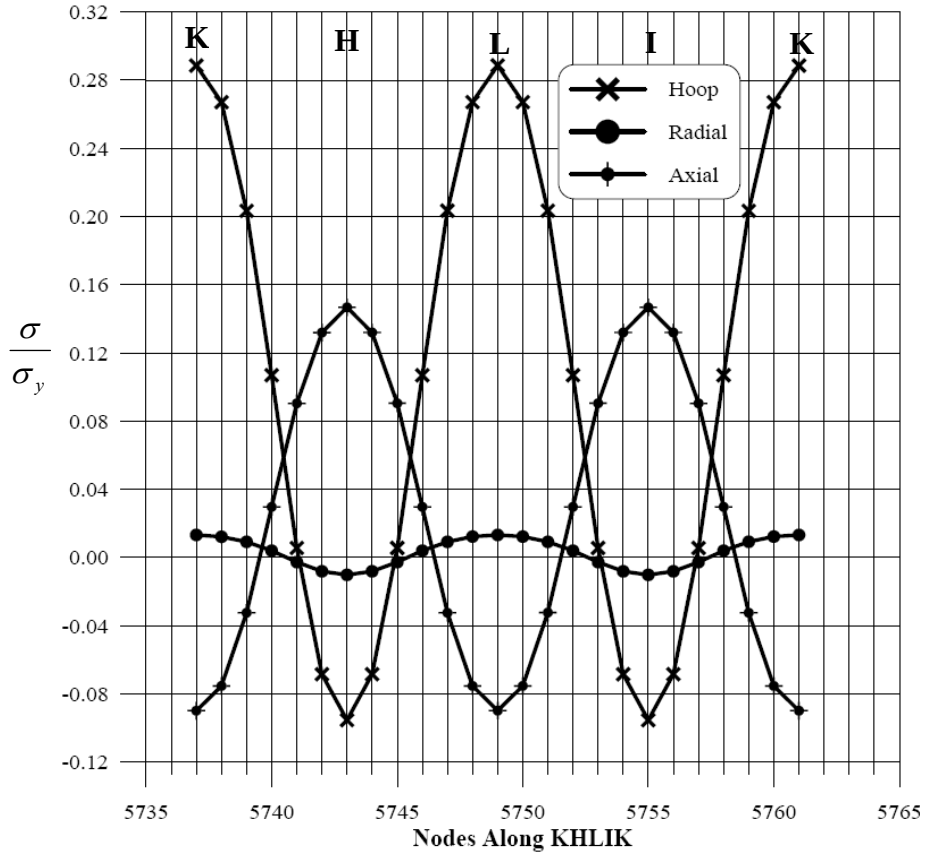

Figure 5-10 Cross-bore cylinder surface intersection stresses – circular cross-bore

Points K and L had a compressive axial stress of a value of about -40 MPa. Points H and I had a tensile axial stress of about 66 MPa. Moving from K to H or L to I, the axial stress increased from -40 MPa to 66 MPa. Moving from H to L or I to K, the axial stress decreases from 66 MPa to -40 MPa.

Points K and L had a tensile radial stress of about 6 MPa. Points H and I had radial stress of about -5 MPa. Moving from K to H or L to I, the radial stress varied smoothly from 6 MPa to -5 MPa. Moving from H to L or I to K, the radial stress increased smoothly from -5 MPa to 6 MPa.

Comparing these stresses with those obtained midway along the cross bore as discussed in section 5.4.4, the hoop stresses have reduced significantly. Moving towards the cylinder outside surface the hoop stress reduces to a minimum. The axial stresses have increased slightly. As discussed in section 5.4.2, the axial stress increased to their maximum in the transverse section at the intersection of the cross-bore and the cylinder outside surface. The radial stresses have increased and formed a smooth curve oscillating about the zero value. As discussed in sections 5.4.1 and 5.4.2 the radial stresses increase to their maximum at the intersection of the cross-bore and the cylinder outside surface.

5.5. ELLIPTICAL CROSS-BORE PARALLEL TO CYLINDER AXIS

In this section, a radial elliptical cross-bore with its major axis oriented parallel to the cylinder axis was considered. Cylinder of thickness ratio $k = 2.0$ was considered. An elliptical cross-bore of cross-sectional area same as a circular cross-bore of cross-bore to cylinder bore radius ratio of $d = 0.15$ were considered to ensure same material weight removal. For the elliptical cross-bore, the ratio of the minor axis to the major axis of $b/a = 0.5$ was considered.

5.5.1. Meridional Stresses

The stresses elastic along the meridional section shown in. Figure 4-3 along the surface BNK or QPL are discussed in this section. Figure 5-11 shows the meridional stresses for an elliptical cross-bore of cross-sectional area same as a circular cross-bore of cross-bore to cylinder bore ratio of d = 0.15. The cross-bore major axis is parallel to the cylinder axis.

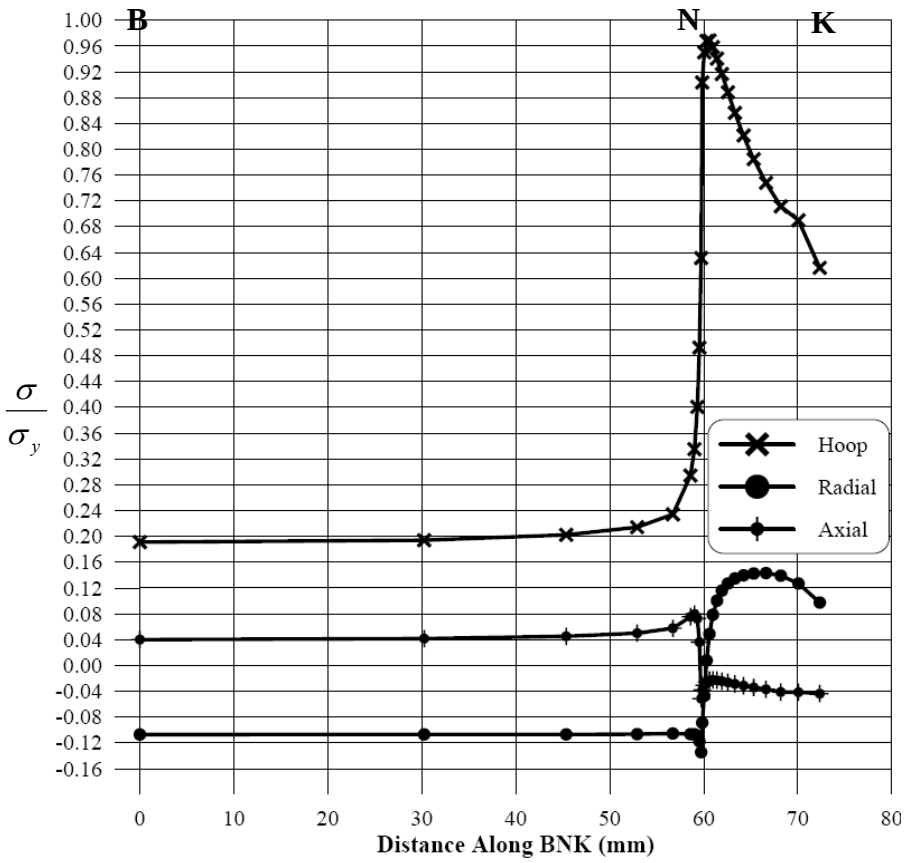

Figure 5-11 Meridional stresses – parallel elliptical cross-bore

Hoop stress was about 86 MPa at point B. It remained constant along the cylinder bore towards N. In the vicinity of the cross-bore, hoop stress increased sharply to 407 MPa at point N. Moving up the cross-bore the hoop stress continued to increase to a value of 436 MPa. The hoop stress then dropped to about 277 MPa at point K on the cylinder surface.

Axial stress was about at 18 MPa at point B and remained constant along the cylinder bore. Approaching the cross-bore it increased to about 36 MPa and than suddenly dropped to -23 MPa at point N. Along the vertical line NK, the axial stress then increased slightly to about -10 MPa and then dropped gradually to about -20 MPa at the intersection of the cross-bore and cylinder outside surface.

Radial stress was about -48 MPa at B and remained a constant along the cylinder bore. Approaching the intersection of the cross-bore and the cylinder bore it dropped sharply to -60 MPa and increased sharply before it smoothly curved off to a value of 64 MPa and then dropped 44 MPa.

Comparing these stresses to those of the circular cross-bore of same area discussed in section 5.4.1 the maximum hoop stress increased by 70 %. The hoop stress at the intersection of cross-bore and cylinder outside surface increased by 113 %. The maximum axial stress (compressive) reduced by half. The maximum radial stress increased by 540 %.

5.5.2. Transverse Stresses

The stresses discussed here are the elastic stresses along the transverse section shown in Figure 4-4 along the surface RSH. Figure 5-12 show the transverse non-dimensional stresses for an elliptical cross-bore of cross-sectional area same as a circular cross-bore of cross-bore ratio of d = 0.15. The cross-bore major axis is parallel to the cylinder axis.

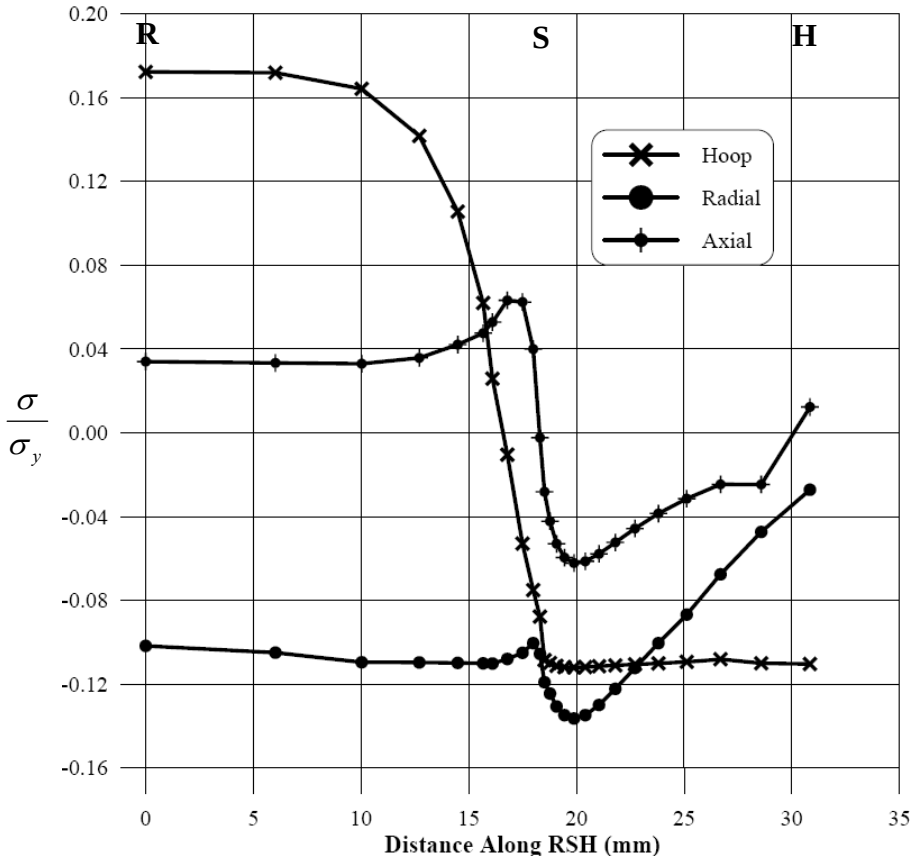

Figure 5-12 Transverse stresses – parallel elliptical cross-bore

Hoop stress was about 78 MPa at point R. Along the cylinder bore it remained constant. Approaching point S it starts falling down to a value of about -40 MPa at point S. Along the vertical line SH, it immediately falls to -49 MPa and continue to fall further to -50 MPa and then remained constant throughout the cross bore length.

Axial stress was about 15 MPa at point R. It then remained constant along the cylinder bore. In the vicinity of the cross bore it rose slightly to 28 MPa. It then dropped to -1 MPa at point S. Along the vertical line SH it dropped to -13 MPa and then further to -28 MPa. It then increased to about 6 MPa at point H on the cylinder surface.

Radial stress was about -46 MPa at point R. Moving towards the cross-bore it dropped slightly to about -50 MPa and then increased to about -45 MPa at point S. Moving up the cross-bore, it dropped in a smooth curve to -61 MPa before starting to rise gradually up to -12 MPa at the cross-bore cylinder outside surface intersection.

Comparing these stresses with those for a circular cross-bore discussed in section 5.4.2, the hoop stress has varied very slightly. The compressive hoop stress along SH increased by between 16 % and 19 %. The axial stress at point S reduced by 98 % and became compressive. The axial stress along the cross-bore was largely compressive. The radial stress changed very slightly. Along the cross-bore immediately after point S the compressive radial stress increased by 17 %.

5.5.3. Cross-Bore Main Bore Intersection Stresses

The stresses discussed here are the elastic stresses at the intersection of the circular cross-bore and the cylinder main bore. Figure 5-13 shows the non-dimensional stresses for an elliptical cross-bore of same cross-sectional area as a circular cross-bore of cross-bore to cylinder bore radius ratio of d = 0.15. The cross-bore major axis is parallel to the cylinder axis.

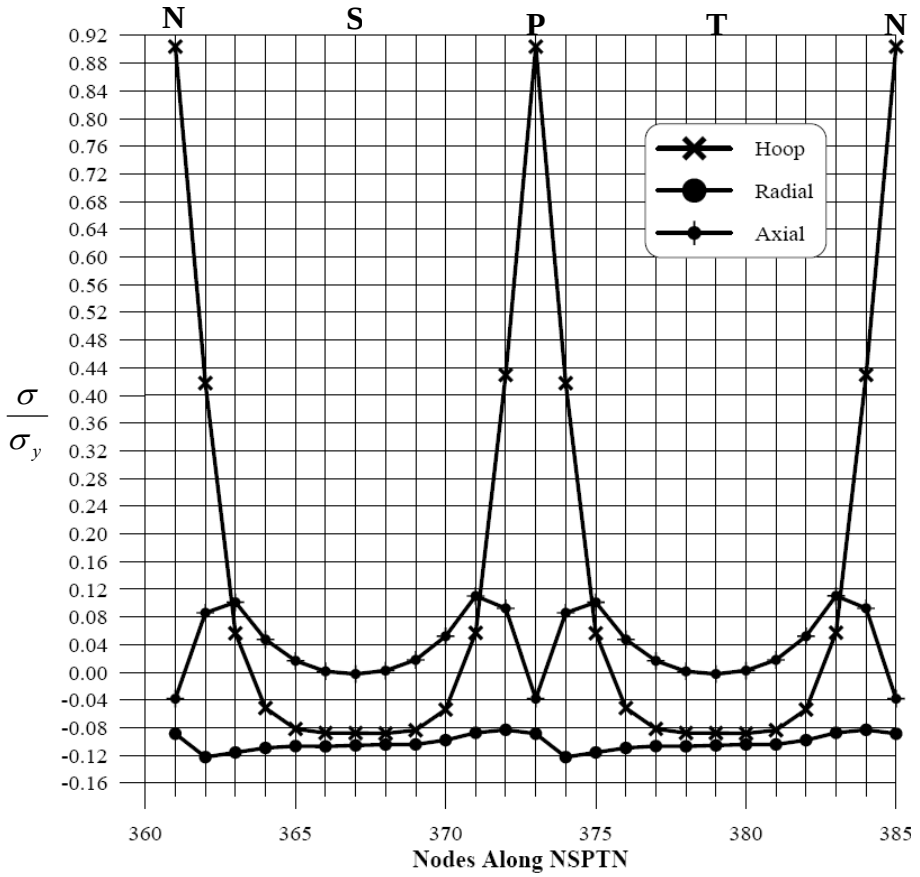

Figure 5-13 Cross-bore main bore intersection stresses – parallel elliptical cross-bore

Points N and P had a tensile hoop stress of about 407 MPa. Points S and T had a compressive hoop stress of about -40 MPa. Moving from N to S or P to T, the hoop stress dropped quickly from 407 MPa to -40 MPa. It then remained constant for the points near S or T. Moving from S to P or T to N, the hoop stress was constant at -40 MPa for some points before it increased quickly to 407 MPa.

Points N and P had a compressive axial stress of a value of about -17 MPa. Points S and T had a tensile axial stress of about 0 MPa. Moving from N to S or P to T, the axial stress increased from -17 MPa to 39 MPa and then 45 MPa. It then dropped in a smooth curve to 0 MPa. Moving from S to P or T to N, the axial stress curved up smoothly from 0 MPa to 45 MPa. It then falls to 39 MPa and then to -17 MPa.

Moving from N to S to P and back to N the radial stress varied between -37 MPa and -55 MPa. At points N and P the radial stress was about -40 MPa. At S and T, the radial stress was -48 MPa. The points around S and T had constant radial stress of about -48 MPa.

Comparing these stresses with those for a circular cross-bore discussed in section 5.4.3, the hoop stress at the crotch corner, that is points N and P, increased by 61 % while the compressive hoop stress at points S and T increased by 14 %. Point S and T and the points around them had the same value of hoop stress. The axial stress profile changed and at points S and T it curved downwards. The axial at points S and

T reduced greatly to about 0 MPa. The radial stress varied slightly. Maximum radial stress increased by 17 %.

5.5.4. Cross-Bore Mid-Way Stresses

The stresses discussed here are the stresses midway along an elliptical cross-bore. Figure 5-14 shows the non-dimensional stresses for an elliptical cross-bore of same cross-sectional area as a circular cross-bore of cross-bore to cylinder bore radius ratio of $d = 0.15$. The cross-bore major axis is parallel to the cylinder axis.

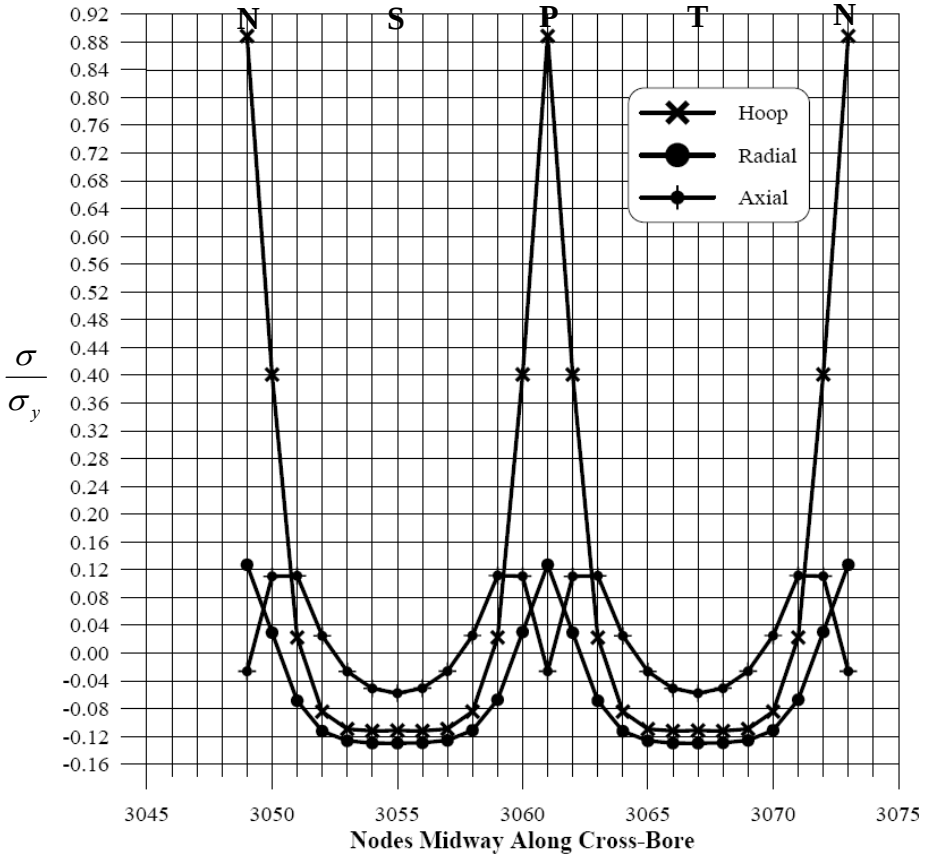

Figure 5-14 Cross-bore midway stresses – parallel elliptical cross-bore

Points N and P had tensile hoop stress of about 400 MPa. Points S and T had a compressive hoop stress of about -50 MPa. Moving from N to S or P to T, the hoop stress dropped from 400 MPa to -50 MPa. It then remained constant for the points near S and T. Moving from S to P or T to N, the hoop stress was constant at about -50 MPa for the points near S or T before it increased to 400 MPa.

Points N and P had a compressive axial stress of a value of about -12 MPa. Points S and T had a compressive axial stress of about -26 MPa. Moving from N to S or P to T, the axial stress increased from -12 MPa to 50 MPa, remained constant and then curved down to -26 MPa. Moving from S to P or T to N, the axial stress curved up from -26 MPa to 50 MPa remained constant and then dropped to -12 MPa.

Points N and P had a tensile radial stress of about 57 MPa. Points S and T had a compressive radial stress of about -59 MPa. Moving from N to S or P to T, the radial stress dropped from 57 MPa to -59 MPa. It then remained constant at -59 MPa for the points near S or T. Moving from S to P or T to N, the radial stress was constant at -59 MPa for the points near S or T before it increased to 57 MPa.

Comparing these stresses with those for a circular cross-bore discussed in section 5.4.4, the hoop stress at points N and P increased 81 %. At points S and T compressive hoop stress increased slightly and they had the same stress as the points around them. The axial stress profile changed. It curved downwards at points S and T and made them have the lowest radial stress. Axial stress reduced 41 % and

changed from tensile to compressive. The radial stress profile changed into two troughs at points S and T. The radial stress at points N and P increased from about 0 MPa to 57 MPa. The compressive radial stress at points S and T increased by 44 %.

Compared to the cross-bore cylinder bore intersection stresses discuss in section 5.5.3, the hoop stresses at points N and P have reduced by 2 % and increased by 25 % at points S and T. Compressive axial stress at point S and T increased from 0 MPa to -26 MPa. Radial stress became more pronounced and formed clear curves and increased by 50 %.

5.5.5. Cross-Bore Cylinder Outside Surface Intersection Stresses

The stresses discussed here are the stresses at the intersection of an elliptical cross-bore and the cylinder outside surface. Figure 5-15 shows the non-dimensional stresses for an elliptical cross-bore of same cross-sectional area as a circular cross-bore of cross-bore to cylinder bore radius ratio of 0.15. The cross-bore major axis is parallel to the cylinder axis.

Points K and L had tensile hoop stress of about 277 MPa. Points H and I had a compressive hoop stress of about -50 MPa. Moving from K to H or L to I, the hoop stress dropped quickly from 277 MPa to -50 MPa. It then remained constant at -50 MPa for the points near H or I. Moving from H to L or I to K, the hoop stress was constant at -50 MPa for the points near H or I before it increased quickly to 277 MPa.

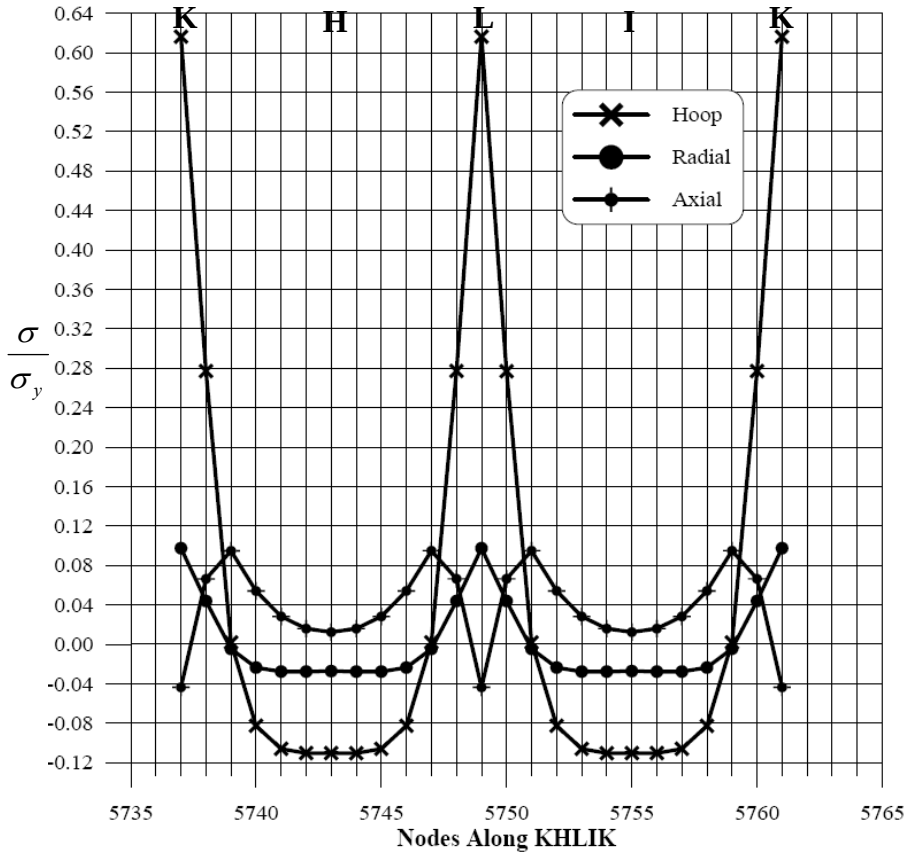

Figure 5-15 Cross-bore cylinder surface intersection stresses – parallel elliptical cross-bore

Points K and L had a compressive axial stress of a value of about -20 MPa. Points H and I had a tensile axial stress of about 6 MPa. Moving from K to H or L to I, the axial stress increased from -20 MPa to 30 MPa and then 43 MPa. It then curved down smoothly to 6 MPa. Moving from H to L or I to K, the axial stress curved up smoothly from 6 MPa to 43 MPa, then drop to 30 MPa and further to -20 MPa.

Points K and L had a tensile radial stress of about 44 MPa. Points H and I had a compressive radial stress of about -12 MPa. Moving from K to H or L to I, the radial

stress reduced from 44 MPa to -12 MPa. It then remained constant at -12 MPa for the points near H or I. Moving from H to L or I to K, the radial stress was constant at -12 MPa for points near H or I, and then increased to 44 MPa.

Comparing these stresses with those for a circular cross-bore discussed in section 5.4.5, the hoop stress at points K and L increased by 113 %. At points H and I compressive hoop stress increased slightly by 16 %. Points H and I had the same stress as the points around them. The axial stress profile changed. It curved downwards at points S and T. At points K and L it reduced by half. At points H and I the axial stress reduced by 91 %. The radial stress profile changed into two troughs at points H and I. The radial stress at points K and L increased by 633 %. The compressive radial stress at points H and I increased by 140 %.

Compared to the cross-bore midway stresses discuss in section 5.5.4, the hoop stresses at points K and L have reduced by 31 %. The hoop stress at points H and I did not change. The axial stress at point H and I reduced by 77 % and changed from compressive to tensile. Radial stress at points K and L reduced by 23 %. Radial stress at points H and I reduced by 80 %.

From the these discussions it can be concluded that when the circular cross-bore was replaced by an elliptical cross-bore with its major axis parallel to the cylinder axis, the hoop stresses in the vicinity of the cross-bore increased. The axial stress reduced. The radial stresses increased.

5.6. ELLIPTICAL CROSS-BORE PERPENDICULAR TO CYLINDER AXIS

In this section, a cylinder of thickness ratio k=2.0 with a radial elliptical cross-bore with its major axis oriented perpendicular to the cylinder axis was considered. The cross-sectional area of the elliptical cross-bore was the same as that of a circular cross-bore of cross-bore to cylinder bore radius ratio of d=0.15 to ensure same material weight removal. The ratio of the minor axis to the major axis of the elliptical cross-bore was b/a=0.5.

5.6.1. Meridional Stresses

The stresses discussed here are along the meridional section shown in Figure 4-3 along the surface BNK. Figure 5-16 shows the non-dimensional stresses for an elliptical cross-bore of same cross-sectional area as a circular cross-bore of cross-bore to cylinder bore radius ratio of d=0.15. The cross-bore major axis is perpendicular to the cylinder axis.

Hoop stress was about 87 MPa at point B. It remained constant along the cylinder bore towards point N. In the vicinity of the cross-bore, hoop stress increased smoothly to 146 MPa at point N. The hoop stress then curved down to 52 MPa at point K on the cylinder surface.

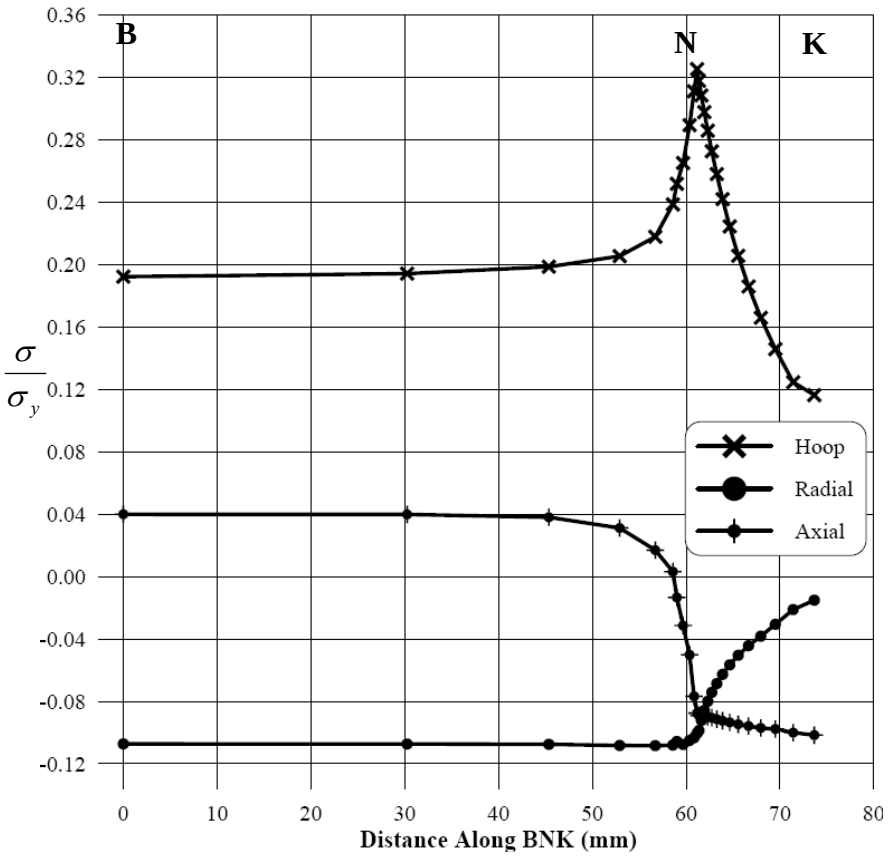

Figure 5-16 Meridional stresses – perpendicular elliptical cross-bore

Axial stress was about 18 MPa at point B and remained a constant along the cylinder bore towards point N. In the vicinity of the cross-bore it starts dropping till -39 MPa at point N. Along the vertical line NK it dropped to -46 MPa at point K.

Radial stress was about -48 MPa at point B and remained a constant along the cylinder bore towards point N. Approaching point N it increased to -45 MPa at the crotch corner. Moving along the vertical line NK, it increased gradually in a curve to -7 MPa at point K.

Comparing these stresses with those for a circular cross-bore discussed in section 5.4.1, the maximum hoop stress reduced by 43 %. Hoop stress at point K reduced by 60 %. The maximum compressive axial stress increased by 15 %. The radial stress at point K increased by 17 %.

Comparing these stresses with those for an elliptical cross-bore with major axis parallel to the cylinder axis discussed in section 5.5.1, the maximum hoop stress reduced by 67 %. The hoop stress at point K reduced by 81 %. The maximum compressive axial stress at point K increased by 130 %. The radial stress at point K reduced by 84 % and changed from tensile to compressive.

5.6.2. Transverse Stresses

The stresses discussed here are along the transverse section shown in Figure 4-4 along the surface RSH. Figure 5-17 shows the non-dimensional stresses for an elliptical cross-bore of same cross-sectional area as a circular cross-bore of cross-bore to cylinder bore radius ratio of d=0.15. The cross-bore major axis is perpendicular to the cylinder axis.

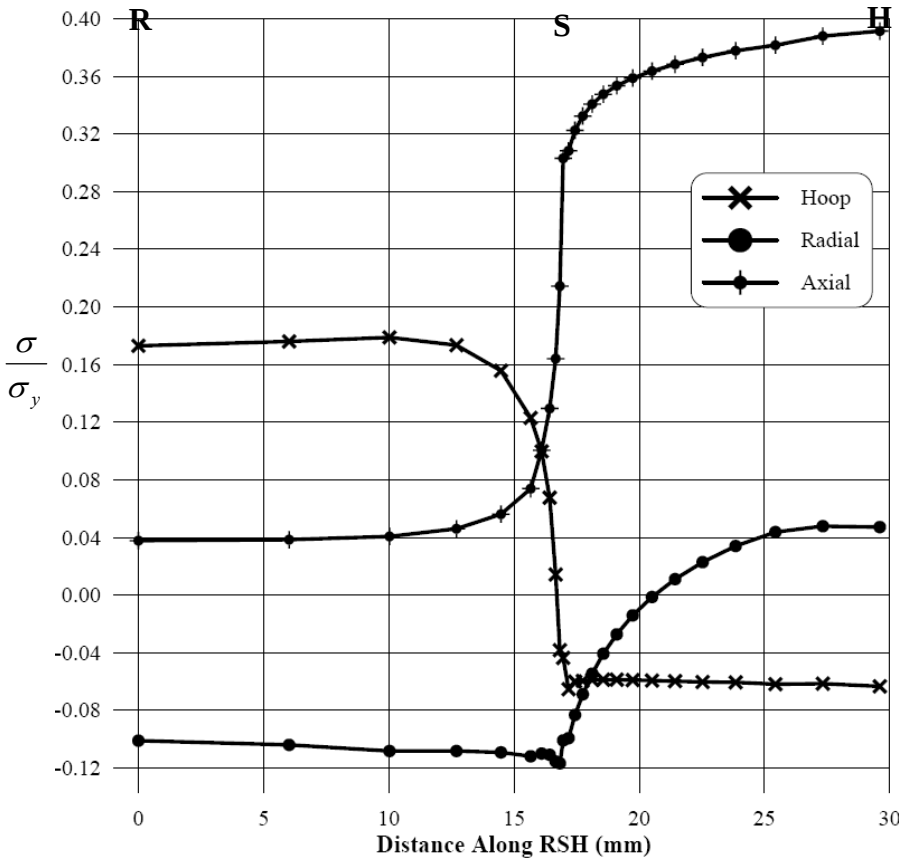

Figure 5-17 Transverse stresses – perpendicular elliptical cross-bore

Hoop stress was about 78 MPa at point R. Along the cylinder bore it remained constant. It then started falling down smoothly and then sharply to a value of about -20 MPa at point S. Moving up the cross-bore it dropped further to -29 MPa. It then increased slightly to -26 MPa, remained constant for several points along the cross bore before it reduced slightly to -29 MPa at point H.

Axial stress was about 17 MPa at point R. It remained constant along the cylinder bore. In the vicinity of the cross bore it raises to 136 MPa at point S. Moving up the cross-bore it increased gradually to about 176 MPa at point H on the cylinder surface.

Radial stress was about -46 MPa at point R. It dropped slightly to about -50 MPa in the vicinity of the cross-bore. At point S the radial stress increased to -45 MPa. Up the cross-bore the radial stress increased in a smooth curve to 21 MPa at point H.

Comparing these stresses with those for a circular cross-bore discussed in section 5.4.2, the maximum compressive hoop stress reduced by 33 %. The axial stresses increased throughout the cross-bore length. At point H axial stress increased by 167 %. The radial stress at point H increased by 320 % and changed from compressive to tensile.

Comparing these stresses with those for an elliptical cross-bore with major axis parallel to the cylinder axis discussed in section 5.5.2, the maximum compressive hoop stress reduced by 42 %. The axial stress at point H increased by 2833 %. The radial stress profile gave a smooth curve along the cross-bore. The radial stress at point H increased by 75 % and changed from compressive to tensile.

5.6.3. Cross-Bore Main Bore Intersection Stresses

The stresses discussed here are the elastic stresses at the intersection of the elliptical cross-bore and the cylinder main bore. Figure 5-18 shows the non-dimensional stresses for an elliptical cross-bore of same cross-sectional area as a circular cross-bore of cross-bore to cylinder bore radius ratio of d=0.15. The cross-bore major axis is perpendicular to the cylinder axis.

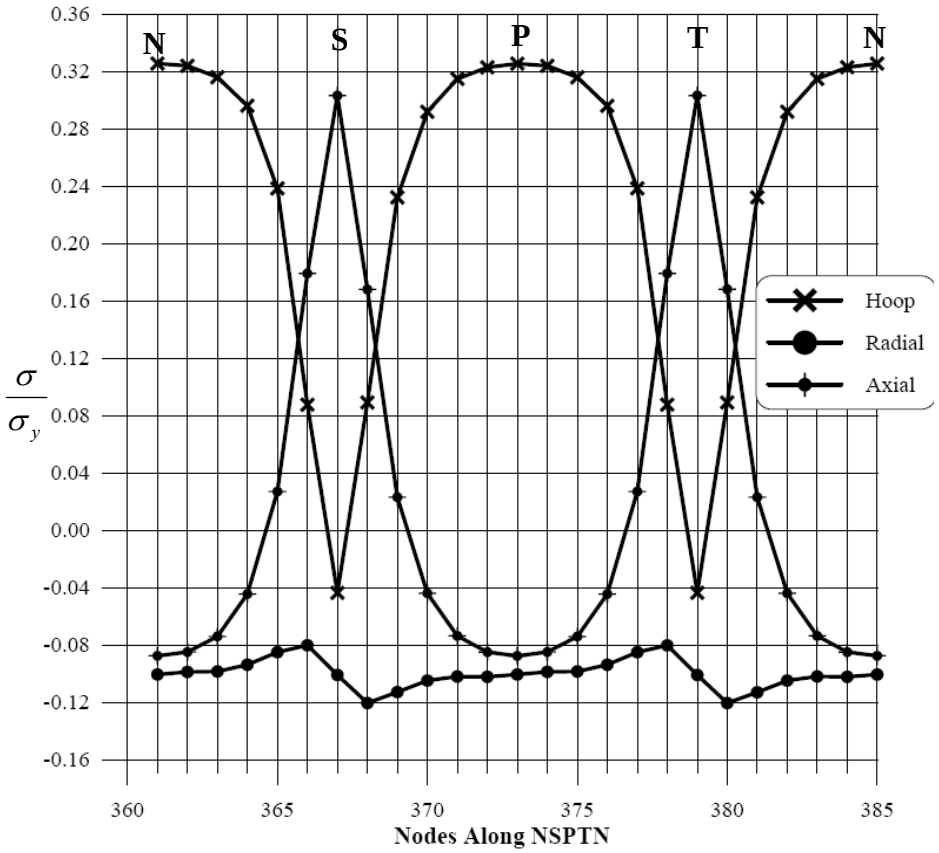

Figure 5-18 Cross-bore main bore intersection stresses – perpendicular elliptical cross-bore

Points N and P, at the cross-bore main bore intersection, had a tensile hoop stress of about 146 MPa. Points S and T had a compressive hoop stress of about -20 MPa. Moving from N to S or P to T, the hoop stress curved down smoothly from 146 MPa to about 107 MPa before it reduced linearly to -20 MPa. Moving from S to P or T to N, the hoop stress increased linearly from -20 MPa to 107 MPa and then curved smoothly to 146 MPa.

Points N and P, at the cross-bore main bore intersection, had a tensile hoop stress of about 146 MPa. Points S and T had a compressive hoop stress of about -20 MPa. Moving from N to S or P to T, the hoop stress curved down smoothly from 146 MPa to about 107 MPa before it reduced linearly to -20 MPa. Moving from S to P or T to N, the hoop stress increased linearly from -20 MPa to 107 MPa and then curved smoothly to 146 MPa.

Points N and P had a compressive axial stress of a value of about -39 MPa. Points S and T had a tensile axial stress of about 136 MPa. Moving from N to S or P to T, the axial stress curved up smoothly from -39 MPa to 12 MPa and then increased linearly to 136 MPa. Moving from S to P or T to N, the axial stress reduced linearly from 136 MPa to 12 MPa before it curved down smoothly to -39 MPa.

The radial stress was compressive and varied between -36 MPa and -54 MPa. At point N and point P the radial stress was about -45 MPa. At point S and point T, the radial stress was -45 MPa. Moving from point N to point S the radial stress increased gradually from -45 MPa to -36 MPa and then dropped to -45 MPa. Moving from point S to point P, radial stress dropped further to -54 MPa before it raised gradually to -45 MPa at point P. This profile is the same for points between P-T-N.

Comparing these stresses with those for a circular cross-bore discussed in section 5.4.3, the hoop stress reduced by 42 % at points N and P while at points S and T it reduced by 43 %. The hoop stress profile is sharp at points S and T and smoothly

curved at points P and N. The axial stress increased slightly at points N and P by 11 % while at points S and T it increased by 157 %. The radial stress at points N and P it increased by 7 % while at points S and T it reduced by 4 %.

Comparing these stresses with those for an elliptical cross-bore with major axis parallel to the cylinder axis discussed in section 5.5.3 the hoop stress at points N and P reduced by 64 % while at points S and T it reduced by half. The hoop stress profile was sharp at points S and T and curved smoothly at points N and P. The axial stress at points N and P increased by 130 % while at points S and T it increased from 0 MPa to 136 MPa. The maximum radial stress reduced by 2 % while the minimum radial stress reduced by 3 %.

5.6.4. Cross-Bore Mid-Way Stresses

The stresses discussed here are the stresses midway along the elliptical cross-bore. Figure 5-19 shows the non-dimensional stresses for an elliptical cross-bore of same cross-sectional area as a circular cross-bore of cross-bore to cylinder bore radius ratio of d=0.15. The cross-bore major axis is perpendicular to the cylinder axis.

Points N and P had a tensile hoop stress of about 109 MPa. Points S and T had a compressive hoop stress of about -27 MPa. Moving from N to S or P to T, the hoop stress curved down smoothly from 109 MPa to about 83 MPa before it reduced

linearly to -27 MPa. Moving from S to P or T to N, the hoop stress increased linearly from -27 MPa to 83 MPa and then curved smoothly to 109 MPa.

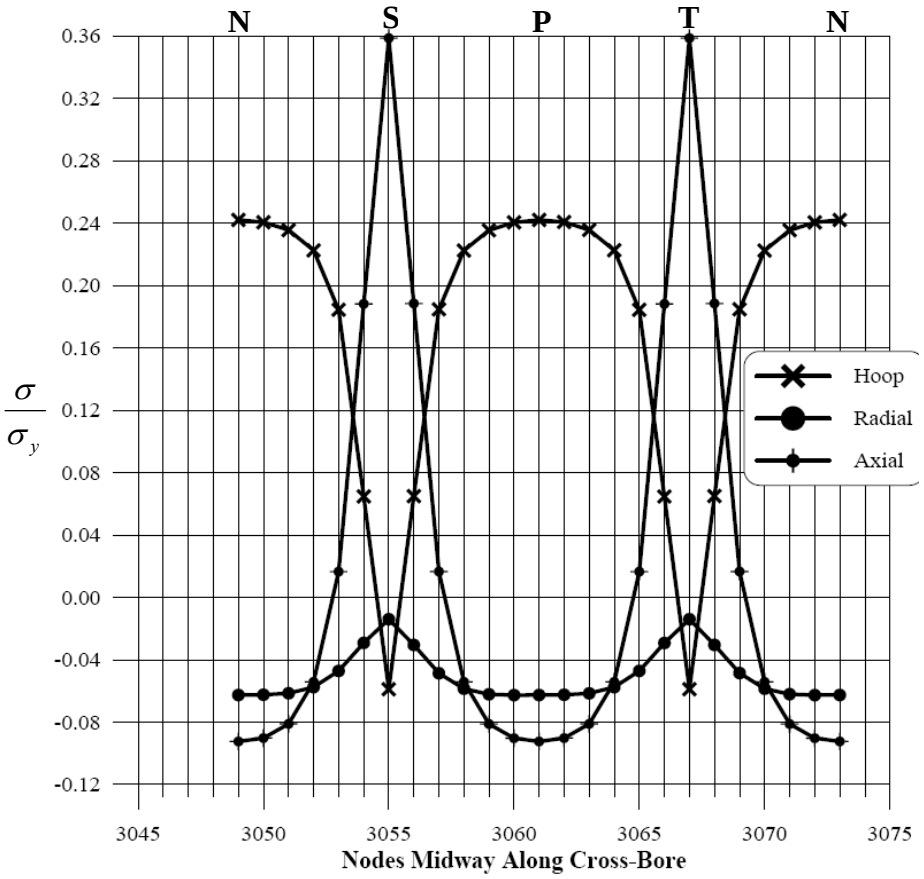

Figure 5-19 Cross-bore midway stresses – perpendicular elliptical cross-bore

Points N and P had a compressive axial stress of a value of about -42 MPa. Points S and T had a tensile axial stress of about 161 MPa. Moving from N to S or P to T, the axial stress curved up smoothly from -42 MPa to about 7 MPa and then increased linearly to 161 MPa. Moving from S to P or T to N, the axial stress reduced linearly from 161 MPa to 7 MPa before it curved down smoothly to -42 MPa.

Radial stress was compressive for all points. Points N and P had a compressive radial stress of about -28 MPa. Points S and T had a compressive radial stress of about -6 MPa. Moving from N to S or P to T, the radial stress curved up smoothly from -28 MPa to -6 MPa. Moving from S to P or T to N, the radial stress curved down smoothly from -6 MPa to -28 MPa.

Comparing these stresses with those for a circular cross-bore discussed in section 5.4.4, the hoop stress reduced by 51 % at points N and P while at points S and T it reduced by 34 %. The axial stress increased slightly at points N and P by 17 % while at points S and T it increased by 266 %. The radial stress at points N and P it changed from 0 MPa and became compressive at -28 MPa while at points S and T it reduced by 85 %.

Comparing these stresses with those for an elliptical cross-bore with major axis parallel to the cylinder axis discussed in section 5.5.4 the hoop stress at points N and P reduced by 73 % while at points S and T it reduced by 46 %. The axial stress at points N and P increased by 250 % while at points S and T it increased by 519 % and changed from compressive to tensile. The radial stress was compressive for all points. The radial stress profile changed with peaks at points S and T. The radial stress at points N and P reduced by 51 % and changed from tensile to compressive, while at points S and T it reduced by 90 %.

5.6.5. Cross-Bore Cylinder Outside Surface Intersection Stresses

The stresses discussed here are the stresses at the intersection of the elliptical cross-bore and the cylinder outside surface. Figure 5-20 shows the non-dimensional stresses for an elliptical cross-bore of same cross-sectional area as a circular cross-bore of cross-bore to cylinder bore radius ratio of d=0.15. The cross-bore major axis is perpendicular to the cylinder axis.

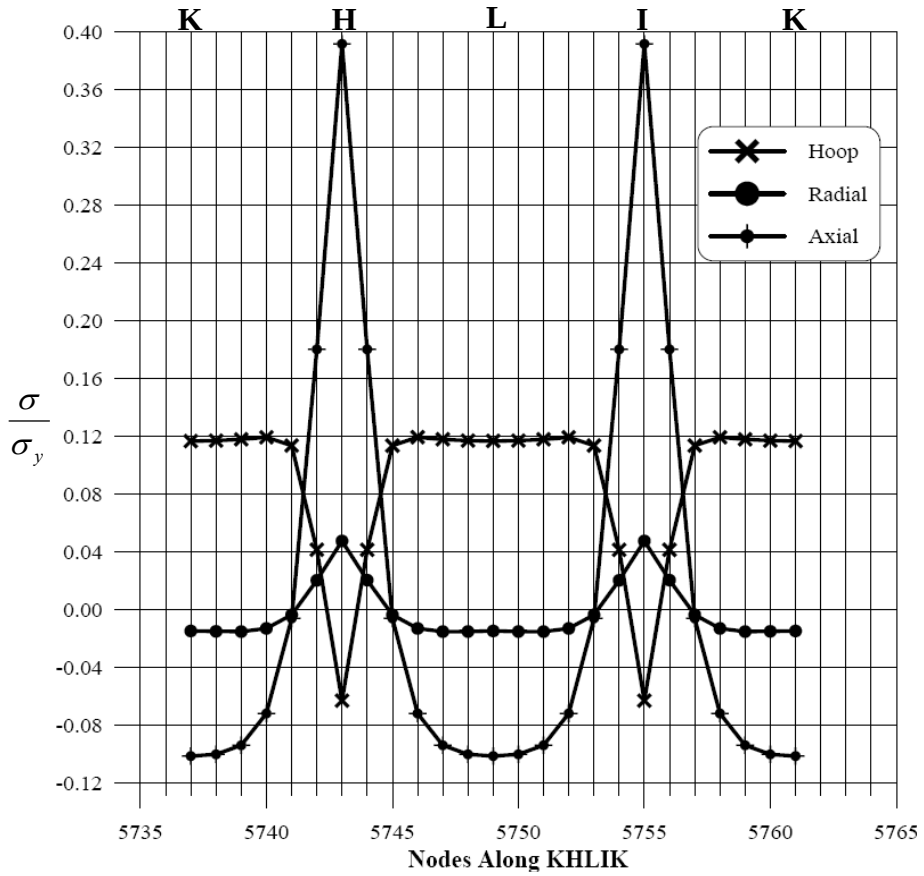

Figure 5-20 Cross-bore cylinder surface intersection stresses – perpendicular elliptical cross-bore

Points K and L had a tensile hoop stress of about 52 MPa. Points H and I had a compressive hoop stress of about -29 MPa. Moving from K to H or L to I, the hoop stress increased from 52 MPa to 54 MPa and then dropped to about 51 MPa. It then dropped to about -29 MPa at point H or I. Moving from H to L or I to K, the hoop stress increased from -29 MPa to 51 MPa and then 54 MPa before dropping to 52 MPa.

Points K and L had a compressive axial stress of about -46 MPa. Points H and I had a tensile axial stress of about 176 MPa. Moving from K to H or L to I, the axial stress curved up smoothly from -46 MPa to about -3 MPa and then increased linearly to 176 MPa. Moving from H to L or I to K, the axial stress reduced linearly from 176 MPa to -3 MPa before it curved down smoothly to -46 MPa.

Points K and L and the points in their vicinity had a compressive radial stress of about -7 MPa. Points H and I had a tensile radial stress of about 21 MPa. Moving from K to H or L to I, the radial stress was initially constant at -7 MPa for before it curved up smoothly to 21 MPa. Moving from H to L or I to K, the radial stress curved down smoothly from 21 MPa to -7 MPa and then remained constant till point L or K.

Comparing these stresses with those for a circular cross-bore discussed in section 5.4.5, the hoop stress at points K and L reduced by 60 %, while at points H and I it reduced by 33 %. The axial stress profile had sharp points at points H and I. The

compressive axial stress at points K and L increased by 15 %. The tensile axial stress at points H and I increased by 167 %. The radial stress profile had peaks at points H and I and constant distribution around points K and L. The radial stress at points K and L increased by 17 % and changed from tensile to compressive. At points H and I the radial stress increased by 320 % and changed from compressive to tensile.

Comparing these stresses with those for an elliptical cross-bore with major axis parallel to the cylinder axis discussed in section 5.5.5, the hoop stress profile changed and had constant regions around points K and L and a sharp dip at points H and I. The hoop stress at points K and L reduced by 81 %, while at points H and I it reduced by 42 %. The axial stress had a sharp peak at points H and I. At points K and L the compressive axial stress increased by 130 %. At points H and I the tensile axial stress increased by 2833 %.

The radial stress profile changed with peaks at points H and I. The radial stress at points K and L reduced by 84 % and changed from tensile to compressive, while at points H and I it increased by 75 % and changed from compressive to tensile.

From the discussions in this section it can be concluded that in the vicinity of the elliptical cross-bore with major axis perpendicular to the cylinder axis when compared to a circular cross bore and also an elliptical cross-bore with major axis parallel to the cylinder axis: the hoop stress reduced and the axial stresses increased. The radial stress had mixed effect with even the nature of the stresses changing.

5.7. STRESS CONCENTRATION FACTORS

In this section, the stress intensities that arise due to the discontinuities created by the cross-bore are discussed. In determining the stress concentration factors, the effective stress was considered, rather than the hoop stress alone. This was due to the special shape of the elliptical cross-bore. Using effective stress in the determination of the stress concentration factors was found to give a better representation of the state of stress in the cylinder. The effective stress was determined using the von Mises failure criteria.

5.7.1. Circular Cross-Bore

Table 5-1 shows the stress concentration factors (SCF) determined for a radial circular cross-bore. Thick-walled cylinders of thickness ratios of 2.0, 2.25, and 2.5 were considered. For each thickness ratio, cross-bore to cylinder bore radius ratios of 0.15, 0.20, and 0.25 were considered.

From Table 5-1, when only the hoop stress was considered, for cylinder thickness ratios of 2.0 and 2.25, the SCF reduced and then increased when the cross-bore to cylinder bore radius ratio was increased from 0.15 to 0.20 to 0.25. For a cylinder thickness ratio of 2.5, the SCF reduced and then remained constant when the cross-bore to cylinder bore radius ratio was increased from 0.15 to 0.20 to 0.25. When the cylinder thickness ratio was increased, the SCF increased for any given cross-bore to

cylinder bore radius ratio. This was with the exception of cross-bore to cylinder bore radius ratio of 0.25 in which the SCF remained constant when the thickness ratio was increased from 2.25 to 2.50.

Table 5-1 SCF for a Circular Radial Cross-Bore

k	***d***	**Hoop Stress**		**Effective Stress**	
		SCF	**Location**	**SCF**	**Location**
2.0	0.15	2.95	Between points N and K or between points P and L	2.50	Between points N and K or between points P and L
	0.20	2.94	Between points N and K or between points P and L	2.52	Point N or P
	0.25	2.97	Point N or P	2.57	Point N or P
2.25	0.15	3.00	Between points N and K or between points P and L	2.47	Between points N and K or between points P and L
	0.20	2.96	Between points N and K or between points P and L	2.48	Point N or P
	0.25	2.98	Point N or P	2.51	Point N or P
2.5	0.15	3.04	Between points N and K or between points P and L	2.45	Point N or P
	0.20	2.97	Between points N and K or between points P and L	2.45	Point N or P
	0.25	2.97	Point N or P	2.47	Point N or P

When only hoop stress was considered, with the exception of cross-bore to cylinder bore radius ratio of 0.25, the SCF occurred away from point N or P, away from the crotch corner. For cross-bore to cylinder bore radius ratios of 0.20 and below, the

hoop SCF occurred away from the crotch corner. For cross-bore to cylinder bore radius ratio of above 0.20 the SCF occurred at the crotch corner.

The maximum hoop stress approaches the crotch corner as the cross-bore to cylinder bore radius ratio increases. Once the cross-bore to cylinder bore radius ratio reaches a critical value, depending on the cylinder thickness ratio, the location of the maximum hoop stress is always at the crotch corner [19].

Though the crotch corner may be considered the geometrically most singular point in the structure, it may not necessarily be the point of maximum global hoop stress. This is due to the interactions of the complex stress systems in the cross-bore and main bore [19]. The location of the maximum global hoop stress is then solely determined by the relative dimensions and dispositions of the cross-bore and the main bore. These are the cross-bore radius, the cylinder bore radius and the cylinder thickness ratio [19].

When effective stress was considered, with the exception of cylinder of thickness ratios of 2.00 and 2.25 with cross-bore to cylinder bore radius ratio of 0.15, the effective SCF occurred at either point N or P also known as the crotch corner, shown in Figure 4-3. For the exceptions, the SCF occurred along the vertical line NK or PL along the cross-bore a short distance from the crotch corner.

When the effective stress was used to determine the SCF, for the cylinder thickness ratios considered, the SCF increased with increase in the cross-bore to cylinder bore radius ratio. Increasing the cylinder thickness ratio, for any given cross-bore to cylinder bore radius ratio, the SCF reduced. The hoop stress gave higher values of SCF when compared to the effective stress. The effective stress gave more consistent results. Therefore, the effective stress was used to determine the SCF when the elliptical cross-bore was rotated.

For a cylinder thickness ratio of 2.0, the SCF was 2.50, 2.52, and 2.57 for cross-bore to cylinder bore radius ratios of 0.15, 0.20 and 0.25 respectively. For a cylinder thickness ratio of 2.25, the SCF was 2.47, 2.48, and 2.51 for cross-bore to cylinder bore radius ratios of 0.15, 0.20 and 0.25 respectively. For a cylinder thickness ratio of 2.5, the SCF was 2.45, 2.45, and 2.47 for cross-bore to cylinder bore radius ratios of 0.15, 0.20 and 0.25 respectively.

5.7.2. Elliptical Cross-Bore with Changing Orientation

The effect of the orientation of the elliptical cross-bore on the stress concentration factors is presented and discussed in this section. Thick-walled cylinders of thickness ratios of 2.0, 2.25, and 2.5 were considered. For each thickness ratio, elliptical cross-bores with cross-sectional area equivalent to circular cross-bores of cross-bore to cylinder bore radius ratios of 0.15, 0.20, and 0.25 were considered. The geometry of the elliptical cross-bore was varied by changing the ratio of the semi-

minor axis to semi-major axis while keeping the cross-sectional area constant. The ratios of elliptical cross-bore semi-minor axis to semi-major axis, b/a, of 0.1, 0.3, 0.5, and 0.7 were considered.

The orientation of the elliptical cross-bore major axis was varied with respect to the cylinder axis. Initially the cross-bore major axis was parallel to the cylinder axis. The orientation of the cross-bore major axis with respect to the cylinder axis was then varied from 0° to 90°, where the major axis was perpendicular to cylinder axis.

Table 5-2 SCF for AOR = 0° and k = 2.00

d	***b/a***	**SCF**	**Location**
0.15	0.1	2.70	Point N or P
	0.3	4.15	Point N or P
	0.5	3.83	Between points N and K or between points P and L
	0.7	3.17	Between points N and K or between points P and L
0.20	0.1	2.61	Point N or P
	0.3	4.04	Point N or P
	0.5	3.85	Between points N and K or between points P and L
	0.7	3.20	Between points N and K or between points P and L
0.25	0.1	2.66	Point N or P
	0.3	4.01	Point N or P
	0.5	3.91	Between points N and K or between points P and L
	0.7	3.25	Between points N and K or between points P and L

Table 5-3 SCF for AOR = 0° and k = 2.25

d	***b/a***	**SCF**	**Location**
0.15	0.1	2.60	Point N or P
	0.3	4.05	Point N or P
	0.5	3.78	Between points N and K or between points P and L
	0.7	3.14	Between points N and K or between points P and L
0.20	0.1	2.47	Point N or P
	0.3	3.90	Point N or P
	0.5	3.77	Between points N and K or between points P and L
	0.7	3.14	Between points N and K or between points P and L
0.25	0.1	2.49	Point N or P
	0.3	3.83	Point N or P
	0.5	3.78	Between points N and K or between points P and L
	0.7	3.16	Between points N and K or between points P and L

Table 5-2, Table 5-3, and Table 5-4 show the SCF for an elliptical cross-bore for angle of rotation equal to zero, for cylinder thickness ratios of 2.0, 2.25, and 2.5 respectively. From the tables, it is seen that the semi-minor to semi-major axis ratio of 0.3 gave the highest SCF for any of the cross-bore to cylinder bore radius ratios considered; while the semi-minor to semi-major axis ratio of 0.1 gave the minimum SCF. For the semi-minor to semi-major axis ratios of 0.1 and 0.3, the maximum SCF occurred at the crotch corner, while for the semi-minor to semi-major axis ratios of

0.5 and 0.7, the maximum SCF occurred away from the crotch corner along the vertical line NK or PL, but near to the crotch corner.

Table 5-4 SCF for AOR = 0° and k = 2.50

d	***b/a***	**SCF**	**Location**
0.15	0.1	2.53	Point N or P
	0.3	3.98	Point N or P
	0.5	3.74	Between points N and K or between points P and L
	0.7	3.11	Between points N and K or between points P and L
0.20	0.1	2.37	Point N or P
	0.3	3.81	Point N or P
	0.5	3.70	Between points N and K or between points P and L
	0.7	3.09	Between points N and K or between points P and L
0.25	0.1	2.35	Point N or P
	0.3	3.70	Point N or P
	0.5	3.69	Between points N and K or between points P and L
	0.7	3.09	Between points N and K or between points P and L

From Table 5-2, Table 5-3 and Table 5-4 it can be seen that the values of SCF obtained for thickness ratio of 2.25 were lower than those for thickness ratio of 2.0; while those obtained for thickness ratio of 2.5 were lower than those for thickness ratio of 2.25. Therefore, increasing the thickness ratio reduced the SCF for a thick walled cylinder with the major axis of an elliptical cross parallel to the cylinder axis.

Table 5-5 SCF for AOR = 45° and k = 2.00

d	***b/a***	**SCF**	**Location**
0.15	0.1	1.96	Cross-bore cylinder bore intersection on cross-bore major axis
	0.3	2.97	Along the cross-bore on vertical line on cross-bore major axis.
	0.5	2.99	Along the cross-bore on a vertical line next to cross-bore major axis.
	0.7	2.61	Along the cross-bore on a vertical line next to cross-bore major axis.
0.20	0.1	1.77	Cross-bore cylinder bore intersection on cross-bore major axis
	0.3	2.77	Cross-bore cylinder bore intersection on cross-bore major axis
	0.5	2.99	Along the cross-bore on a vertical line next to cross-bore major axis.
	0.7	2.62	Along the cross-bore on a vertical line next to cross-bore major axis.
0.25	0.1	1.81	On cylinder bore next to cross-bore major axis
	0.3	2.63	Cross-bore cylinder bore intersection on cross-bore major axis
	0.5	3.01	Along the cross-bore on a vertical line next to cross-bore major axis.
	0.7	2.67	Cross-bore cylinder bore intersection away from cross-bore major axis

Table 5-6 SCF for AOR = 45° and k = 2.25

d	***b/a***	**SCF**	**Location**
0.15	0.1	1.92	Cross-bore cylinder bore intersection on cross-bore major axis
	0.3	2.93	Along the cross-bore on vertical line on cross-bore major axis.
	0.5	2.97	Along the cross-bore on a vertical line next to cross-bore major axis.
	0.7	2.58	Along the cross-bore on a vertical line next to cross-bore major axis.
0.20	0.1	1.72	Cross-bore cylinder bore intersection on cross-bore major axis
	0.3	2.72	Along the cross-bore on vertical line on cross-bore major axis.
	0.5	2.95	Along the cross-bore on a vertical line next to cross-bore major axis.
	0.7	2.58	Cross-bore cylinder bore intersection away from cross-bore major axis
0.25	0.1	1.76	On cylinder bore next to cross-bore major axis
	0.3	2.55	Cross-bore cylinder bore intersection on cross-bore major axis
	0.5	2.94	Along the cross-bore on a vertical line next to cross-bore major axis.
	0.7	2.61	Cross-bore cylinder bore intersection away from cross-bore major axis

Table 5-7 SCF for AOR = 45° and k = 2.50

d	***b/a***	**SCF**	**Location**
0.15	0.1	1.88	Cross-bore cylinder bore intersection on cross-bore major axis
	0.3	2.91	Along the cross-bore on vertical line on cross-bore major axis.
	0.5	2.94	Along the cross-bore on a vertical line next to cross-bore major axis.
	0.7	2.57	Along the cross-bore on a vertical line next to cross-bore major axis.
0.20	0.1	1.67	Cross-bore cylinder bore intersection on cross-bore major axis
	0.3	2.69	Along the cross-bore on vertical line on cross-bore major axis.
	0.5	2.91	Along the cross-bore on a vertical line next to cross-bore major axis.
	0.7	2.55	Cross-bore cylinder bore intersection away from cross-bore major axis
0.25	0.1	1.71	On cylinder bore next to cross-bore major axis
	0.3	2.51	Along the cross-bore on vertical line on cross-bore major axis.
	0.5	2.89	Along the cross-bore on a vertical line next to cross-bore major axis.
	0.7	2.57	Cross-bore cylinder bore intersection away from cross-bore major axis

Table 5-5, Table 5-6, and Table 5-7 show the SCF for an elliptical cross-bore for angle of rotation equal to 45°, for cylinder thickness ratios of 2.0, 2.25 and 2.5

respectively. For each of the cross-bore to cylinder bore radius ratios considered, the semi-minor to semi-major axis ratio of 0.5 gave the highest SCF; while the semi-minor to semi-major axis ratio of 0.1 gave the minimum SCF. The SCF for these cases occurred on or near the cross-bore major axis; and near cross-bore cylinder bore intersection.

From Table 5-5, Table 5-6, and Table 5-7 it is seen that the values of SCF obtained for thickness ratio of 2.25 were lower than those for thickness ratio of 2.0; while those obtained for thickness ratio of 2.5 were lower than those for thickness ratio of 2.25. Therefore, increasing the thickness ratio reduced the SCF for a thick walled cylinder with the major axis of an elliptical cross parallel to the cylinder axis.

Table 5-8, Table 5-9, and Table 5-10 show the SCF for an elliptical cross-bore for angle of rotation equal to 90°, for cylinder thickness ratios of 2.0, 2.25, and 2.5.

From Table 5-8, Table 5-9, and Table 5-10 it can be seen that for all of the cross-bore to cylinder bore radius ratios investigated, the semi-minor to semi-major axis ratio of 0.7 gave the highest SCF; while the semi-minor to semi-major axis ratio of 0.1 gave the minimum SCF. For the semi-minor to semi-major axis ratio of 0.7, the SCF occurred at the crotch corner. For the semi-minor to semi-major axis ratios of 0.1, 0.3, and 0.5, the SCF occurred in the transverse plane. For semi-minor to semi-major axis ratio of 0.3 the SCF occurred at the intersection of the cross-bore and the

cylinder outside surface. For semi-minor to semi-major axis ratios of 0.3 and 0.7, the SCF reduced as the cylinder thickness was increased.

Table 5-8 SCF for AOR = 90° and k = 2.00

d	***b/a***	**SCF**	**Location**
0.15	0.1	1.40	Point S or T
	0.3	1.80	Point H or I
	0.5	1.64	Cross-bore cylinder bore intersection away from cross-bore major axis
	0.7	1.97	Point N or P
0.20	0.1	1.31	On cylinder bore next to cross-bore major axis
	0.3	1.76	Point H or I
	0.5	1.62	Cross-bore cylinder bore intersection away from cross-bore major axis
	0.7	1.97	Point N or P
0.25	0.1	1.43	On cylinder bore on cross-bore major axis
	0.3	1.73	Point H or I
	0.5	1.65	Point H or I
	0.7	1.98	Point P or N

Table 5-9 SCF for AOR = 90° and k = 2.25

d	***b/a***	**SCF**	**Location**
0.15	0.1	1.39	Point S or T
	0.3	1.80	Point H or I
	0.5	1.63	Cross-bore cylinder bore intersection away from cross-bore major axis
	0.7	1.96	Point N or P
0.20	0.1	1.33	On cylinder bore next to cross-bore major axis
	0.3	1.74	Point H or I
	0.5	1.63	Point H or I
	0.7	1.95	Point N or P
0.25	0.1	1.48	On cylinder bore on cross-bore major axis
	0.3	1.71	Point H or I
	0.5	1.66	Point H or I
	0.7	1.95	Point P or N

Table 5-10 SCF for AOR = 90° and k = 2.50

d	*b/a*	SCF	Location
0.15	0.1	1.38	Point S or T
	0.3	1.79	Point H or I
	0.5	1.63	Cross-bore cylinder bore intersection away from cross-bore major axis
	0.7	1.95	Point N or P
0.20	0.1	1.34	On cylinder bore next to cross-bore major axis
	0.3	1.73	Point H or I
	0.5	1.64	Point H or I
	0.7	1.94	Point N or P
0.25	0.1	1.51	On cylinder bore on cross-bore major axis
	0.3	1.68	Point H or I
	0.5	1.66	Point H or I
	0.7	1.93	Point P or N

5.7.3. SCF Constants for a Radial Elliptical Cross-Bore

Figure 5-21, Figure 5-22 and Figure 5-23 show the variation of the SCF with the orientation of an elliptical cross-bore which had the same cross-sectional area as a circular cross-bore of cross-bore to cylinder bore ratio of 0.15, 0.20 and 0.25 respectively.

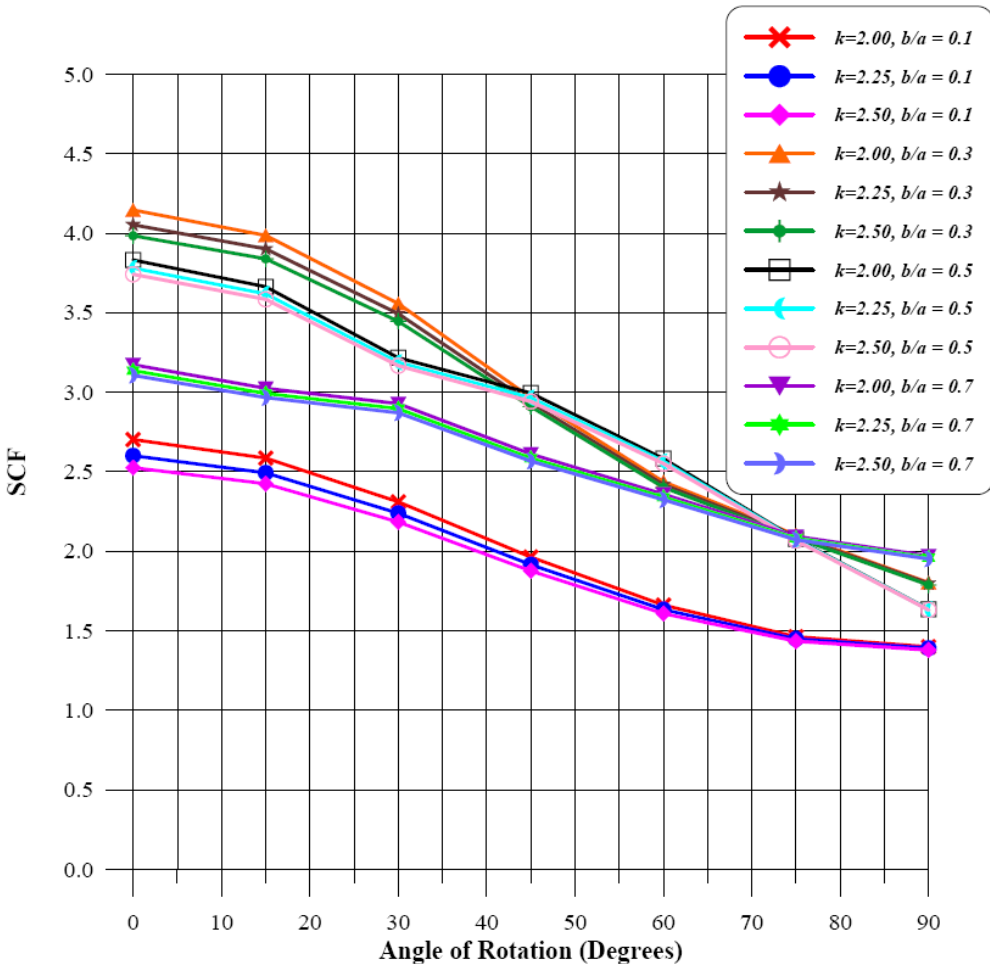

Figure 5-21 SCF vs. Angle of Rotation for d = 0.15

From Figure 5-21 to Figure 5-23, it can be seen that as the angle of rotation increased from 0° to 90° for any condition, the SCF reduced from a maximum to a minimum value. Therefore, an elliptical cross bore oriented perpendicular the cylinder axis gave the minimum SCF for any geometry considered. This can be explained by considering the orientation of the elliptical cross-bore with respect to the directions of the stresses.

The hoop stress is normally the highest stress in thick walled cylinders. In thick walled cylinder studies, emphasis is normally laid on the behaviour of the hoop stress since it is normally the highest and involves separation of material leading to failure of the structure [19].

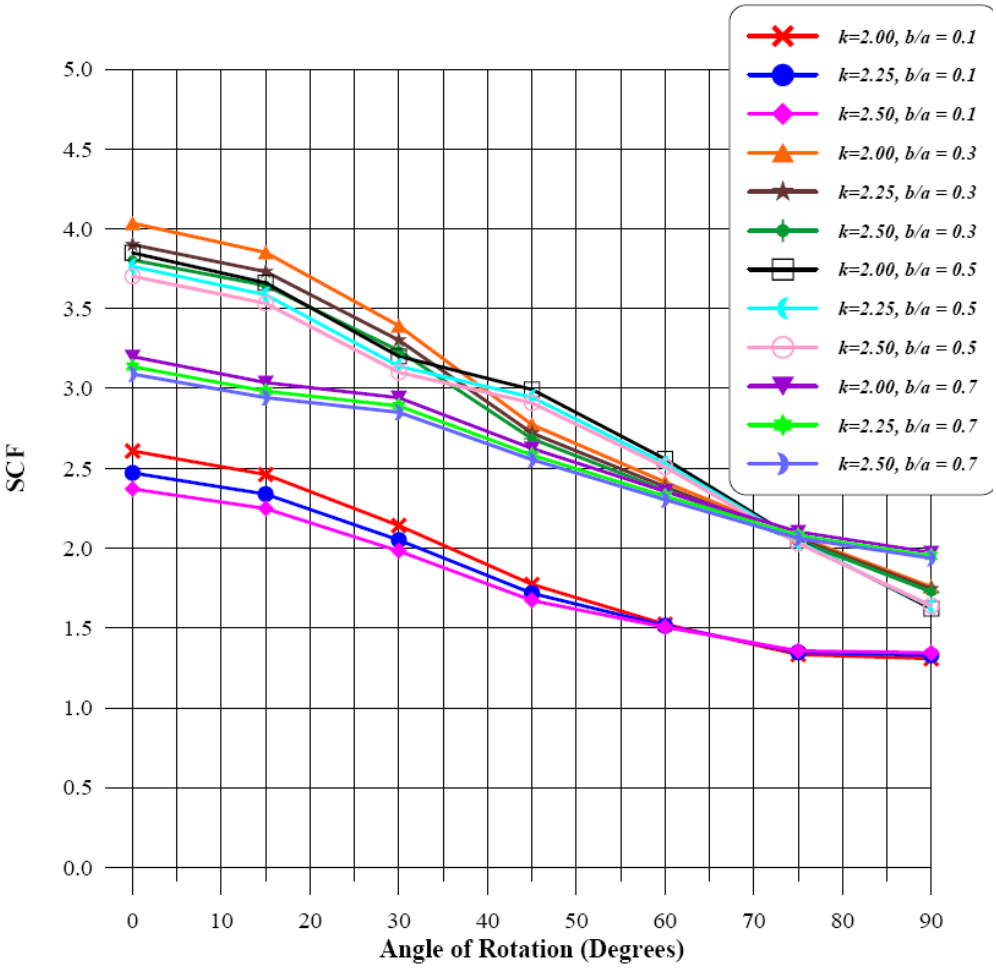

Figure 5-22 SCF vs. Angle of Rotation for d = 0.20

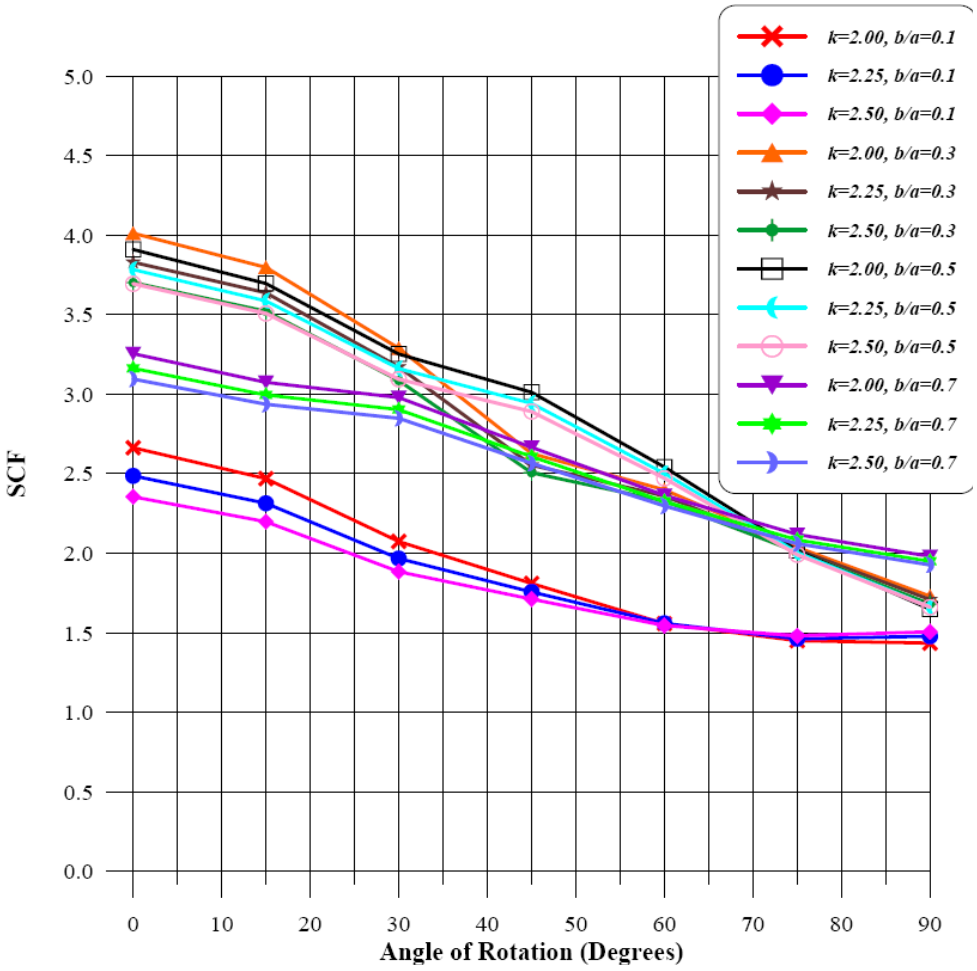

Figure 5-23 SCF vs. Angle of Rotation for d = 0.25

When the angle of rotation was zero, the cross-bore major axis was aligned perpendicular to the direction of the hoop stresses as shown in Figure 3-2. As indicated in section 3.4, the maximum stress and therefore the maximum SCF will be at the end of the major axis. In this case, the meridional plane. This was observed in section 5.5. The high SCF when angle of rotation was zero can be attributed to this. This explains the location of SCF indicated in Table 5-2, Table 5-3, and Table 5-4.

When the cross-bore is rotated, the orientation of the cross-bore major axis with hoop stresses changed until they were parallel. From equation (3.9) the factor *a/b* becomes a less than 1.0. Therefore the SCF reduces. When the cross-bore major axis is perpendicular to the cylinder axis, it also aligned perpendicular to the axial stresses. From section 5.6, the axial stresses are of great magnitudes. These axial stresses play a big role in the SCF. The axial stresses as shown in Figure 5-17 are a maximum in the transverse cross-section at the intersection of the cross-bore and cylinder outside surface. This explains the location of SCF indicated in Table 5-8, Table 5-9, and Table 5-10.

For any given thickness ratio, when $b/a = 0.1$, the SCF was a minimum. When b/a was increased to 0.3, the SCF increased to the maximum. When b/a was changed to 0.5, the SCF reduced. When $b/a = 0.7$, the SCF reduced further but did not fall below those obtained for $b/a = 0.1$.

Thus the size and orientation of geometric discontinuities with respect to applied stress play a large role in determining the stress concentration. Stress concentration factor is a function of the type of discontinuity (hole, fillet, or groove), the geometry of the discontinuity, and the type of loading being experienced [46].

When the thickness ratio was increased from 2.00 to 2.25 to 2.50, the SCF reduced. The magnitude of the difference declined as the angle of rotation changed from 0° to 90°. This trend continued as the cross-bore was rotated, until when nearing angle 90°

when the reverse occurred for some cases of cross-bore to cylinder bore radius ratios of 0.2 and 0.25.

From Figure 5-21, for cylinder of thickness ratios of 2.0, 2.25, and 2.5, and an elliptical cross-bore, whose cross-sectional area is equivalent to a circular cross-bore of cross-bore to cylinder bore radius ratio of 0.15, the SCF was a constant at 2.1 when the cross-bore major axis was rotated 74.5°, with respect to the cylinder axis, for values of *b/a* of 0.3, 0.5, and 0.7.

From Figure 5-22, for cylinder of thickness ratios of 2.0, 2.25, and 2.5, and an elliptical cross-bore, whose cross-sectional area is equivalent to a circular cross-bore of cross-bore to cylinder bore radius ratio of 0.20, the SCF was a constant at 2.1 when the cross-bore major axis was rotated 73°, with respect to the cylinder axis, for values of *b/a* of 0.3, 0.5, and 0.7. For *b/a* of 0.1, the SCF was a constant at 1.45 when the cross-bore major axis was rotated 66° with respect to the cylinder axis.

From Figure 5-23, for cylinder of thickness ratios of 2.0, 2.25, and 2.5, and an elliptical cross-bore, whose cross-sectional area is equivalent to a circular cross-bore of cross-bore to cylinder bore radius ratio of 0.25, the SCF was a constant at 2.1 when the cross-bore major axis was rotated 72.5°, with respect to the cylinder axis, for values of *b/a* of 0.3, 0.5, and 0.7. For *b/a* of 0.1 the SCF was a constant at 1.55 when the cross-bore major axis was rotated 66° with respect to the cylinder axis.

CHAPTER 6

CONCLUSIONS AND RECOMMENDATIONS

6.1. CONCLUSIONS

This study involved the development a finite element method computer program to analyze elastic stresses in a plain thick walled cylinder and in a thick walled cylinder with an elliptical cross-bore. The frontal solution technique was used to solve the linear equations that resulted from the finite element method formulation. The frontal solution technique was used to overcome the computer memory limitation that occurs when dealing with a large number of elements. Investigations were carried out to determine the stress profiles and stress concentration factors for various cross-bore geometries and for various cross-bore orientations with respect to the cylinder axis. The stress profiles have been presented using graphs and discussed. The stress profiles and the stress concentration factors indicate the critical points to be considered when designing a cylinder with an elliptical cross-bore.

In determining the stress concentration factors in the vicinity of an elliptical cross-bore, the following conclusions have been made:

1. The radial elliptical cross-bore has the maximum SCF when its major axis is positioned in the meridional plane.

2. The radial elliptical cross-bore has the minimum SCF when its major axis is positioned in the transverse plane.

In determining the elliptical cross-bore geometry and orientation that gives the minimum stress concentration factor, the following conclusions have been made:

1. For all the orientations of a radial elliptical cross-bore major axis with respect to the cylinder axis, the semi-minor to semi-major axis ratio of 0.1 gives the minimum SCF.

2. For a radial elliptical cross-bore with its major axis in the meridional plane, the semi-minor to semi-major axis ratio of 0.3 gives the highest SCF.

3. For a radial elliptical cross-bore with its major axis inclined at 45° to the cylinder axis, the semi-minor to semi-major axis ratio of 0.5 gives the highest SCF.

4. For a radial elliptical cross-bore with its major axis in the transverse plane, the semi-minor to semi-major axis ratio of 0.7 gives the highest SCF.

In determining the effect of the orientation of an elliptical cross-bore on the stress profiles and the stress concentration factors, the following conclusions have been made:

1. When the cylinder thickness ratio is increased from 2.00 to 2.25 to 2.50, the SCF reduced. The magnitude of the difference of SCF between any two thickness rations declines as the angle of rotation with respect to the cylinder axis changes from 0° to 90°.

2. For cylinder of thickness ratios 2.0, 2.25, and 2.5, with a radial elliptical cross-bore of cross-sectional area equivalent to a circular cross-bore of cross-bore to cylinder bore radius ratio of 0.15, the SCF is a constant at 2.1 when the cross-bore major axis is inclined at 74.5° with respect to the cylinder axis for *b/a* between 0.3 and 0.7.

3. For cylinder of thickness ratios 2.0, 2.25, and 2.5, with a radial elliptical cross-bore of cross-sectional area equivalent to a circular cross-bore of cross-bore to cylinder bore radius ratio of 0.20, the SCF is a constant at 2.1 when the cross-bore major axis is inclined at 73° with respect to the cylinder axis for *b/a* between 0.3 and 0.7. For *b/a* of 0.1 the SCF is a constant at 1.45 when the cross-bore major axis is inclined at 66° with respect to the cylinder axis.

4. For cylinder of thickness ratios 2.0, 2.25, and 2.5, with a radial elliptical cross-bore of cross-sectional area equivalent to a circular cross-bore of cross-bore to cylinder bore radius ratio of 0.25, the SCF is a constant at 2.1 when the cross-bore major axis is inclined at 72.5° with respect to the cylinder axis for *b/a*

between 0.3 and 0.7. For *b/a* of 0.1 the SCF is a constant at 1.55 when the cross-bore major axis is inclined at 66° with respect to the cylinder axis.

6.2. RECOMMENDATIONS

The data obtained in this research should be used in guiding the design of pressure vessels with elliptical cross-bores. The data obtained on SCF constants should be used to enable quick design. This information should be shared with the industry involved in manufacture of thick walled pressure vessels. Also the finite element program that has been developed should be commercialized for industrial and academic research.

Fundamental areas for future study:

1. Practical experimental work using strain gauge methods should be done to obtain supporting data for the elliptical cross-bore with varying orientations.

2. In this research, a single cross-bore was assumed. Research should be done to investigate the effect of two or more elliptical cross-bores which are close to one another.

3. Research should be done for a thick walled cylinder with an elliptical cross-bore with varying orientations for plastic stresses, that is, the case of autofrettage.

REFERENCES

[1] J. F. Harvey, *Theory and Design of Pressure Vessels*, 2nd ed: Chapman & Hall, 1991

[2] D. P. Kendall, "A Short History of High Pressure Technology From Bridgham to Division 3," *Journal of Pressure Vessel Technology*, vol. 122, pp. 229 - 233, 2000.

[3] W. R. D. Manning, "Strength of Cylinders," *Industrial and Engineering Chemistry*, vol. 49, pp. 1969 - 1978, 1957.

[4] J. M. Kihiu, S. M. Mutuli, and G. O. Rading, "Stress Characterization of Autofrettaged Thick Walled Cylinders," *International Journal of Mechanical Engineering Education*, vol. 31, pp. 370 - 389, 2003.

[5] J. M. Kihiu, G. O. Rading, and S. M. Mutuli, "Overstraining of Flush Plain Cross-Bored Cylinders," *Proceedings of Institution of Mechanical Engineers, Part C: Journal of Mechanical Engineering Science*, vol. 218, pp. 143-153, 2004.

[6] L. M. Masu, "The Effect of Cross Bore Geometry on the Strength of Pressure Vessels," PhD Thesis, The University of Leeds, 1989.

[7] A. Hameed, R. D. Brown, and J. Hetherington, "A Study of the Residual Stress Distribution in an Autofrettaged, Thick-Walled Cylinder with Cross-Bore," *Journal of Pressure Vessel Technology*, vol. 126, pp. 497 - 503, 2004.

[8] J. H. Faupel and D. B. Harris, "Stress Concentration in Heavy-Walled Cylindrical Pressure Vessels," *Industrial and Engineering Chemistry*, vol. 49, pp. 1979 - 1986, 1957.

[9] H. Fessler and B. H. Lewin, "Stress Distribution in a Tee Junction of Thick Pipes," *British Journal of Applied Physics*, vol. 7, pp. 76 - 79, 1956.

[10] J. L. M. Morrison and B. Crossland, "Fatigue Strength of Cylinders with Cross Bores," *Journal of Mechanical Engineering Science*, vol. 1, pp. 207 - 210, 1959.

[11] J. C. Gerdeen, "Analysis of Stress Concentrations in Thick Cylinders with Sideholes and Crossbores," *Transactions of ASME, Journal of Engineering for Industry*, vol. 94, pp. 815 - 824, 1972.

[12] B. N. Cole, G. Craggs, and I. Ficenec, "Strength of Cylinders Containing Radial or Offset Cross-Bores," *Journal of Mechanical Engineering Science*, vol. 18, pp. 279 - 285, 1976.

[13] C. L. Tan, "Stress Redistributions in Thick-Walled Cylinders due to the Introduction of Cross-Bore After Autofrettage," *Journal of Strain Analysis*, vol. 21, pp. 177 - 183, 1986.

[14] L. M. Masu, "Fatigue Strength of Thick-Walled Cylinders Containing Cross Bores with Blending Features," *Proc. Instn. Mech. Engrs*, vol. 206, pp. 299 - 309, 1992.

[15] L. M. Masu, "Plastic Analysis and Cross Bore Size Effects on the Fatigue Strength of Thick Walled Cylinders," *East African Journal of Engineering*, vol. 1, pp. 22 - 40, 1994.

[16] L. M. Masu, "Numerical Analysis of Cylinders Containing Circular Offset Cross-Bores," *International Journal of Pressure Vessel and Piping*, vol. 75, pp. 191 - 196, 1998.

[17] L. M. Masu, "Cross Bore Configuration and Size Effects on the Stress Distribution in Thick-Walled Cylinders," *International Journal of Pressure Vessel and Piping*, vol. 72, pp. 171 - 176, 1997.

[18] E. A. Badr, J. R. Sorem, S. M. Tipton, and S. Yang, "An Analytical Procedure for Estimating Residual Stress in Blocks Containing Cross Bores," *International Journal of Pressure Vessel and Piping*, vol. 77, pp. 737 - 749, 2000.

[19] J. M. Kihiu, "Numerical Stress Characterization in Cross-Bored Thick walled Cylinders Under Internal Pressure," PhD Thesis, The University of Nairobi, 2002.

[20] W. Zhao, R. Seshadri, and R. N. Dubey, "On Thick-Walled Cylinder Under Internal Pressure," *Journal of Pressure Vessel Technology*, vol. 125, pp. 267 - 273, 2003.

[21] J. M. Kihiu, G. O. Rading, and S. M. Mutuli, "Geometric Constants in Plain Cross Bore Cylinders," *Journal of Pressure Vessel Technology*, vol. 125, pp. 446 - 453, 2003.

[22] J. M. Kihiu, G. O. Rading, and S. M. Mutuli, "Universal SCFs and Optimal Chamfering in Cross-Bored Cylinders," *International Journal of Pressure Vessels and Piping*, vol. 84, pp. 396 - 404, 2007.

[23] B. N. Cole, "Strategy for cross-bores in high pressure containers," *Journal of Mechanical Engineering Science*, vol. 11, pp. 151–161, 1969.

[24] N. E. Dowling, *Mechanical Behaviour of Materials - Engineering Methods for Deformation, Fracture and Fatigue*: Prentice Hall International Editions, pp. 240 - 252, 1993

[25] K.-J. Bathe, *Finite Element Procedures*: Prentice Hall, Englewood Cliffs, New Jersey, pp. 465 - 466, 1996

[26] W. D. Pilkey and D. F. Pilkey, *Peterson's Stress Concentration Factors*, 3rd ed: John Wiley and Sons, pp. 3 - 5, 2008

[27] S. P. Timoshenko, *Strength of Materials Part II: Advanced Theory and Problems*, 3rd ed: Krieger, 1958

[28] R. D. Dixon, D. T. Peters, and J. G. M. Keltjens, "Stress Concentration Factors of Cross-Bores in Thick Walled Cylinders and Blocks," *Transactions of ASME, Journal of Pressure Vessel Technology*, vol. 126, pp. 184 - 187, 2004.

[29] "Editorial," *International Journal for Numerical Methods in Engineering*, vol. 1, pp. 1, 1969.

[30] A. D. Staff, "The Eight-Node Hexahedral "Brick" Element in Finite Element Analysis," 2008.

[31] D. R. J. Owen and E. M. Salonen, "Three-Dimensional Elasto-Plastic Finite Element Analysis," *International Journal for Numerical Methods in Engineering*, vol. 9, pp. 209 - 218, 1975.

[32] J. N. Reddy, *An Introduction to the Finite Element Method*: McGraw Hill International, 1993

[33] P. V. Marcal and I. P. King, "Elastic-Plastic Analysis of Two-Dimensional Stress System by the Finite Element Method," *International Journal of Mechanical Sciences*, vol. 9, pp. 143 - 155, 1967.

[34] O. C. Zienkiewicz and R. L. Taylor, *The Finite Element Method*, vol. 1: Basic Formulation and Linear Problems, 4th ed: McGraw-Hill Book Company, London, 1994

[35] L. J. Segerlind, *Applied Finite Element Analysis*, 2nd ed: John Wiley and Sons, New York, 1984

[36] C. S. Krishnamoorthy, *Finite Element Analysis - Theory and Programming*, 2nd ed: Tata McGraw-Hill Publishing Company Limited, New Delhi, 1995

[37] O. C. Zienkiewicz, *The Finite Element Method in Engineering Science*: McGraw-Hill, London, pp. 369 - 390, 1971

[38] C. S. Desai and J. F. Abel, *Introduction to the Finite Element Method*: Van Nostrand Reinhold Company, New York, 1972

[39] E. Hinton, F. C. Scott, and R. E. Ricketts, "Local Least Squares Stress Smoothing for Parabolic Isoparametric Elements," *International Journal for Numerical Methods in Engineering*, vol. 9, pp. 235 - 238, 1975.

[40] G. J. Mraz and E. G. Nisbett, "Design, Manufacture and Safety Aspects of Forged Vessels for High-Pressure Services," *Transactions of ASME, Journal of Pressure Vessel Technology*, vol. 102, pp. 98 - 106, 1980.

[41] Y. K. Cheung and M. F. Yeo, *A Practical Introduction to Finite Element Analysis*: Pitman Publishing Limited, London, pp. 117 - 138, 1979

[42] J. W. Dally and W. F. Riley, *Experimental Stress Analysis*, 2nd ed: McGraw Hill Book Company, pp. 10 - 13, 1978

[43] M. F. Yeo, "A More Efficient Front Solution: Allocating Assembly Locations by Longevity Considerations," *International Journal for Numerical Methods in Engineering*, vol. 7, pp. 570 - 573, 1973.

[44] B. M. Irons, "A Frontal Solution Program for Finite Element Analysis," *International Journal for Numerical Methods in Engineering*, vol. 2, pp. 5 - 32, 1970.

[45] D. J. Chen, D. K. Shah, and W. S. Chan, "Using Stress Smoothing for Interlaminar Stress Distribution in Finite Element Analysis of Composite Laminates," *Key Engineering Material*, vol. 121-122, pp. 203-224, 1996.

[46] B. J. Hamrock, S. R. Schmid, and B. O. Jacobson, *Fundamentals of Machine Elements*, 2nd ed: McGraw-Hill Professional, pp. 226 - 235, 2004

[47] A. C. Ugural and S. K. Fenster, *Advanced Strength and Applied Elasticity*, 2nd SI ed: Elservier, pp. 262, 1987

[48] E. P. Popov, *Engineering Mechanics of Solids*, 2nd ed: Prentice Hall, pp. 190 - 197, 1998

[49] S. Singh, *Theory of Plasticity*: Khan Publishers, 1981

APPENDICES

APPENDIX A

Thick Walled Pressure Vessels

Thick walled pressure vessels are those whose wall thickness exceeds the inner radius by more than 10 % [47]. The stresses experienced in thick walled cylinders are hoop stress, σ_c, axial stress, σ_a and radial stress, σ_r. Their values compare as follows:

$$\sigma_r < \sigma_a < \sigma_c \tag{A.1}$$

These stresses are the principal stresses at any given point in the cylinder body. When written in principal stress notation, they become: $\sigma_1 = \sigma_c, \sigma_2 = \sigma_a, \sigma_3 = \sigma_r$

Hoop and radial stresses vary with radius. Lame's Equations for hoop and radial stresses at any point in thick walled cylinders in the elastic range are given by [48]:

$$\sigma_c = A - \frac{B}{r^2} \tag{A.2}$$

$$\sigma_r = A + \frac{B}{r^2} \tag{A.3}$$

where *r* is the radius, *A* and *B* are constants to be determined by boundary conditions. The axial stress is dependent on end conditions. For an open ended cylinder, the axial stress is equal to zero. For a closed ended cylinder under either internal or external pressure, the elastic axial stress is given by [49]:

$$\sigma_a = \frac{\sigma_c + \sigma_r}{2} \tag{A.4}$$

$\sigma_c+\sigma_r$ is constant over the whole cross sectional area of the cylinder [48]. Thus the axial stress, σ_a, is also constant over the entire cross-sectional area of the thick walled cylinder.

The maximum shear stress at any point in the cylinder is given by [27]:

$$\tau_{\max} = \frac{\sigma_1 - \sigma_3}{2} = \frac{\sigma_c - \sigma_r}{2} \tag{A.5}$$

APPENDIX B

Cylinder Under Internal Pressure

For a cylinder under internal pressure only, the hoop and radial stresses at radius r are given by [27]:

$$\sigma_c = p\frac{r_i^2}{r_o^2 - r_i^2}\left(1+\frac{r_o^2}{r^2}\right) \tag{A.6}$$

$$\sigma_r = p\frac{r_i^2}{r_o^2 - r_i^2}\left(1-\frac{r_o^2}{r^2}\right) \tag{A.7}$$

where r_i is the inside radius, r_o is the outside radius and p is the applied internal pressure.

The axial stress is tensile but constant throughout the cylinder wall and is given by [47]:

$$\sigma_a = p\frac{r_i^2}{r_o^2 - r_i^2} \tag{A.8}$$

σ_c is tensile throughout and it is maximum at $r = r_i$. σ_r is compressive throughout and it is maximum at $r = r_i$. $|\sigma_c|$ is greater than $|\sigma_r|$ at any radius [27]. The maximum value of σ_c is always numerically greater than the internal pressure, and the minimum value of σ_c is always less than that at the inner surface by the value of the applied pressure [1].

Maximum shear stress will occur at $r = r_i$ and its value is given by [1]:

$$\tau_{\max} = p\frac{r_o^{\,2}}{r_o^{\,2} - r_i^{\,2}} \tag{A.9}$$

The maximum hoop stress and the maximum shear stress both occur at the bore of the cylinder. In thick walled cylinders, emphasis is normally on the behaviour of the hoop stress since it is normally the highest and involves separation of material leading to failure of structure [21].

APPENDIX C

Gaussian Sampling Points

The Gaussian sampling points for an eight noded element are [25]:

Table A-1 Eight Noded Element Gaussian Sampling Points

Gauss Point	ξ	η	ρ
1	-0.5773502692	-0.5773502692	-0.5773502692
2	0.5773502692	-0.5773502692	-0.5773502692
3	0.5773502692	0.5773502692	-0.5773502692
4	-0.5773502692	0.5773502692	-0.5773502692
5	-0.5773502692	-0.5773502692	0.5773502692
6	0.5773502692	-0.5773502692	0.5773502692
7	0.5773502692	0.5773502692	0.5773502692
8	-0.5773502692	0.5773502692	0.5773502692

APPENDIX D

Main Program Module

Below is the main program module that was developed for this research:

Program to determine the elastic stress profile and stress concentrations for elliptic cross-bore with changing orientation with respect to the cylinder axis.

Main variables

BETA - Angle of rotation of cross-bore counter-clockwise

C - Elastic stress-strain matrix

CL - Half cylinder length

CR - Ratio of circular cross-bore radius to the cylinder inside radius

D - Displacement vector

E - Young's modulus

EC - Eccentricity of the elliptic cross-bore

EF - Element load vector

ESM - Element stiffness matrix

EX - Element nodal cartesian coordinates

GF - Global load vector of active nodes

GR - Radial geometric ratio

GSM - Global stiffness matrix of active nodes

MC - Connectivity matrix

NDOF - Number of degrees of freedom in the structure

NEL - Number of elements in the structure

NFW - Maximum frontal width

NODES - Number of nodes in the structure

NR - Number of divisions in the radial direction

P - Change in internal pressure

Q - First term of a geometric ratio

R1 - Cylinder inside radius

R2 - Cylinder outside radius

RA - Semi-major axis of the elliptical cross-bore

RB - Semi-minor axis of the elliptical cross-bore

RBA - Ratio semi-minor axis to semi-major axis of the cross-bore

SIGMA - Array for stresses in Cartesian coordinate system

STRESS - Array for stresses in Polar coordinate system

TR - Thickness ratio

V - Poisson's ratio

YS - Yield stress

```
PARAMETER(MAXDOF=22000,MAXFW=3000,MAXNEL=6000,MAXNOD=70
00)
COMMON/BLOCK1/ADJ,BETA,CL,CR,E,EC,GR,GR1,GR2,GR3,GR4,P,PI,Q,Q1,
Q2,Q3,Q4
COMMON/BLOCK2/NA3,NC1,NC2,NC4,NDOF,NEL,NEP1,NEP2,NEP3,NFW,N
ODES,
```

```
PF,NR,NR1
COMMON/BLOCK3/R1,R2,RA,RB,RBA,TR,V,YS
COMMON/BLOCK4/C(6,6),D(MAXDOF),EF(24),ES(MAXNOD),ESM(24,24),EX
(8,3),GF(MAXFW)
COMMON/BLOCK5/GSM(MAXFW,MAXFW),LOADED(MAXNEL,3),MC(MA
XNEL,8),NEDV(MAXNEL,8)
COMMON/BLOCK6/SIGMA(MAXNEL,48),STRESS(MAXNOD,6),X(MAXNOD,
3)
OPEN (1,FILE='INPUT1')
OPEN (3,FILE='OUTPUT3',STATUS='REPLACE')
OPEN (4,FILE='OUTPUT4.DAT',STATUS='REPLACE')
OPEN (5,FILE='OUTPUT5.DAT',STATUS='REPLACE')
OPEN (7,FILE='OUTPUT7.DAT',STATUS='REPLACE')
OPEN (8,FILE='OUTPUT8.DAT',STATUS='REPLACE')
OPEN (9,FILE='OUTPUT9.DAT',STATUS='REPLACE')
OPEN (10,FILE='OUTPUT10.DAT',STATUS='REPLACE')
OPEN (11,FILE='OUTPUT11.DAT',STATUS='REPLACE')
OPEN (12,FILE='OUTPUT12.DAT',STATUS='REPLACE')
OPEN (13,FILE='OUTPUT13.DAT',STATUS='REPLACE')
OPEN (14,FILE='OUTPUT14.DAT',STATUS='REPLACE')
OPEN (15,FILE='OUTPUT15.DAT',STATUS='REPLACE')
OPEN (16,FILE='OUTPUT16.DAT',STATUS='REPLACE')
OPEN (17,FILE='OUTPUT17.DAT',STATUS='REPLACE')
```

```
OPEN (18,FILE='OUTPUT18.DAT',STATUS='REPLACE')
OPEN (19,FILE='OUTPUT19.DAT',STATUS='REPLACE')
OPEN (20,FILE='OUTPUT20.DAT',STATUS='REPLACE')
OPEN (21,FILE='OUTPUT21.DAT',STATUS='REPLACE')
OPEN (22,FILE='OUTPUT22.DAT',STATUS='REPLACE')
OPEN (23,FILE='OUTPUT23.DAT',STATUS='REPLACE')
READ (1,*) R1,TR,CR,RBA,E,V,NR,P,BETA
DO 280 CR=0.15,0.26,0.05
CALL INPUT
DO 20 I=1,6
DO 10 J=1,6
C(I,J)=0.0
10CONTINUE
20CONTINUE
CN=E/((1.0-2.0*V)*(1.0+V))
DO 30 I=1,3
C(I,I)=CN*(1.0-V)
30CONTINUE
DO 40 I=4,6
C(I,I)=CN*(1.0-2.0*V)/2.0
40CONTINUE
DO 60 I=1,2
DO 50 J=I+1,3
```

```
C(I,J)=V*CN

C(J,I)=V*CN

50CONTINUE

60CONTINUE

DO 270 BETA=0.0,90.0,15.0

REWIND (3)

CALL DISCRITIZE

CALL CONNECTIVITY

CALL PREFRONT

DO 80 I=1,NEL

DO 70 J=1,48

SIGMA(I,J)=0.0

70CONTINUE

80CONTINUE

CALL ASSEMBLE

CALL BACKSUB

CALL STRESSES

CALL SMOOTH

HMAX=0.0

DO 90 I=1,NODES

IF (ABS(STRESS(I,1)).GT.HMAX) THEN

HMAX=ABS(STRESS(I,1))

I1=I
```

```
ENDIF
90CONTINUE
EMAX=0.0
DO 100 I=1,NODES
IF (ES(I).GT.EMAX) THEN
EMAX=ES(I)
I2=I
ENDIF
100  CONTINUE
SCF1=HMAX/STRESS(NC2/2+1,1)
SCF2=EMAX/ES(NC2/2+1)
IF (CR.EQ.0.15) THEN
WRITE(20,290)BETA,SCF1,SCF2,I1,I2,TR,CR,RBA
ELSEIF (CR.EQ.0.20) THEN
WRITE (21,290)BETA,SCF1,SCF2,I1,I2,TR,CR,RBA
ELSEIF (CR.EQ.0.25) THEN
WRITE (22,290)BETA,SCF1,SCF2,I1,I2,TR,CR,RBA
ELSEIF (RBA.EQ.0.7) THEN
WRITE (23,290)BETA,SCF1,SCF2,I1,I2,TR,CR,RBA
ENDIF
R=R1*1000.0
J=0
N1=1
```

```
N2=N1+NPF*NR
DO 110 I=N1,N2,NPF
I1=I*3-2;I2=I*3-1
RD=SQRT(D(I1)**2+D(I2)**2)
WRITE(17,*) R,RD
WRITE(4,*) R,STRESS(I,1),STRESS(I,2),STRESS(I,3)
R=R+Q*(GR**J)*1000.0
J=J+1
110  CONTINUE
R=R1*1000.0
J=0
N1=NC2/2+1
N2=N1+NPF*NR
DO 120 I=N1,N2,NPF
I1=I*3-2;I2=I*3-1
RD=SQRT(D(I1)**2+D(I2)**2)
WRITE(18,*) R,RD
WRITE(5,*) R,STRESS(I,1),STRESS(I,2),STRESS(I,3)
R=R+Q*(GR**J)*1000.0
J=J+1
120  CONTINUE
R=R1*1000.0
J=0
```

```
N1=NC2+1
N2=N1+NPF*NR
DO 130 I=N1,N2,NPF
I1=I*3-2;I2=I*3-1
RD=SQRT(D(I1)**2+D(I2)**2)
WRITE(19,*) R,RD
WRITE(7,*) R,STRESS(I,1),STRESS(I,2),STRESS(I,3)
R=R+Q*(GR**J)*1000.0
J=J+1
130  CONTINUE
N1=NC2/2+1
N2=N1+(NC2+1)*NA3
DO 140 I=N1,N2,NC2+1
DS=(X(I,3)-X(NC2/2+1,3))*1000.0
WRITE(8,*) DS,STRESS(I,1),STRESS(I,2),STRESS(I,3)
140  CONTINUE
DO 150 J=0,NR1-2
I=((NC2+1)*(NA3+1)+(NC4+1)*(NC1-1))*2+1+NC1*4*J
DS=(X(I,3)-X(NC2/2+1,3))*1000.0
WRITE(8,*) DS,STRESS(I,1),STRESS(I,2),STRESS(I,3)
150  CONTINUE
N1=((NC2+1)*(NA3+1)+(NC4+1)*(NC1-1))*2+1+NC1*4*(NR1-1)
N2=N1+NPF*NR
```

```
DO 160 I=N1,N2,NPF
DS=(X(I,2)-X(N1,2)+X(N1,3)-X(NC2/2+1,3))*1000.0
WRITE(8,*) DS,STRESS(I,1),STRESS(I,2),STRESS(I,3)
160  CONTINUE
N1=(NC2+1)*(NA3+1)+(NC4+1)*NC1/2-NC4
N2=N1+NC4
DO 170 I=N1,N2
DS=PI*R1*ASIND(X(I,2)/R1)*1000.0/180.0
WRITE(9,*) DS,STRESS(I,1),STRESS(I,2),STRESS(I,3)
170  CONTINUE
DO 180 J=0,NR1-2
I=((NC2+1)*(NA3+1)+(NC4+1)*(NC1-1))*2+(NC1+1)+NC1*4*J
DS=PI*R1*ASIND(X(I,2)/R1)*1000.0/180.0
WRITE(9,*) DS,STRESS(I,1),STRESS(I,2),STRESS(I,3)
180  CONTINUE
N1=((NC2+1)*(NA3+1)+(NC4+1)*(NC1-1))*2+(NC1+1)+NC1*4*(NR1-1)
N2=N1+NPF*NR
DO 190 I=N1,N2,NPF
DS=(X(I,2)-X(N1,2)+PI*R1*ASIND(X(N1,2)/R1)/180.0)*1000.0
WRITE(9,*) DS,STRESS(I,1),STRESS(I,2),STRESS(I,3)
190  CONTINUE
R=R1*1000.0
J=0
```

```
N1=(NC2+1)*(NA3+1)+(NC4+1)*NC1/2-NC4
N2=N1+NPF*NR
DO 200 I=N1,N2,NPF
WRITE(10,*) R,STRESS(I,1),STRESS(I,2),STRESS(I,3)
R=R+Q*(GR**J)*1000.0
J=J+1
200  CONTINUE
R=R1*1000.0
J=0
N1=(NC2+1)*(NA3+1)+(NC4+1)*(NC1-1+NC1/2)
N2=N1+NPF*NR
DO 210 I=N1,N2,NPF
WRITE(11,*) R,STRESS(I,1),STRESS(I,2),STRESS(I,3)
R=R+Q*(GR**J)*1000.0
J=J+1
210  CONTINUE
N1=NPF-(NC1*4-1)
N2=NPF
DO 220 I=N1,N2
WRITE(12,*) I,STRESS(I,1),STRESS(I,2),STRESS(I,3)
220  CONTINUE
WRITE(12,*) N2+1,STRESS(N1,1),STRESS(N1,2),STRESS(N1,3)
N1=NPF-(NC1*4-1)+NPF*(NR/2)
```

```
N2=NPF+NPF*(NR/2)
DO 230 I=N1,N2
WRITE(13,*) I,STRESS(I,1),STRESS(I,2),STRESS(I,3)
230  CONTINUE
WRITE(13,*) N2+1,STRESS(N1,1),STRESS(N1,2),STRESS(N1,3)
N1=NPF-(NC1*4-1)+NPF*NR
N2=NODES
DO 240 I=N1,N2
WRITE(14,*) I,STRESS(I,1),STRESS(I,2),STRESS(I,3)
240  CONTINUE
WRITE(14,*) N2+1,STRESS(N1,1),STRESS(N1,2),STRESS(N1,3)
R=R1*1000.0
J=0
N1=((NC2+1)*(NA3+1)+(NC4+1)*(NC1-1))*2
N2=N1+NPF*NR
DO 250 I=N1, N2, NPF
WRITE (15,*) R,STRESS(I,1),STRESS(I,2),STRESS(I,3)
R=R+Q*(GR**J)*1000.0
J=J+1
250  CONTINUE
R=R1*1000.0
J=0
N1 = ((NC2+1)*(NA3+1)+(NC4+1)*(NC1-1))*2-NC2
```

```
N2=N1+NPF*NR
DO 260 I=N1, N2, NPF
WRITE(16,*) R,STRESS(I,1),STRESS(I,2),STRESS(I,3)
R=R+Q*(GR**J)*1000.0
J=J+1
260  CONTINUE
270  CONTINUE
280  CONTINUE
290 FORMAT(F12.5, 1X, F12.5, 1X, F12.5, 1X, I5, 1X,I5, 1X, F12.5, 1X, F12.5,
1X, F12.5)
END
```